ACCSCIENCE PUBLISHING

International Journal of Bioprinting

REVIEW ARTICLE

Designing methacrylic anhydride-based hydrogels for 3D bioprinting

Naisi Shen[1], Zhen Li[1], Pu Yang[1], Xiangjun Liu[1], Yikun Ju[1], Yue Hu[1], Bairong Fang[1]*, and Liangle Liu[2]*

[1]Department of Plastic and Aesthetic (Burn) Surgery, The Second Xiangya Hospital of Central South University, Changsha, Hunan, China

[2]Department of Spinal Surgery, The Third Affiliated Hospital of Wenzhou Medical University, Wenzhou, Zhejiang , China

(This article belongs to the Special Issue: *New matrix materials for 3D Bioprinting*)

Abstract

Methacrylic anhydride (MA)-based hydrogels, derived by introducing methacryloyl groups to various polymer side chains, are promising bioinks for three-dimensional (3D) printing in medical applications. These hydrogels combine the inherent biocompatibility and therapeutic benefits of their parent polymers with the unique photocrosslinking properties conferred by the methacryloyl groups, allowing precise control over their mechanical properties through light-curing parameters. Using 3D biological compression, these hydrogels serve as bioinks for producing scaffolds with optimal porosity, facilitating cell adhesion, proliferation, and differentiation. This technology enables the precise spatial distribution of bioactive substances, offering targeted therapeutic treatment and controlled release. This review delved into recent advancements in bioprinting technologies, outlined the preparation of MA-based bioinks, and summarized factors influencing the resulting biological and mechanical properties of bioscaffolds. Additionally, the properties and applications of methylpropionic anhydride-based hydrogels in various medical fields were discussed, addressing current limitations and future challenges in integrating these hydrogels with 3D bioprinting for clinical applications.

Keywords: 3D printing; 3D-printed scaffold; Bioink; Light curing; Methacrylic anhydride-based compound

***Corresponding authors:**
Bairong Fang
(fbrfbr2004@csu.edu.cn)

Liangle Liu
(liuliangle@wmu.edu.cn)

Citation: Shen N, Li N, Yang P, et al. Designing methacrylic anhydride-based hydrogels for 3D bioprinting. *Int J Bioprint*. 2025;11(1):84-138. doi: 10.36922/ijb.4650

Received: August 24, 2024
Revised: October 3, 2024
Accepted: October 14, 2024
Published Online: October 15, 2024

Copyright: © 2024 Author(s). This is an Open Access article distributed under the terms of the Creative Commons Attribution License, permitting distribution, and reproduction in any medium, provided the original work is properly cited.

Publisher's Note: AccScience Publishing remains neutral with regard to jurisdictional claims in published maps and institutional affiliations.

1. Introduction

Three-dimensional (3D) bioprinting employs bioactive materials and biounits, such as bioink, as well as 3D printing technology, to create personalized biofunctional scaffolds. From a macrostructural perspective, conventional 2D cell culture technology cannot replicate the intricate complexity of actual tissues and organ systems. On a molecular and cellular level, the absence of mechanical induction and signaling crosslinking in 2D cultures results in a cellular state that significantly diverges from the physiological morphology observed in the human body compared with *in vivo* and 3D cell cultures. The 2D cellular environment lacks essential nutrients, as well as cellular and other factors present in native tissues, thus eliminating crucial stimuli that guide cell behavior. Moreover, 2D cell cultures exhibit a flat morphology, are limited by single growth

conditions, and display minimal cellular connections, resulting in inadequate differentiation and proliferation. Consequently, a higher incidence of apoptosis, reduced drug resistance, and diminished resilience to mechanical stress are observed in 2D cultures.[1]

Spatially distributed cells cultured in 3D not only exhibit different signaling cascades and drug sensitivities, but can also be induced to adhere, proliferate, and differentiate. Moreover, 3D culture enables the spatial localization and co-cultivation of different cell populations to observe their interactions. With the aid of microengineering (microfluidics), the effects of pathway modulators on tissue compartmentalization, cellular differentiation, and sequential sorting can be quantitatively and systematically investigated.[2] The assembly of multilayered 3D cellular structures can only be achieved through the use of scaffolds. In recent years, increasing research has centered around the advancement of 3D cell culture techniques to circumvent the limitations of 2D cell culture. Microtissue cellular scaffolds, such as scaffolds based on hydrogel, polymer rigid material, or hydrophilic glass fiber, have an enormous influence on cell differentiation and proliferation.[3] Notably, 3D printing technology can be used to generate 3D structures with adequate precision and mechanical performance, which can be combined with substrates, cells, and bioactive cues to produce 3D bioscaffolds.

The biomaterials used for 3D printing are called bioinks. Aqueous formulations of polymers or hydrogel precursors that contain biological factors would be considered biomaterial inks. Bioink varies from biomaterial ink as it contains cells. This is important because this biological component significantly restricts the choice of biomaterials and processing methods.[4] Bioink can also be loaded with microcarriers, such as cell-active substances, drugs, and various types of nanoparticles, which can be used to release functional drugs or improve the rheological and mechanical properties of bioink.[5] Bioinks need to have good biocompatibility and mechanical properties. The former ensures that printed cells can survive and establish connections, whereas the latter provides good fluidity during the printing process, enables rapid curing and molding after printing, and supports subsequent applications. Emerging bioprinting technologies allow the printing process to personalize the distribution of bioink on the x–y axes and form biological scaffolds with 3D spatial microscopic properties through multilayer print stacking on the z-axis. The power source for the droplets generated by inkjet 3D printing is the deformation of the printer head, which is squeezed against the bioink to generate tiny, discontinuous hydrogel droplets that are deposited on the receiving plane. In contrast to inkjet printing, laser-assisted printing uses focused laser pulses to stimulate a small area of the absorbing layer and generate high-pressure bubbles that propel the bioink to avoid direct contact with the dispenser. This printing method can maintain high cell viability (typically above 95%) because it does not subject cells to high mechanical stress.[6] Extrusion 3D printing utilizes a syringe-needle style nozzle that, by applying constant pressure to it, can produce a continuous filamentary hydrogel that is deposited on the receiving table. Based on extrusion 3D printing, fused deposition 3D printing introduces individualized temperature regulation of the nozzle and receiving panel, which is more suitable for bioinks with different mechanical properties at different temperatures.

Furthermore, digital light processing (DLP) and stereolithography (SLA) employ photocurable hydrogels, which are cured by using light sources of varying wavelengths; each corresponding layer of bioink is light-cured layer by layer to obtain high-precision 3D scaffolds. In addition, 4D printing, an emerging technology, employs 3D printing technology to print biological scaffolds that can change properties over time or have adjustable stability.[7] The power source for the property change can be a smart reactive hydrogel or living cells.[8] This holds significant potential for the engineering of tissues and organs whose primary function is mechanical, such as skeletal and smooth muscles. These 3D printing methods have their respective merits and demerits. Notably, 3D printing using light-cured hydrogels provides enhanced maneuverability, yielding reactive scaffolds that better simulate biological tissues in terms of mechanical strength. Notably, the light-curing process can be combined with different printing modalities at various stages: pretreatment of the bioink, curing upon completion of each layer, and consolidation curing after the print.

Methacrylic anhydride (MA)-based hydrogels, derived from MA and various polymers, serve as photosensitive biohydrogel materials suitable to be used as 3D printing bioinks. Upon ultraviolet (UV) or visible light exposure, the methacrylate side chains generate free radicals, promoting crosslinking and transitioning from sol–gel to gel. Variations in ink concentrations, UV wavelengths, and irradiation concentrations yield hydrogels with differing elastic modulus, hardness modulus, and adhesion strength, making them suitable for various biological tissue replacements. Methacryloyl anhydride group-modified bioactive substances, notably gelatin methacrylate (GelMA), feature a universal arginine-glycine-aspartic acid (RGD) tripeptide similar to that in extracellular matrix (ECM) proteins, enhancing cellular activities. Through meticulous control of reaction conditions, the substitution rate of methacryloyl anhydride groups can be adjusted, influencing scaffold physical properties

under identical light conditions. The light curing process allows for manipulation of the mechanical strength of each printed layer and overall scaffold by selecting photoinitiators and adjusting the light source's wavelength, intensity, duration, and distance. In summary, MA-based hydrogels used as bioinks offer versatility in 3D printing methods, enabling the customization of mechanical properties for personalized, biocompatible 3D tissues in medical applications.

By choosing different compounds for polymerization, different biological properties and therapeutic significance can be obtained. The spatial distribution of cells, drugs, bioactives, exosomes, or other factors introduced into the MA-based hydrogel can be managed through 3D printing technology, enabling the construction of 3D tissues that better resemble the structure of target tissues. By changing the printing and light-curing parameters or mixing polymer hydrogels with high mechanical strength but poor bioactivity with MA-based hydrogels, it is possible to create bioscaffolds with high mechanical strength that meet the varying mechanical modulus requirements of the human body, from skin to bone.

In this paper, we first introduce 3D printing technology and the associated materials used and systematically summarize the preparation methods of MA hydrogels. We then introduce MA-modifiable compounds or active substances, followed by the biological potential of these precursors, which provides insights and guidance for the future application and development of MA hydrogel. By applying MA-based bioink in 3D printing technology, we can directionally distribute cells and other active components to produce 3D scaffolds with good biocompatibility and mechanical properties. We not only review the applications of these 3D scaffolds in tissue engineering but also discuss their use in organ-on-a-chip systems, organoids, biosensors, and bioglues. These applications can provide ideas for clinical treatment of various systemic diseases. Ultimately, we highlight the trends and shortcomings of MA-based hydrogels for 3D bioprinting and provide directions for their future development.

2. 3D printing technology and materials

2.1. 3D printing technology and characteristics

2.1.1. Inkjet 3D printing

As one of the earliest printing technologies,[9] inkjet 3D printing can be traced back to traditional inkjet 2D printers used for text printing. In fact, as early as 1988, Klebe used collagen as bioink and inkjet 3D printing technology in his experiments.[10] Similar to the construction of traditional 2D inkjet printers, the cartridge containing the bioink is connected to the printer head. During the electronically controlled printing process, the printer head is deformed and extruded, producing average-sized droplets (resolution can be as high as 50 μm). Depending on the power source, the printer head can be categorized as a piezoelectric, thermal, or electrostatic inkjet[11] (Figure 1A). Piezoelectric actuators work by utilizing the vibration of a polycrystalline piezoelectric ceramic actuator when energized, causing the head to eject ink. A major problem with this method is that the high frequencies (15–25 kHz) used in this bioprinter may disrupt cell membranes, leading to cell damage.[12] Thermal piezoelectrics operate by heating the printer head to create small bubbles inside the bioink; the kinetic energy generated by these bubbles squeezes and ejects the bioink. Even after being exposed to temperatures up to 300°C in the nozzle, cells can still be ejected with up to 90% viability, as they are only heated for 2 μs, resulting in a temperature increase of 4–10°C.[13] Electrostatic inkjets exploit the deformation of the platen when the circuit is turned on or off to extrude ink droplets. The advantages of inkjet printing are as follows: (i) low cost due to a commercial printer-like construction; (ii) high print speed; and (iii) relatively high cell viability. However, current printer heads are based on microelectromechanical system devices; hence, thermal or piezoelectric actuation at the nozzle opening produces relatively small deformation blockages.[14] Another disadvantage of inkjet printing is the settling effect.[15] When the bioinks are initially loaded into the cartridges, they typically mix well. However, throughout the printing process, cells begin to deposit in the cartridge, increasing the viscosity of the bioinks during subsequent printing and often clogging the printer head. In terms of material selection, the non-contact nature of inkjet printing and its reliance on gravity limit the utilization of biomaterials to those with low viscosity, restricting its ability to create fine 3D structures with suitable mechanical properties. Additionally, a certain degree of splattering may occur during the printing process, thus affecting the accuracy of inkjet printing (Table 1).[11]

2.1.2. Laser-assisted 3D printing

Laser-assisted printing is a 3D printing method based on the principle of focused laser-induced transfer of bioink in bioink carriers (cartridges). Laser-assisted 3D printing produces discontinuous droplets of bioink similar to inkjet 3D printing. The difference with inkjet 3D printing lies in its power source during the printing process: focused laser pulses generate high-pressure bubbles at the boundary of the bioink layer, propelling the bioink particles suspended within.[16] Accordingly, laser-assisted printing circumvents many of the drawbacks of inkjet 3D printing by eliminating the need for physical contact and mechanical pressure on cells, leading to optimal cell survival rates, typically

above 95%.[6] Experiments have demonstrated that mesenchymal stem cells (MSCs) can survive and maintain their function throughout the printing process.[17] In addition, laser-assisted printing allows for the printing of more diverse types of bioinks. However, as no nozzles are used to deliver the bioink to the desired plane, the entire cartridge is filled with bioink, leading to material wastage. Moreover, high-resolution and high-intensity laser diodes are expensive. Laser-assisted 3D printing instruments are also bulkier than other 3D printers due to the complexity of the control technology (Table 1).

2.1.3. Extrusion 3D printing

As one of the most common biological 3D printing methods, extrusion 3D printing, also known as pressure-assisted 3D printing, involves assembling bioink in a printer head. By applying pressure to it, the bioink is extruded out of the printer head to form a continuous strand that is deposited onto a surface, forming a 2D structure[18]; a 3D structure is then created layer by layer. The pressure applied to the bioink during the deposition and extrusion process can be carried out using either pneumatic, piston, or screw systems[19] (Figure 1B). To build complex tissue structures, more advanced extrusion bioprinting fabrication methods, such as multi-dispenser printing, coaxial bioprinting, and hybrid bioprinting, have been developed.[19] By using multi-dispenser printing and hybrid bioprinting, simultaneous printing of multiple bioinks can be achieved for constructing complex organ tissues; however, the key to this method is to prevent contact and mixing between the different bioinks.[20] Coaxial bioprinting utilizes different diameters of print heads on the same longitudinal axis to print hollow structures and vertical filament structures (e.g., blood vessels[21] and small intestine villi[22]). A wide range of bioinks are available for extrusion bioprinting. The cost and commercial availability of this printing method are also among its advantages. Extrusion-based bioprinting can also result in cell damage, primarily due to shear stress exerted on the hydrogel and cells, which is the main force leading to this damage. Other influencing factors include needle type and size, dispensing pressure, and bioink concentration.[23,24] A larger print head diameter would reduce the shear stress and print precision (>100 nm), limiting the ability to print finer biological tissues; when the dispensing pressure, which is the pressure exerted directly on the bioink, is increased, shear stress increases; in addition, when printing bioink with higher viscosity, the increased pressure exerted by the machine leads to greater shear stress, increasing the risk of damaging the cell membrane (Table 1).

2.1.4. Depositional 3D printing

Currently, depositional 3D printing, also called fused deposition modeling (FDM), is the most common, economical, and commercially available form of 3D printing.[25] The key characteristic of FDM is the temperature difference between the nozzle and platform, which enables the bioink to exhibit varying mechanical properties at different spatial and temporal scales (Figure 1C). Before being extruded by the nozzle, the bioink is heated to a semi-solid state at a relatively high temperature, and after being deposited on the relatively low-temperature platform, it reverts back to a solid state. Other polymerization methods, such as photopolymerization, can also help improve the mechanical properties of bioink. The printing process, akin to extrusion 3D printing, involves nozzle movement along the x–y axes to follow the in-plane shape of the final object, while stacking layers on the z-axis. Temperature control is critical in depositional printing, as the heat-sensitive bioink can lead to poor material connectivity if the printed filament cools too quickly after extrusion. This cooling may create gaps in the material, affecting its mechanical properties.[26] If the printing process requires an extended duration of elevated temperature, this can affect the activity of the active bioink ingredients; for example, some industrial sectors require nozzle temperatures of up to 400°C.[27] However, various studies have attempted to minimize the potential negative effects of thermal conditions through different approaches, such as adding polymers or excipients to lower the temperature or scaling down the heating time (Table 1).

2.1.5. Stereolithography

SLA differs from traditional extrusion and inkjet printing technologies, as it does not require a nozzle or extrusion head to stack the bioink; it relies on a light source to cure the bioink. The fundamental principle of SLA molding technology involves utilizing a UV laser (350–410 nm). Under the programmable instructions, a vibrating mirror system is employed to scan the liquid surface point by point, gradually curing 2D hydrogel layers. After stacking along the z-axis, a 3D scaffold is formed through this curing process[28] (Figure 1E). Compared with the aforementioned 3D printing methods, SLA has more stringent material requirements, as the utilized bioinks must be easily photocrosslinked upon light exposure. As most light-sensitive materials require photoinitiators during the curing process, the potential toxicity of these initiators can also affect the bioactives in bioinks. The main advantages of this method are its enhanced precision and print quality, as the precise movement and tiny dimensions of the laser enable improved detail and resolution. However, this enhanced quality comes at the cost of print speed, as plotting each layer can be more time-consuming (Table 1).

2.1.6. Digital light processing

The process of DLP, also called projection-based 3D printing, involves the construction of a 2D hydrogel image

on the x–y axes, followed by layer-by-layer printing to realize the superposition on the z-axis, ultimately obtaining a 3D hydrogel body. DLP and SLA differ mainly in the way that each layer of hydrogel is constructed due to the difference in the light sources used. If the SLA's light source is a dot-shaped light source moving relative to the bioink, the DLP's light source is a static, surface-shaped light source with image properties relative to the bioink. The DLP system projects a 2D light image onto the bioink layer, triggering a photopolymerization reaction in the hydrogel solution, allowing for personalized single-material 3D printing.[35] A simple projected 3D printing device uses a UV emitter at the bottom as the light source, with the hydrogel being contained in a solution chamber above and separated from the UV emitter by a glass substrate (Figure 1E).[36] The light source of the DLP device is capable of emitting light at a wavelength range of 350–450 nm, with corresponding intensities varying according to wavelength, peaking at 405 nm (Figure 1E).[37] Due to its high manufacturing speed and resolution, DLP has become a significant focus in biomanufacturing technology. Compared to extrusion 3D printing, which has the smallest extrusion diameter of 100 μm, DLP can reach resolutions of up to 10 μm or less, resulting in significantly higher print quality,[38] allowing

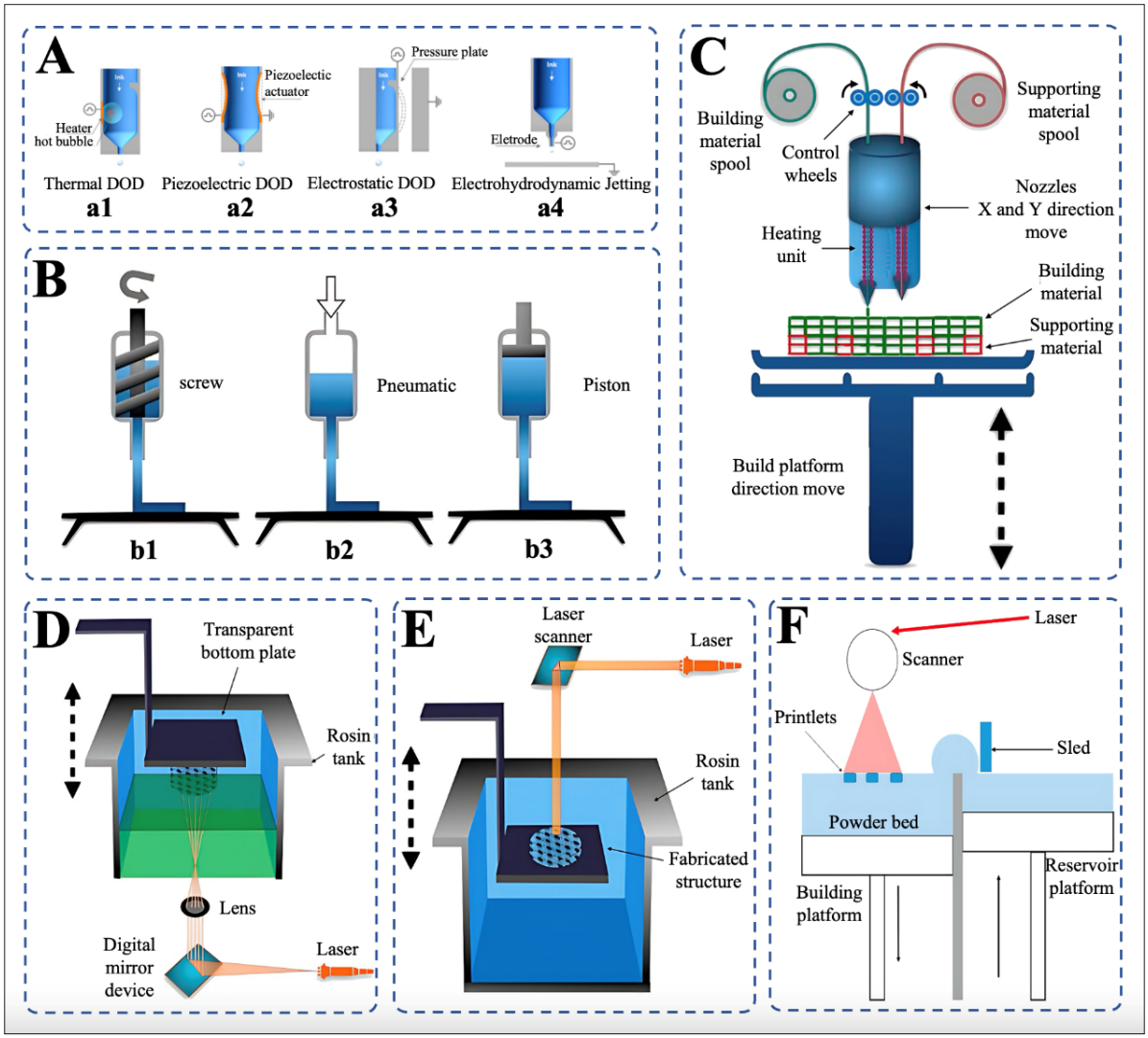

Figure 1. Overview of 3D printing. (A) Simple nozzle models for inkjet 3D printing: (a1) hot inkjet produces water droplets by heating bubbles; (a2) piezoelectric inkjet produces droplets by the vibration of the piezoelectric actuator; (a3) electrostatic inkjet ejects droplets through deformation of the pressure plate; (a4) high voltage electric field produces droplet. Adapted with permission from Li et al.[11] (B) Power sources of extruded heads: (b1) screw, (b2) pneumatic, (b3) piston. (C) FDM 3D printing with two different materials. (D) SLA printing model. (E) DLP printing model. Adapted with permission from Su et al.[32] (F) SLS printing model. Adapted with permission from Kafle et al.[33] Abbreviations: DOD, drop-on-demand; FDM, fused deposition modeling; SLA, stereolithography; SLS, selective laser sintering.

for the printing of finer tissues.[39] Additionally, projection-based 3D printing is more efficient than SLA, with manufacturing speeds typically ranging from 0.5 to 15 mm/s, allowing cell viability to be consistently maintained at 85–95%.[38] By assessing the adenosine triphosphate (ATP) content, Tahouni et al. demonstrated that DLP produced the highest number of viable cells compared with extrusion and inkjet 3D printing.[40] However, DLP has its drawbacks, such as potential DNA inducibility of the light source and photoinitiator toxicity (Table 1).[41]

2.1.7. Selective laser sintering

Selective laser sintering (SLS), known as solid-state sintering, is a process that uses one or more lasers to produce an object from a powder material. Any powder material that can be heated to form an atomic bond can be used as a molding material for SLS. A computer-controlled laser heats the powder, causing the particles in the powder to polymerize into a solid form. After sintering layer by layer, the 3D structure is successfully printed. Once the process is complete, the remaining powder is extracted from the platform (Figure 1F). The unsintered material can be reused, thus reducing waste and costs. Due to its distinct printing principle and process, SLS is seldom used to print cell-laden bioinks. SLS employs thermoplastic polymer, similar to fused deposition 3D printing; the material precursor for the former is powder, whereas for the latter, it is filament. SLS can achieve high printing accuracy with a minimum resolution of 20 μm if the laser is tightly focused.[29] However, its application is currently limited by its high cost and slow printing speed, which prevents rapid printing over large areas (Table 1).[30,31]

2.1.8. 4D printing

4D printing introduces a new dimension to the *x*–*y*–*z* spatial dimensions of 3D printing, i.e., time. By applying stimulus-responsive bioink, 4D bioprinting can create dynamic biostructures that can alter their shapes or behaviors in reaction to a range of stimuli (Figure 2A), more closely resembling the biological state of the original tissue (Figure 2B),[34] thereby offering significant promise for tissue engineering of tissues and organs with mechanical primary functions (Figure 2C). One such example is the use of electrical stimulation to activate cardiomyocytes cultured in 3D fibrin hydrogel environments that mimic the natural environment of these cells and enable the reshaping of their structure to produce contractility under electrical pacing conditions.[35] However, one of the limitations of 4D bioprinting also stems from its dependence on external stimuli, as excessive stimulation may damage and kill living cells; therefore, stimuli must be adapted. One of the simplest mechanisms that can be employed in 4D printing is using non-homogeneous materials with different properties to enable folding and unfolding under different conditions (e.g., swelling). The power source for 4D-printed biomaterials to undergo a trait change can be an intelligent hydrogel substance or cells. The available hydrogel substances are categorized into light-responsive hydrogels,[36] temperature-responsive hydrogels,[37,38] acidity-responsive hydrogels,[39] humidity-responsive hydrogels,[40] magnetic,[41] and electric[42] reactive hydrogels, and acoustic reactive hydrogels,[43] or combinations of these. Additionally, material changes can also be achieved using cellular forces, where cells can generate traction in their matrix, originating from intracellular actin polymerization and antiglobulin interactions.[44] Kuribayashi-Shigetomi et al. cultured cells on microtiter plates and then used cellular traction to fold these cells into 3D microstructures.[45]

2.2. Materials

Bioinks typically comprise a solution of hydrogel prepolymer and cells (Figure 3A). In the 3D printing process, cells interact with the hydrogel material. Hence, choosing suitable biomaterials to simulate the physiological *in vivo* environment is essential for cells to proliferate in the microenvironment provided by the hydrogel.[49] However, the printing properties of the hydrogel vary to a certain extent due to the incorporation of cells (Figure 3B).[50] Therefore, selecting suitable hydrogel solutions and cells, and using proper printing and crosslinking methods are significant.

2.2.1. Hydrogel solutions

Hydrogel solutions play a critical role in bioinks because they provide the immediate environment on which cells depend on and must have the required physical and chemical properties.

Given that most current 3D printing approaches support dispensing liquid materials and that subsequent cell proliferation necessitates a scaffold with adequate mechanical strength, the printability of the hydrogel solution in both liquid and gel states while maintaining its solidity after printing is essential. Consequently, hydrogels designed for 3D printing must exhibit responsiveness to specific optical,[51] chemical,[52] and thermal[53] stimuli. This responsiveness is crucial for forming solid scaffolds with the requisite mechanical strength under controlled conditions. Moreover, these hydrogel properties should remain relatively stable in a biological environment, minimizing susceptibility to changes.

The interaction between hydrogels and cells is dynamic, which is important for cell adhesion and growth.[54] The hydrogel's mechanical characteristics, including shear stress, mass expansion, strain, and compression modulus, precisely determine its interaction with cells. For some soft

Table 1. Comparison of various 3D printing technologies

3D printing method	Printing form	Printing speed	Resolution (μm)	Vertical stability	Cell viability	Cell density	Printing cost	Ref.
Inkjet 3D printing	Droplet	Fast	50–100	Poor	>85%	Low	Low	[11]
Laser-assisted 3D printing	Punctiform	Medium	10–100	Good	>95%	Medium	High	[46]
Extruded 3D printing/ FDM	Filamentous	Slow	200–1000	Good	40–90%	High	Medium	[23,47]
DLP/SLA	Layered	Fast	<50	Good	>85%	Medium	High	[29,48]

Abbreviations: FDM, fused deposition modeling; DLP, digital light processing; SLA, stereolithography.

tissues, tissue functionality lies in the mechanical properties they provide; therefore, the resulting hydrogel must first be well-adapted and can withstand the stresses and tensions that the tissue would otherwise be subjected to.

Biocompatibility requires that cells survive, differentiate, and proliferate in the hydrogel after 3D printing. Hydrogels need to have good porosity to facilitate nutrient delivery. The problem of vascularization is a major limitation for printing structures on a large scale.[55] These are just the basic requirements for *in vitro* applications. When hydrogels are used *in vivo*, they not only need to have the basic requirements for *in vitro* applications described above but also avoid adversely affecting the organism or being metabolized to produce toxic by-products. In addition, the ideal implantable tissue needs to have good degradability, gradually combining with human tissue through metabolic degradation.[56]

2.2.2. Cells

Cells selected for bioink production are typically divided into two main categories: differentiated functional or support cells[57,58] and stem cells with differentiation potential.[59,60] such as induced pluripotent stem cells (iPSCs), MSCs, neural stem cells (NSCs), adipose-derived stem cells (ADSCs), embryonic stem cells (ESCs), or embryoid bodies (EBs) made up of multiple ESCs.[61] When using differentiated cells, parallel printing is needed as multiple cell types must be embedded in one or more hydrogels concurrently or sequentially. This complicates real-time alignment and printing control, introducing challenges in preventing interference between bioinks due to varied excitation conditions, potentially leading to errors in bioprinting processes. Stem cell printing streamlines the variety of bioinks but increases complexity in subsequent steps, particularly in inducing differentiation. Precise deposition of growth factors and differentiation stimulators is essential for controlling differentiation during subsequent post-printing culturing. Currently, two methods exist for cell insertion during printing: (i) mixing a hydrogel solution with cells in a cartridge and acting as a bioink, or (ii) applying cells directly to a scaffold of cured material after printing with a hydrogel solution.[50] Notably, a reliable cell source remains a long-term challenge for bioprinting, especially for clinical applications, where cells should ideally be isolated from the body of the patient to prevent immune reactions.[62]

3. MA-based hydrogel bioinks

3.1. Preparation

3.1.1. Introduction of methacryloyl groups

The preparation of MA-based hydrogels involves grafting methacryloyl anhydride groups to the hydroxyl or carboxyl

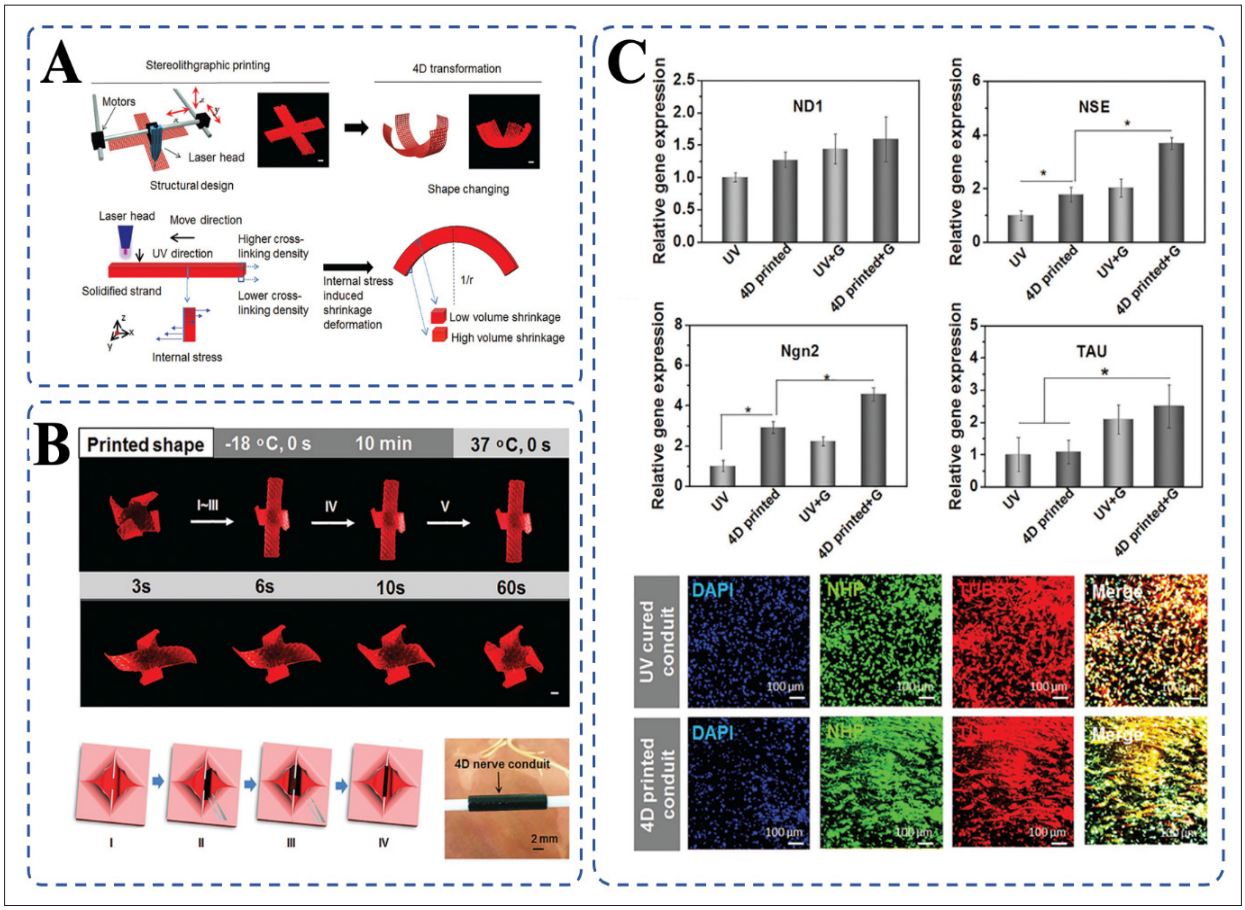

Figure 2. A novel multi-responsive architecture through stereolithography (SLA)-based 4D bioprinting, using a naturally derived, photocrosslinkable monomer (soybean oil epoxidized acrylate [SOEA]). (A) A claw structure obtained by SLS printing technology and its deformation mechanism. (B) Images displaying the reversible shape change process of a 4D-printed structure and its application in nerve repair. (C) The 4D-printed graphene hybrid conduit significantly improved the neurogenic differentiation of hMSCs. Adapted with permission from ref.[36] Abbreviations: SLS, selective laser sintering; hMSCs, human mesenchymal stem cells.

groups on their side chains by mixing different hydrogels with compounds capable of introducing MA groups under certain conditions, generating an amidation or an esterification reaction. At present, owing to simplicity and cost, the most common modification reaction used is the esterification of MA or glycidyl methacrylate (GMA).[64] Alternatively, aminoethyl methacrylate (AEMA) and hydroxyethyl methacrylate (HEMA) may be used.[64] AEMA, HEMA,[65] and methacryloyl chloride[66] can also be used for the introduction of methacryloyl anhydride groups. Different concentrations of MA can result in different methacrylic acid (MAA) graft substitution conversions in the resulting material (Table 2). The substitution conversion ratio of MAA is a key parameter for measuring GelMA performance. When the substitution rate is low, the formed MA compounds can better retain their original biocompatibility and other active properties; however, when the substitution rate increases, the crosslinking and mechanical properties increase significantly; when the rate of substitution exceeds 15% for light-curing crosslinking, the degree of methacrylation can reach up to 90%.[67] By adjusting the GMA content and reaction time, the degree of methacrylation can also be changed, reaching up to 90%.[68] Nichol et al.[69] prepared three batches of GelMA with methacrylation degrees of 81.4% (high), 53.8% (middle), and 19.7% (low) by adding 20, 1.25, and 0.25 vol.% MAA, respectively, into the synthesis reaction. The compressive modulus was significantly higher for low, medium, and high degrees of methacrylation at both the 15% and 10% (w/v) GelMA concentrations. Holding the hydrogel percentage constant, the mass swelling ratio increased significantly with a decreasing degree of methacrylation at all three hydrogel concentrations, demonstrating that the degree of methacrylation had a significant effect on the material's ability and propensity for attracting and storing water within the polymer network (Figure 4B).[69]

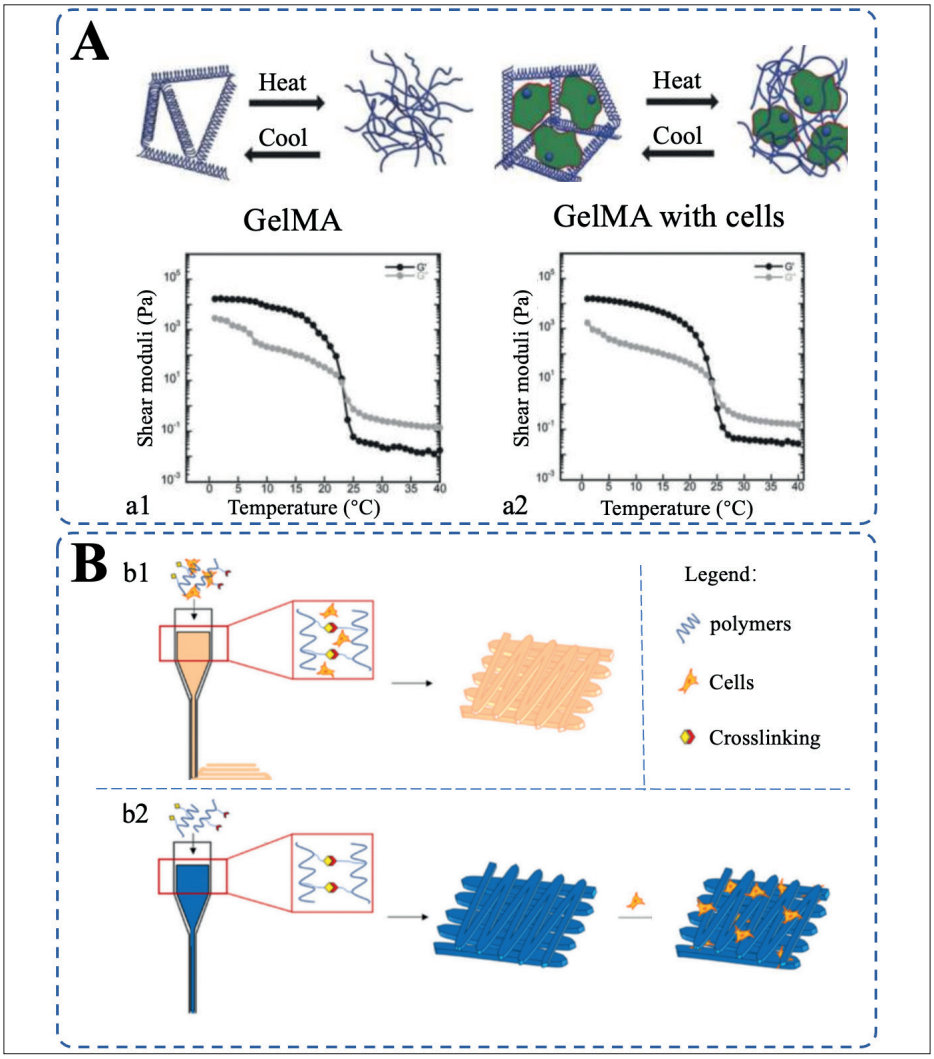

Figure 3. Basic form of a bioink. (A) Schematic representation of temperature-responsive gels (top); corresponding shear elasticity and loss modulus of pure GelMA (a1) and fibroblast-containing GelMA bioink (a2). Adapted with permission from Kolesky et al.[63] (B) Cell coating methods for 3D printing using bioink: printing with cells (b1), or using scaffold adhesion cells (b2). Adapted with permission from Cadamuro and Nicotra.[50] Abbreviation: GelMA, methacrylated gelatin.

3.1.2. Photocrosslinking reactions and photoinitiators

MA-based hydrogels can be crosslinked and molded by light reactions because they contain many photosensitive groups, usually unsaturated double bonds. Unlike the polymerization process of traditional materials that form a 1D linear structure, photosensitive hydrogels require a certain light wavelength and photoinitiator to polymerize. This reaction mainly consists of three steps: proliferation, termination, and closure reaction (Figure 4C).

Only two factors influence the formation of light-cured hydrogels: hydrogel precursor properties and crosslinking conditions. The latter include temperature, exposure time and intensity, and light wavelength.[72] The printability of hydrogel materials is mainly determined by the degree of crosslinking. He et al. found that utilizing fast crosslinking printing and slow crosslinking followed by printing can improve the printability of hydrogels by two to four times. Fast crosslinking printing refers to a printing method that utilizes high exposure intensity and short exposure time, forming a hydrogel with a lower crosslinking degree. By contrast, slow crosslinking post-printing utilizes low exposure intensity and long exposure time, forming a hydrogel with a higher crosslinking degree underneath. By adjusting the exposure parameters, this strategy achieves higher cell viability. Hence, the properties of cured materials can be improved to a large extent by personalizing the light reaction parameters in the photocrosslinking reaction.[73]

Table 2. Common MA reactants

Reactants	Reaction solvent	Reactant concentration	Reaction pH	Reaction temperature	Response time (h)	Ref.
MA	Water, PBS	4–6%	8–10	Indoor temperature	2–4	[68,70]
GMA	PBS	1%	3.5–5.5	50–60°C	24	[64]
AEMA	MES buffer	0.38%	6.5	Indoor temperature	24	[64]
HEMA	DMAP, Boc_2O	-	-	45°C	20	[65]
Methacryloyl chloride	Anhydrous chloroform	-	-	0°C to room temperature	14	[66]

Abbreviations: AEMA, aminoethyl methacrylate; Boc_2O, di-tert-butyl decarbonate; DMAP, dimethyl sulfoxide; GMA, glycidyl methacrylate; HEMA, hydroxyethyl methacrylate; MA, methacrylic anhydride; PBS, phosphate-buffered saline.

Photosensitizers can absorb energy at a certain wavelength and produce free radicals and cations, triggering the polymerization of monomers, crosslinking, and curing. Lithium phenyl-2,4,6-trimethylbenzoylphosphinate (LAP), a kind of phosphine derivative with good spectral properties and high water-solubility, is the most commonly used photoinitiator in the photopolymerization of MA-based hydrogel. Studies have reported that using different types of photosensitizers results in varying resolutions. Using a high-intensity light source that is scattered or refracted by other substances amplifies the effect of the photosensitizer.[74] Additionally, certain photoinitiators may pose potential toxicity to cells. Therefore, when designing a photocrosslinking reaction, the choice of photoinitiator and its absorbance properties should be cautiously considered.

3.1.3. Advantages and disadvantages of modified hydrogel bioinks

Most hydrogels crosslinked by ionic, chemical, or temperature reactions have poor mechanical strength and reversible crosslinking disadvantages. Photopolymerization offers numerous advantages over other methods. Firstly, light is non-invasive and can be manipulated remotely without additional reagents. Secondly, by adjusting the illumination parameters (intensity, wavelength, and illumination time), the irradiation dose can be controlled, thereby imparting precise regulation of the degree of light reaction.[75] Under certain light reaction conditions, a gum can form quickly and be crosslinked in a few seconds. This can greatly improve the efficiency of 3D printing. However, this poses challenges for 3D printing; for example, in extrusion 3D printing, the extrusion speed of the precursor solution of hydrogel needs to be controlled to match the gelation speed of the hydrogel. Otherwise, if the extrusion speed is too fast while the gelation time is too little, this will cause the collapse of the stent; conversely, if the extrusion speed is too slow while the gelation time is too long, the pre-cured hydrogel will block the nozzle. The UV light utilized in the photocrosslinking process also affects cell viability and DNA stability. When cells are exposed to UV light for more than 10 min, up to 90% of cells can be damaged.[76] Although UV light and free radicals may attack the cell membrane during crosslinking, this can be easily controlled by adjusting the light source and dose of photoinitiator.

To maintain cell viability during and after printing, the low toxicity and high biocompatibility of the printed scaffolds are imperative, especially for implantable tissue structures. From a materials science perspective, the biggest factor that influences the biocompatibility of biological scaffolds is their microscopic morphology.

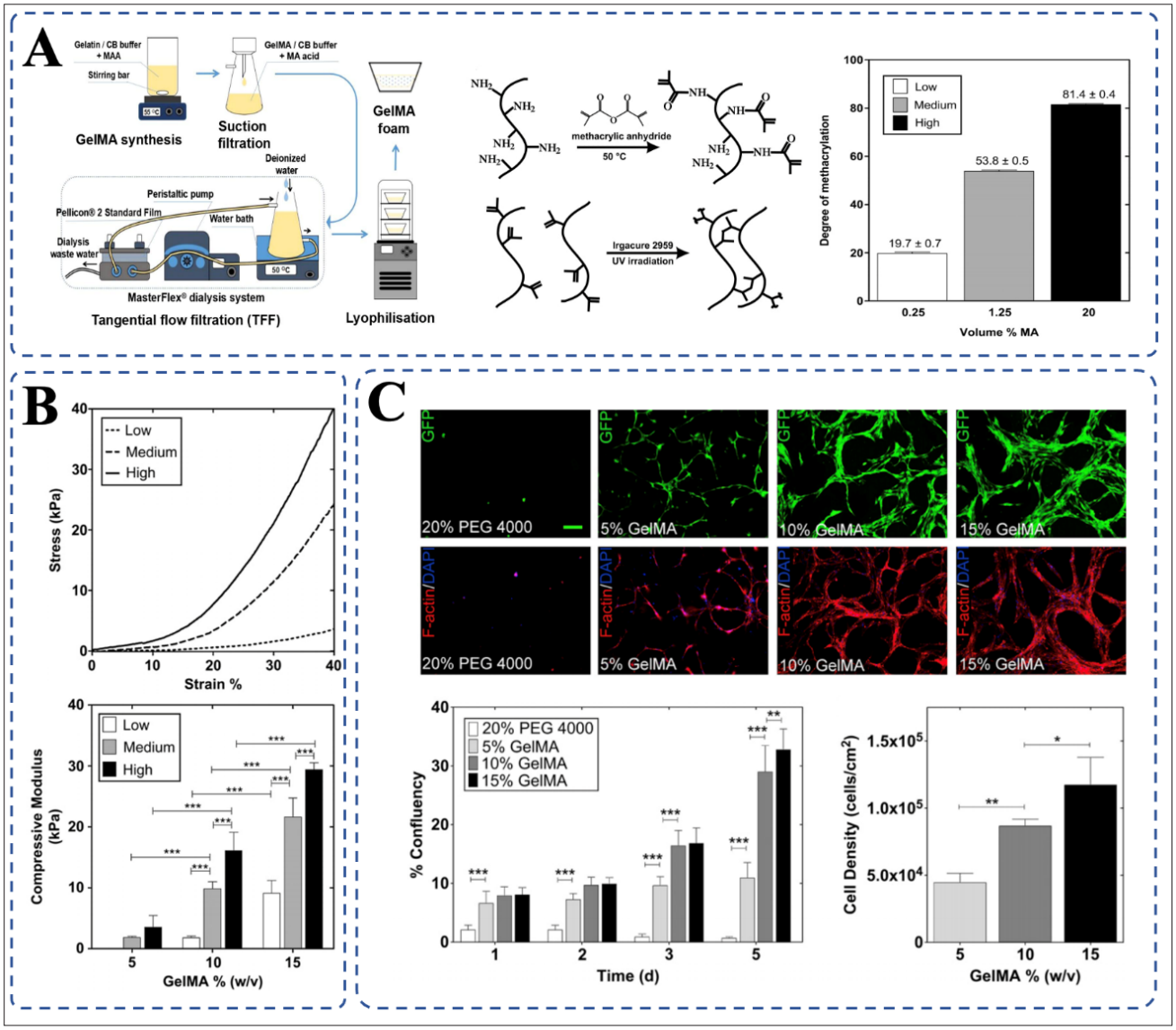

Figure 4. Gelatin methacrylate (GelMA) hydrogels with different substitution rates have different properties. (A) GelMA hydrogels with different substitution rates can be obtained by changing the feed ratio. Adapted with permission from Zhu et al.[71] (B) GelMA hydrogels with different substitution rates have different physical properties. (C) GelMA hydrogels with different concentrations have different biocompatibility. Adapted with permission from Nichol et al.[69] Abbreviations: CB, carbonate-bicarbonate; MAA, methacrylic acid; MA, methacrylic anhydride; PEG, polyethylene glycol, GelMA, methacrylated gelatin.

Thus, by adjusting the printing parameters and methods, 3D printing and photoreactive hydrogels can be utilized to develop bionic cues that favor cell adhesion.[77]

Regarding the microscopic morphology, the pore size and porosity of hydrogels are critical for cell migration, nutrient and oxygen distribution, and cell–cell interactions. Of note, adequate pore size and porosity mediate vascularization, as they provide an optimal physical microenvironment for human umbilical vein endothelial cell (HUVEC) migration. When pore size ranges from 200 to 250 μm, cell migration and proliferation are favored.[78] Porosity and pore size are largely determined by the precision of the printing process and material properties. The fidelity of the printed hydrogel determines whether the subsequent scaffold can maintain these biological cues. With the increasing number of layers, the geometry of the hydrogel may collapse under its own weight. As bioink cannot sustain unsupported fibers, vertical pores may close as they expand, whereas lateral pores may collapse.[79] The final filament width in a hydrogel material increases due to its water-absorbing and swelling properties, resulting in a

decrease in the final filament spacing when exposed to body fluids. The swelling of hydrogels in simulated body fluid environments leads to notable pore closure, affecting cell migration and nutrient penetration. However, advocating solely for high porosity is not that simple, as increased porosity and pore size inevitably diminish the mechanical properties of the hydrogel. Therefore, a balance must be achieved to optimize both porosity and mechanical strength based on specific tissue load-bearing requirements.

3.2. Material classification and finishing

3.2.1. Proteins

GelMA: Gelatin has an amino acid sequence similar to that of its precursor, collagen, and is widely utilized in the food manufacturing and pharmaceutical sectors. Unmodified gelatin can self-form a crosslinked network under chemical or enzymatic crosslinking conditions, though exhibiting poor mechanical properties.[80] By introducing methacryloyl substituents to the reactive groups on its side chains, GelMA can be obtained, which can be crosslinked and cured into a gel using photoinitiators and UV/visible light. GelMA has good biocompatibility because the gelatin backbone contains biologically active sequences of collagen for cell attachment, such as RGD peptides and matrix metalloproteinase-sensitive degradation sites.[67] 3D GelMA hydrogels closely resemble some of the fundamental properties of natural ECM.[81] In addition, GelMA possesses good temperature-sensitive gel properties and degradability, while a broad spectrum of stiffness and viscoelastic characteristics can be provided by controlling the methacryloyl substitution rate. With the increasing methacryloyl substitution rate, hydrogels exhibit increased stiffness and smaller pore sizes, but they are also less favorable to cellular translocation. As no accurate standard method exists for determining and quantifying the substitution rate of MAA in hydrogels, the amount of MAA used to synthesize GelMA macromolecules is generally used as a measure of the degree of GelMA functionalization.[82] Typically, the compression modulus of hydrogels is in the range of 5–180 kPa, as the concentration of macromolecules varies from 5% to 20%.[83] GelMA, the most widely used MA-based hydrogel, has been used in tissue engineering of various systems of the human body.[70]

Silk protein- and silk gelatin-methacrylate: As a natural fiber, silk mainly comprises silk fibroin (SF) and silk sericin (SS) proteins, both of which have good biocompatibility and biodegradability. Silk fibers have a core–shell structure, with the inner core made up of sericin protein and the outer shell comprising silk gelatin protein. SF protein makes up the central fiber of silk, comprising approximately 75% of the total weight; SS can be used as an adhesive to maintain the structural integrity of the fiber, accounting for approximately 25% of the total weight.[84] SF, derived from the degumming of silk, is a polymer polypeptide composed of various amino acids, with serine, aspartic acid, and glycine being the three most significant amino acids.[85] The SF polypeptide comprises a hydrophobic light chain (with a molecular weight of 26 kDa) and a hydrophilic heavy chain (with a molecular weight of 390 kDa). This structure allows the generation of various secondary conformations of proteins and interconversion between them. Moreover, the degradation products of SF, primarily amino acids and peptides, can serve as nutrients for cells, rendering SF a promising candidate for tissue engineering. As the heavy chain of SF contains more repetitive sequences, which gives it excellent mechanical properties (maximum elongation at break: 4%; ultimate Young's modulus: 300–700 MPa; toughness: 70–78 MJ/m^3), it has been used in bone, blood vessel, and wound dressings.[86] SF solution is a semi-stable colloidal solution that can undergo gelation when induced by various factors, including shear force, ultrasound, temperature, and organic solvents. However, controlling the gelation process is challenging, limiting its adaptation to cell culture and 3D printing.[87] Methacryloylated SF (SilMA) is a methacryloylated modification of SF by glycidyl methacrylate, which introduces a double bond on the SF molecule. SilMA possesses excellent mechanical and rheological properties.[88] SilMA bioinks are ideally suited for DLP printing processes, enabling the construction of highly complex organ structures with excellent structural stability and biocompatibility.[89] In contrast, SS hydrogels exhibit inherent biological properties that support wound healing, moisturization, anticoagulation, and epithelial and connective tissue repair. They are widely applied as antioxidants, food additives, cosmetic additives, drug delivery carriers, polymer grafting devices, chemical protectors, UV radiation protectants (sunscreens), and anticancer compounds.[90] The antioxidant activity of methacryloylated SS (SerMA) is considered a fundamental property contributing to its biological effects, though the exact mechanism remains unclear. Reportedly, SerMA hydrogels have excellent biocompatibility. Moreover, they have demonstrated mechanical properties and degradation rates similar to those of other hydrogels. Diverse restoration needs can be readily accommodated by altering the extent of methacryloyl modification of SS.[91]

Bovine serum albumin (BSA) methacrylate: BSA is a non-glycosylated protein in the circulatory system that is ubiquitous in the human serum. BSA can function as a pH buffer to maintain homeostasis in the internal environment. Given the biodegradability, non-immunogenicity, cost-effectiveness, and remarkable biocompatibility of BSA, it has gained significant attention for biomedical applications,

especially in the treatment of various diseases and tissue engineering.[92] BSA can form hydrogel crosslinking networks under acid-based excitation, photoinitiation, and thermal excitation. However, the high cost and complexity of photoinitiation and temperature excitation can lead to cell inactivation and protein denaturation; thus, acid-based excitation is the optimal choice.[93] The introduction of a methyl amide group enables the synthesis of photoreactive BSA methacrylate (BSAMA), which exhibits slower gelation kinetics and enzymatic degradation than GelMA. In a study by Chen et al., BSAMA demonstrated higher cell survival than GelMA (BSAMA: 99.43 ± 0.57%; GelMA: 97.14 ± 0.69%). However, BSAMA gels were not as suitable as GelMA gels for cell proliferation and migration.[94] The group synthesized and formulated an aqueous resin using BSAMA to print precise 3D objects, exhibiting favorable cell viability after 21 days of incubation.

Methacrylate collagen: Collagen is the main component of animal connective tissue and the most abundant and widely distributed functional protein in mammals, as it can be found in skin, bones, joints, and hair.[95] Conventional collagen mainly derives from animal tissues such as pig skin, cow Achilles tendon, and fish skin. However, these sources entail inherent disease risks and may lead to human exclusivity and reduced efficacy due to structural disruption during extraction. By comparison, recombinant collagen presents no viral risk, demonstrating outstanding biological compatibility and efficacy, along with low immunogenicity. Collagen, which cannot directly support cells, can only be bioprinted by modifying it or mixing it with other hydrogels to form hybrid bioinks, posing a challenge in achieving the proper spatial distribution of cells. Furthermore, collagen exhibits low printability and stability. Toxic chemicals used in the crosslinking process limit cell viability in the bioprinting process.[96] Human recombinant collagen modified with MAA is crosslinked under photoexcitation and initiator conditions with better biocompatibility, printability, and mechanical strength, demonstrating great potential in tissue engineering and regenerative medicine.[97] Cardiomyocytes and cardiac fibroblasts can survive in MAA-modified human recombinant collagen for >14 days, allowing stiffness control of the 3D microenvironment and monitoring of cardiac cellular responses.[98]

3.2.2. Polysaccharides

Methacrylate chitosan: Chitosan, also known as deacetylated or soluble chitin, is derived through deacetylation (removal of the acetyl group from C2) of chitin. Chitosan presents a novel nanomedicine carrier, with a core factor being its unique mucosal property. The biodegradability, low toxicity, and good biocompatibility of chitosan have led to its widespread use in biomedicine and formulations.[99] It exhibits antimicrobial activity against various bacterial, fungal, and viral pathogens, as well as antacid, antiulcer, and wound healing properties.[100–102] Chitosan possesses hydroxyl and amino groups that facilitate intermolecular hydrogen bonding and enable chemical modification of chitosan chains.[103] However, the robust hydrogen bonding between chitosan molecules renders its solubility in both water and organic solvents challenging, thereby restricting its practical utility. Modification of chitosan with MAA involves introducing methacrylic groups into the chitosan molecular chain, enabling light curing.[104] This modification results in chitosan methacrylate, which exists in solution form, possesses injectability and favorable physicochemical properties, and can be rapidly light-cured into a glue.[105] Another derivative, methacrylated carboxymethyl chitosan (CMCSMA), is obtained through the carboxymethyl substitution of active hydrogen on chitosan, retaining the excellent properties of chitosan, including its biocompatibility, biodegradability, and bioadhesion, while enhancing its water solubility.[134] Structurally, CMCSMA, in addition to its light-curing ability from the methacrylic group, contains abundant –COOH and $–NH_2$ groups, allowing for multifunctionalities through chemical modification. Chitosan methacrylate and CMCSMA biohydrogels retain the strong adhesion, good biocompatibility, and antimicrobial properties of chitosan, while also enhancing the versatility of the hydrogel base. This allows for mixing with other drugs or compounds, making them applicable in wound healing,[106–108] bone tissue engineering,[109,110] nerve repair,[111] and other biomedical applications.

Methacryloylated dextran: Glucans are homopolysaccharides composed of glucose connected by glycosidic bonds. The structure of dextran, a complex glucan, varies depending on the microbial species and growth conditions. Based on the type of glycosidic bond, glucans can be categorized into α- and β-glucans. β-glucan is more physiologically active and plays more roles than α-glucan.[112] Additionally, dextran can obtain multifunctional active derivatives through modification of the groups on its side chain. Based on these characteristics, dextran has been widely used in tissue repair,[113] wound dressings,[114] and drug delivery.[112] Compared with other polysaccharides, dextran is popular for its relative bioinertness, biodegradability, and modifiability. However, pure dextran hydrogels exhibit poor mechanical properties.[115] MAA has been utilized to introduce MA groups and generate dextran methacryloyl (DexMA), which can be photocrosslinked to improve its mechanical strength. DexMA is characterized by transparency, flexibility, excellent physical morphology, and high viscosity, as well as stable gel-forming properties

and good biocompatibility.[116] It also exhibits stable adhesive properties and retains biophilicity. In practical applications, DexMA is not only combined with other biopolymers to form macroporous scaffolds for drug delivery, but it is also made into hydrogel microneedles for subcutaneous release.[117,118] DexMA has also been utilized as a platform for angiogenesis and tissue repair.[118,119] In contrast to other derivatives, DexMA retains its beneficial properties in the crosslinked network and possesses tunable mechanical properties that facilitate the renewal and use of composite systems.

Sodium alginate methacrylate: Sodium alginate (Alg) possesses favorable characteristics such as good biocompatibility, stability, solubility, inertness, low cost, and ease of production.[120] Sodium Alg exhibits versatility and can be employed under both extreme and gentle conditions. It can readily form gels through chemical crosslinking. The gelation process under mild conditions is advantageous in preventing the inactivation of active substances.[121] However, the lower mechanical strength of sodium Alg crosslinked hydrogels limits their range of application.[122] Methacrylated sodium Alg (AlgMA) can greatly compensate for this shortcoming, as their crosslinking is highly versatile, and they exhibit good internal gel homogeneity. The introduction of methacrylate groups into AlgMA enables dual crosslinking, which enhances its mechanical properties. Tests revealed that at the same concentration, AlgMA hydrogel mesh scaffolds exhibited enhanced molding fidelity and mechanical strength compared with those of Alg hydrogels.[123,124] Currently, AlgMA is extensively used in the biomedical field as an effective scaffolding material for loading cells, drugs, or other active substances.[125,126]

Methacrylated chondroitin: Chondroitin sulfate (Chs) is a sulfated linear glycosaminoglycan widely distributed in mammalian cells and crucial for the function of the extracellular matrix methacrylate (ECMMA).[127] Chs is found in large quantities in tissues where it serves crucial physiological functions.[128] Chs is most commonly used in combination with glucosamine in the treatment of osteoarthritis.[129] Chs can regulate growth factors and promote injury healing.[130] It acts as a neuroprotective agent[131,132] and possesses anti-inflammatory, antioxidant,[133,134] and antitumor[133,135] activities. Incorporation of a methacrylate group into the molecular chain of Chs forms methacryloylated Chs (ChSMA) with light-curing capability. Utilizing a versatile crosslinking molding method and exhibiting excellent biocompatibility, ChSMA-based material systems have found extensive applications in various biomedical research areas, including serving as effective drug carriers.[136] ChSMA has displayed promise in osteoarthritis treatment,[137] cartilage and heart regeneration,[68] neurological repair,[138] and bone–tendon interface reconstruction.[139]

Methacrylated hyaluronic acid: Hyaluronic acid (HA) is the simplest glycosaminoglycan and a major component of ECM.[140] The chain length of HA can range from 0.200 to 10 MDa, with the most common size range being 2–5 MDa. HA is a scaffolding material secreted *in vivo* by cells and has good water retention and moisturizing properties. The distinctive characteristic of reduced viscosity under shear makes HA suitable as a lubricant. In static conditions, HA offers elasticity. Additionally, apart from creating a hydration space around cells, HA influences the transport of growth factors and other signals through its pore size and charge density. Hyaluronic acrylate methacrylate (HAMA) imparts HA with a light-curing ability. Due to their versatile molding method and good biocompatibility, HAMA-based materials have been used in many biomedical research areas, including chondrocyte and cartilage regeneration,[141,142] infection or diabetic wound repair,[143,144] anti-inflammation, antioxidative stress,[145] corneal reconstruction,[146] tumor modeling,[147] drug-controlled release,[148] biosensors,[149] and post-surgery anti-adhesion.[150]

3.2.3. Other substances

In addition to the natural proteins and polysaccharides mentioned above, numerous substances can be modified with MA groups. Theoretically, as long as a substance is rich in amino and hydroxyl groups, it can potentially incorporate the methacrylate group, thus acquiring photocurable properties. ECM is a natural scaffold prepared from a tissue or organ by removing cellular components and retaining the 3D structure and some natural fiber components of the tissue or organ. As the living environment of cells, it contains various proteins, polysaccharides, and a large number of bioactive factors. ECM can be potentially modified with MA. Growth factors are keys to the biological function of ECM. A study comparing ECM and ECMMA hydrogels revealed that most growth factors and cytokines were retained in ECMMA hydrogels.[151]

Liu et al. prepared polyamide-amine by introducing the MA group into the side chain of polyamides and prepared cartilage repair scaffolds by adding GelMA and ADSCs. The obtained hydrogel displayed sufficient potential for promoting cartilage regeneration.[152] In the study by Lim et al.,[153] a new type of biological resin was constructed by adding GelMA to polyvinyl alcohol polyvinyl methacrylate. Using a visible photoinitiator system that displays high Mohr absorbance, constructs with high-resolution features were bioprinted in the 25–50 μm range. Simaan-Yameen et al.[154] synthesized FibMA by methacrylation of

denatured fibrinogen using MA. Studies have reported that MAA does not alter the important biological properties of fibrinogen, including the ability to support cell adhesion, 3D cell culture, and proteolysis.[154]

4. Applications

4.1. Tissue engineering scaffolds

We summarize the application of various types of methacrylic anhydride hydrogel 3D printing scaffolds in biological tissue engineering in Table 3.

4.1.1. Skin trauma

The main focus in skin tissue engineering is the treatment of chronic ulcers, which are a leading cause of death worldwide.[155]. Chronic wounds are caused by hypoxia and lack of tissue nutrition, with pathogenic infections often being responsible for prolonged non-healing.[156] For example, impaired angiogenesis in patients with diabetes leads to reduced infiltration of inflammatory cells, while growth factors and elevated glucose levels make wounds more susceptible to infection.[185] Furthermore, severe injuries may cause impaired wound healing in the skin, with excessive and sustained myofibroblast activation further leading to scar tissue formation.[157] In summary, a more effective treatment for skin wound tissues is necessary.

Tissue-engineered scaffolds for skin healing should provide isolation and protection to the wound bed by exerting anti-inflammatory and anti-infection effects. Additionally, the scaffolds should promote vascularization, thereby accelerating skin tissue regeneration while concurrently inhibiting scar tissue formation. The bioengineering approach to skin regeneration primarily relies on the utilization of hydrogels and factors, such as vascular endothelial growth factor (VEGF) or stem cells of diverse origins, including human skin fibroblasts,[157] adipose-derived stem cells, and epidermal stem cells. These components are mixed to create bioinks for the formation of hydrogel scaffolds through a combination of extrusion and light-cured printing (Figure 5A). In a study by Chen et al., *in situ* printing on a whole skin incision mice model was achieved using a robot.[158] Multiple animal experiments have demonstrated that 3D scaffolds can attenuate inflammatory response, increase periwound blood perfusion, and promote re-epithelialization, collagen deposition and alignment, and angiogenesis, thereby facilitating wound regeneration. Moreover, the addition of skin-derived precursors (SKPs) printed in a hydrogel incorporating stem cells not only maintains their properties but also promotes their proliferation.[158] By printing the epidermis, dermis, and vascular network in layers, constructing a structure that approximates a full skin layer is made possible.[159] The regenerated skin contains the epidermis, dermis, blood vessels, hair follicles, and sebaceous glands similar to natural skin. These approaches provide an effective strategy for *in vitro* epidermal reconstruction.

4.1.2. Bone defects

Bone tissue consists of a mixture of living cells and minerals (mainly calcium and phosphorus) that provide support and protection. Due to the high mechanical properties that bone tissues possess, the biological replacement of large volumes of bone tissue is still limited to inorganic compounds. In addition to inorganic metallic materials, many organic materials have been used in clinical bone defect repair due to their superior biological properties. For example, synthetic hydroxyapatite (HAp), β-tricalcium phosphate (β-TCP), and their composites have been widely used in orthopedic reconstructive surgeries due to their similar composition to normal bone.[160] Polycaprolactone (PCL) scaffolds regulate cell proliferation and differentiation by promoting cellular senescence, cell cycle, and deoxyribonucleic acid replication pathways, accelerating osteogenesis, and healing tissue formation within cartilage. Bioceramic (e.g., β-TCP) scaffolds specifically enhance osteoclast differentiation and extracellular fluid pathway gene expression, promoting osteoclast differentiation and bone remodeling. During these processes, specific biomaterial properties can be used to direct cell behavior and regulate molecular networks in the symbiotic microenvironment, thus minimizing the existing regeneration and repair barriers.[161]

In recent years, efforts have been made to combine methacrylate-based hydrogels with biologically active and functionalized nanomaterials to enhance the physicochemical and biological properties of methacrylate-based hydrogels (Figure 5B). Currently, the mainstream application is to print 3D scaffolds with high mechanical properties, utilizing the aforementioned nanomaterials, and then apply surface coating[162] or fill the interior with[163] methacrylamide hydrogels. The benefits of this approach are as follows:

(i) Enhanced mechanical properties.[164,165]

(ii) Modulation of viscoelastic properties to allow 3D printing of bioinks.

(iii) Presentation of electro/magnetic properties to produce electro/magnetically active hydrogels for the repair of specific tissues (e.g., muscles, nerves). In particular, MXene exhibits a robust photothermal and sterile effect under infrared irradiation. In addition, GelMA/β-TCP/sodium alginate (Sr2+)/MXene (Ti3C2) (GTAM) scaffolds constructed in

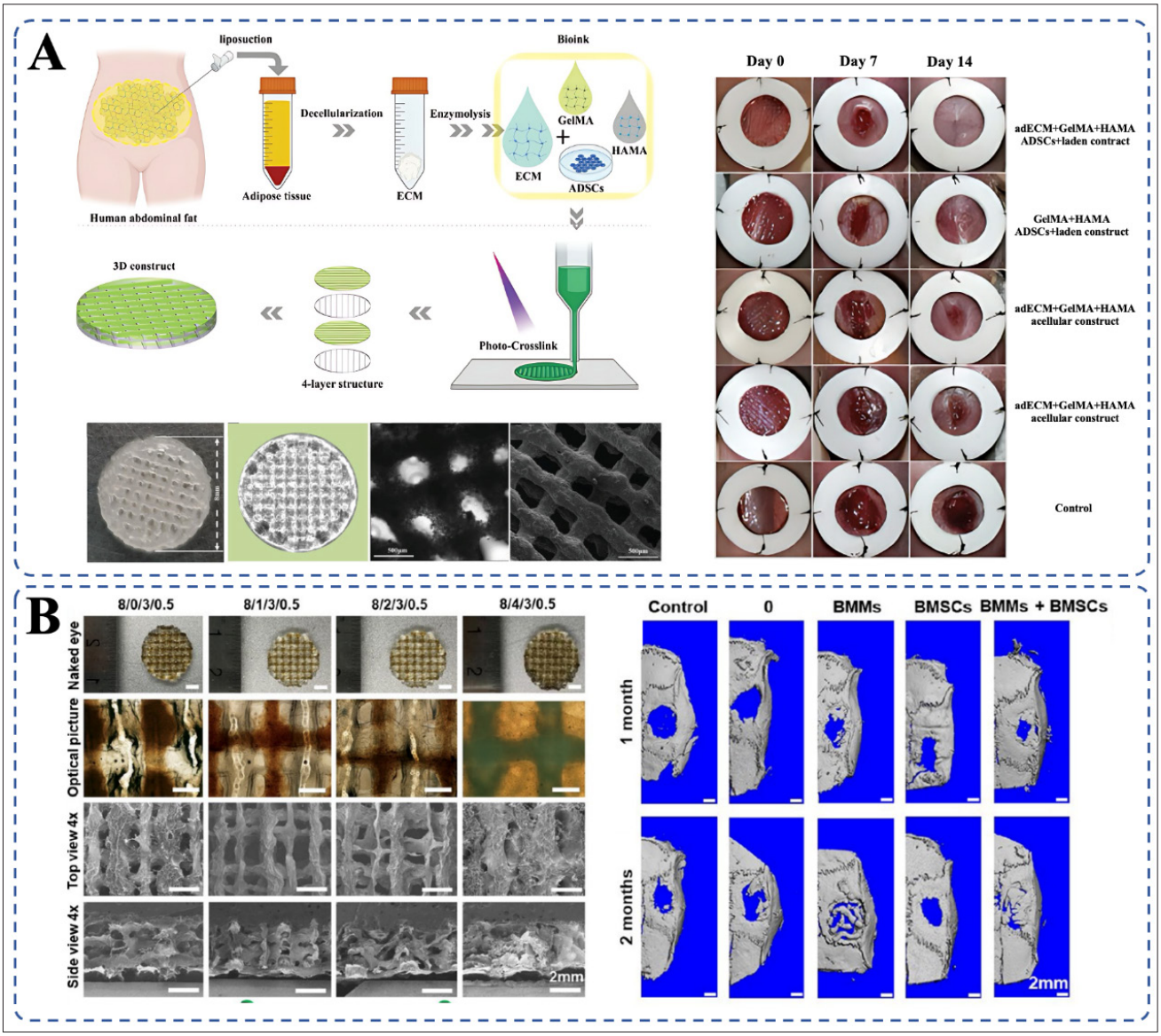

Figure 5. The application of bioink composed of GelMA and HAMA in wound healing and bone repair. (A) The adECM-GelMA-HAMA 3D-printed scaffold loaded with ADSCs can accelerate wound healing. Adapted with permission from Zhang et al.[173] (B) 3D-bioprinted GelMA-HAMA scaffolds encapsulated with rat bone marrow-derived macrophages (BMMs) and bone marrow mesenchymal stem cells (BMSCs) can promote bone repair. Adapted with permission from Yu et al.[174] Abbreviations: adECM, adipose derived extracellular matrix; ADSC, adipose-derived stem cell; GelMA, gelatin methacrylate; HAMA, hyaluronic acrylate methacrylate.

conjunction with GelMA have antimicrobial and osteogenic applications.[166]

(iv) Active delivery of therapeutic molecules, including HAp, MnCO, and desferrioxamine nanoparticles (DFO), to hinder osteoclast differentiation. The Fenton-like reaction between MnCO delivered by GelMA hydrogel and endogenous hydrogen peroxide generated at the implantation site triggers the sustained release of CO and Mn^{2+}. This process significantly reduces inflammatory responses by upregulating the macrophage M2 phenotype. Furthermore, DFO contributes to inflammation reduction by promoting the M2 phenotype of macrophages, thereby synergizing with it to promote vascularization and inhibit osteoclast differentiation.[166]

(v) Therapeutic capabilities, such as antioxidant effects, during tissue repair. 3D-printed GelMA-

g-glutathione scaffolds not only scavenge reactive oxygen species (ROS) by delivering glutathione, but also accelerate bone repair under diabetic conditions by activating the PI3K/Akt signaling pathway to promote osteoblast proliferation and differentiation.[167] Dutta et al. prepared polyphenolic carbon quantum dots (CQDs)-GelMA loaded with antitumor drugs (≈49%), which effectively killed osteosarcoma cells and treated bone defects caused by malignant osteosarcoma.[168]

(vi) Enhanced oxygen transport and erythrocyte development to improve angiogenesis, thereby stimulating tissue regeneration and reconstruction.[169]

(vii) Enhanced osteoblast proliferation and differentiation and mineral salt deposition. Specifically, strontium mesoporous bioactive glass nanoparticles (Sr-MBGNs)-GelMA bioscaffolds release Sr, Ca, and Si ions to enhance osteogenesis, angiogenesis, and immunomodulatory properties. They also regulate ECM reconstruction, promoting cellular adhesion through the activation of lysyl oxidase to form healthy, enzymatically crosslinked collagen, modulate osteoblast differentiation, and mimic biomineralization.[170] By loading and releasing parathyroid hormone (PTH), ultrastructural PCL/GelMA- methacryloylated SF (SilMA) scaffolds can repair bone defects by promoting angiogenesis and osteogenic processes.[171]

(viii) Inhibition of osteoclastogenesis.[172] In addition, more biosimilar-rich spatially distributed bioscaffolds can be constructed using coaxial 3D printing. Ghahri et al. utilized quadruple coaxial extrusion 3D bioprinting with polyethylene glycol as the hollowing agent. The layers mimicked blood vessels, VEGF, and bone, respectively. This approach improved osteoblast differentiation and increased mechanical modulus from 35 to 80 kPa.[164]

4.1.3. Cartilage defect

Due to the complexity of its tissue structure and the absence of blood vessels, nerves, and lymphatic vessels, osteochondral tissue regeneration is challenging.[175] The use of 3D printing enables the construction of a 3D biomimetic structure that mimics cartilage tissue (Figure 6A). By manipulating and adjusting the bioink during the 3D printing process and incorporating diverse cell types, active substances, drugs, and hormone-binding peptides, various induction pathways can be employed. This approach prompts chondrocyte proliferation and facilitates the generation of cartilage material (Figure 6B). Currently, the primary cells incorporated into bioinks consist of chondrocytes from different sources and stem cells with the potential for chondrocyte differentiation. The addition of ECM stroma or MA-based modified ECM stroma to bioink not only enhances its biocompatibility but also promotes chondrocyte maturation. This process can also make the printed 3D structures more viscous and elastic, with enhanced microfinesse[176,177] (Figure 6C). Furthermore, the addition of bioactive factors to bioinks can induce the chemotaxis and differentiation of chondrocyte stem cells. For example, transforming growth factor (TGF)-β1 is a potent chondrogenic cytokine and the most widely utilized biofactor for articular cartilage bioscaffold construction.[178,179] Incorporating platelet-derived growth factor-BB (PDGF-BB), chondro-inducing molecules (e.g., kartogenin [KGN],[175] interleukin [IL]-4,[180] bioglass [BG], and Mn^{2+} [181]), hormones,[182] drugs, and exosomes[183] to bioinks enables their continuous delivery through hydrogel constructs. These additions exert anti-inflammatory effects, contributing to the treatment of arthritic cartilage defects. Moreover, bioinks can carry various bioactive substances, such as platelet-rich plasma (PRP). A PRP-GelMA hydrogel was reported to be involved in macrophage immunomodulation and M1-M2 conversion, showcasing excellent properties for cartilage and subchondral bone repair.[184,185]

Methacrylic compounds provide robust crosslinking and mechanical properties for the construction of cartilage scaffolds with good biocompatibility. Methacryloyl anhydride-based compounds can be constructed with good fineness, fidelity, and biocompatibility for cartilage tissues, including ear and nasal cartilages,[51,76,176] providing a novel source of biostructures for otoplasty and rhinoplasty, which typically use rib cartilage. The most significant challenge in this process is to ensure the good mechanical properties of the bioscaffold. Cartilage is structurally composed of several regions (superficial, transitional, intermediate, and calcified) from superficial to deep. The compression modulus of the layers in a gradient scaffold increases gradually from the topmost layer 3 to the bottom layer 1, forming a gradient structure. The compressive modulus of the superficial and deeper layers is 1–7 MPa, and articular cartilage should ideally have a compressive modulus of 10 MPa.[186] To mimic the realistic structure of cartilage, a layered printing approach is often employed in studies. The bottom layer is simulated using a bioink with good mechanical properties, whereas the middle or top layer utilizes an ink with similar characteristics (cell recruitment and differentiation-inducing biofactors).[187,188] Alternatively, bioinks with anti-inflammatory properties, such as HAMA, can be directly applied.[189]

Currently, the main bioinks utilized are based on GelMA and HAMA; the addition of HAMA to GelMA improves cartilage formation compared with GelMA alone

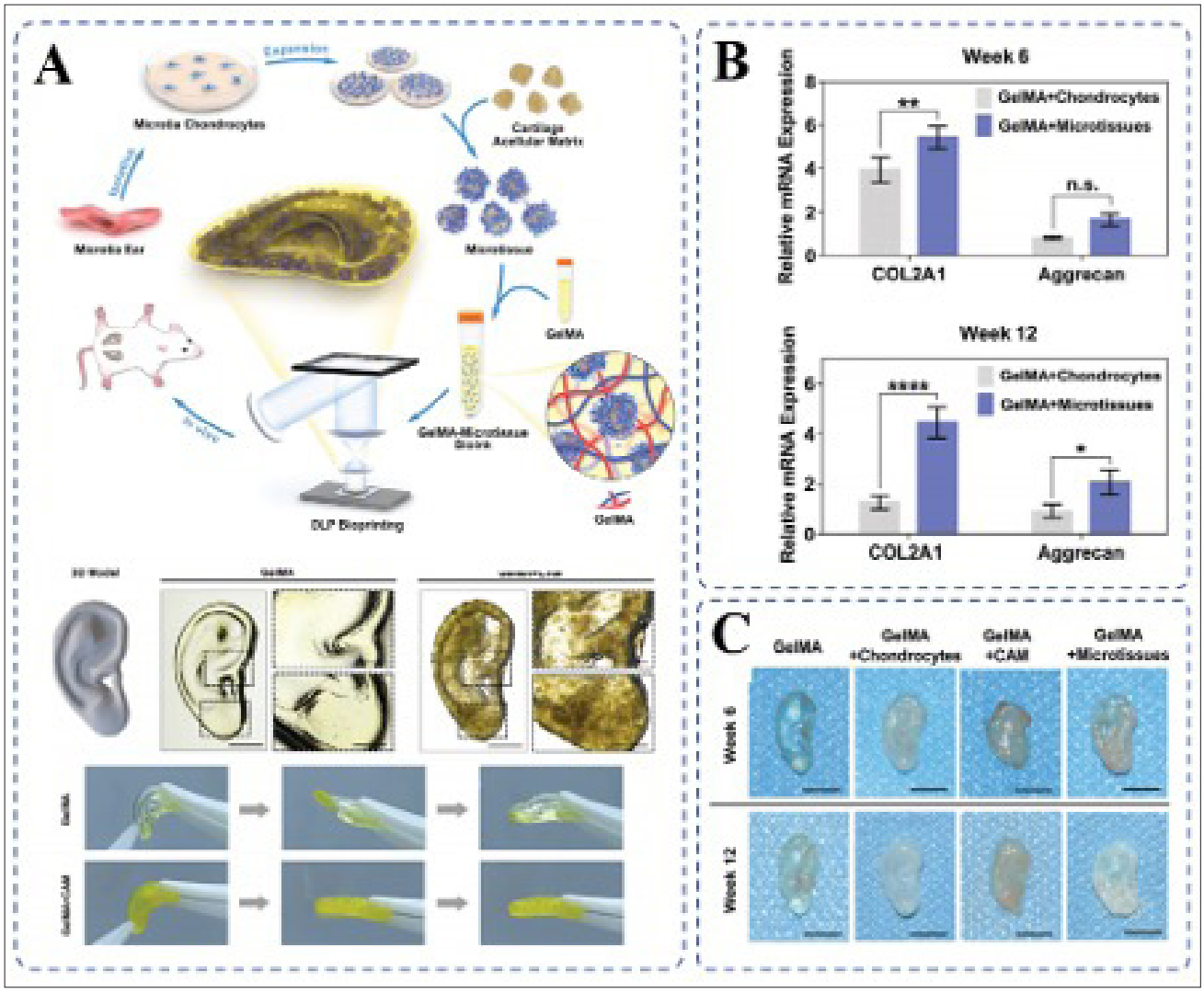

Figure 6. GelMA can be used as bioink to print ear-shape 3D scaffolds with good performance. (A) The bioink was prepared by mixing microtia chondrocytes and cartilage acellular matrix (CAM) with GelMA solution, printed to the auricular shape by a DLP-based 3D bioprinter. The printed auricular scaffold displayed flexibility. (B) The mRNA expression analysis of chondrocytes in auricular constructs at weeks 6 and 12 revealed good biocompatibility of the 3D-printed scaffolds. (C) Images of *in vivo* constructs at weeks 6 and 12 demonstrate the stability of the 3D-printed scaffolds. Adapted with permission from Xie et al.[176] Abbreviations: DLP, digital light processing; GelMA, gelatin methacrylate.

(15%).[190] However, their physical and biological properties need improvement, which is often achieved by blending the hydrogel with other more durable, less hydrophilic polymers.[191] Research suggests that the addition of polyesters (PCL,[76] PEDGA,[178,186,192] poly(propyleneglycolide)-glycolide[193]), bacterial nanocellulose (BNC), and HAp[187,188] to the original methacryloyl anhydride-based hydrogels increase the mechanical strength to better simulate the complex structure of osteochondral tissue. Furthermore, Xia et al. utilized GelMA with HAMA to develop a lyophilized hydrogel preparation method, which further increased the mechanical strength of 3D-printed hydrogels and reduced their degradation rate to match cartilage regeneration.[194]

Moreover, Wang et al. utilized electrostatically spun polylactic acid (PLA) staple fibers, ammonolyzed them to generate PLA crushed microfibers, and incorporated them into oxidized Alg and GelMA bioinks. The inclusion of polylactic acid (PLA) staple fibers improved printing fidelity and resulted in structures with higher mechanical strength. By optimizing the bioink composition, constructs with a compressive stress of approximately 150 kPa were obtained even after 100 cycles of compressive loading (up to 40% strain). This mechanically enhanced

sodium Alg/gel dual network bioink demonstrated good biocompatibility and supported *in vitro* BMSC cartilage formation.[195] These findings suggested that this method is capable of printing engineered grafts with irregular sizes and mechanical properties similar to cartilage, making it a promising approach for functional tissue regeneration.

4.1.4. Skeletal muscle defects

The muscle is one of the few organs that maintains the lifelong ability to regenerate. However, when a large portion of muscle mass is lost due to trauma, disease, or surgical ablation, the natural regenerative capacity of the muscle is overwhelmed. Conversely, when skeletal muscle heals excessively, active fibrosis can lead to volumetric muscle loss, resulting in scar tissue formation. The primary goal of tissue engineering for skeletal muscle repair is to promote myocyte survival and alignment and functional reconstruction of myofibers. Currently, the most utilized hydrogel for tissue engineering reconstruction of skeletal muscle defects is GelMA, followed by AlgMA[196] and SilMA.[197] Using 3D-printing technology, cell-containing GelMA constructs were processed with a functional nozzle featuring topographical cues and an optic-fiber-assisted bioprinting process, which induced the uniaxial alignment of C2C12 and human ASCs. A significantly higher degree of cellular alignment and myogenic activity was observed in cell-loaded GelMA structures compared with cellular constructs printed using conventional crosslinking methods.[198] The GelMA constructs were printed in a light-responsive hydrogel. In addition, by adding iron oxide to the photo-responsive hydrogel, the cells in the hydrogel were mechanically stretched in a 3D manner using a magnetic bioreactor to ensure that cell differentiation could mimic the 3D human environment. The magnetic bioreactor system promoted the differentiation of mouse adult myoblasts in the hydrogel by increasing the diameter and length of myotubes.[197] By incorporating gold nanoparticles (AuNPs)/2D transition metal carbides (MXene nanosheets), which led to an increase in the electrical conductivity of GelMA (up to 0.8 ± 0.07 and 0.9 ± 0.12 S/m, respectively), an enhancement in the differentiation ability of encapsulated adult myoblasts was observed that enabled the printing of a highly viable (97%) stable construct.[199]

4.1.5. Spinal cord repair

Due to the poor self-regeneration ability of damaged neurons, no effective treatments are currently available for neurological impairments. With the in-depth development of stem cell therapy, NSCs, with their self-renewal ability and potential to differentiate into various neural cells, have become ideal candidates for spinal cord injury repair. Bioengineered spinal cord-like scaffolds with microchannel structures are prepared using 3D bioprinting technology. Different types of neural progenitor cells are precisely placed in the scaffolds, which can promote the regeneration and functional reconstruction of the spinal cord. In addition to low cell survival, transplanted NSCs often tend to differentiate into glial cells rather than neurons in the complex pathological microenvironment of spinal cord injury, which is another major cause of nerve regeneration failure.[200] Therefore, a substantial increase in the survival rate and neuronal differentiation of transplanted NSCs is necessary for the effective treatment of spinal cord injury.

Many bioscaffolds have been investigated for therapeutic effects using a wide range of nerve injury models. These bioscaffolds are neuroprotective, promote repair, reduce injury volume, and improve functional recovery in animal models; however, many challenges remain before they can be routinely applied in clinical practice. One of the most pressing challenges is the fabrication of 3D scaffolds capable of maintaining the survival and guiding the proliferation, functional differentiation, and transplantation of replacement or supportive cells.[201] OSMI-4, acrylic β-cyclodextrin (Ac-β-CD), and GelMA bioscaffolds constructed using GelMA significantly enhanced intrinsic neuronal differentiation of neural stem cells by inhibiting Notch signaling through sustained delivery of OsMI-4. This promoted neuronal regeneration and axon growth in a spinal cord injury rat model, leading to significant motor recovery.[202] PCL-GelMA-Alg builds EBs that give rise to neural progenitor cells, which are responsive to morphogenic factors and can differentiate into different neuronal identities. PCL scaffolds constructed using 3D printing technology displayed a regular tubular structure consisting of two concentric cylinders in micro-computed tomography (μCT) images. To enable the availability of oxygen and nutrients for the cells within the hydrogel cylinder supply, the internal PCL cylinder was printed as a macroporous structure. Macropores were generated on the cylinder surface by printing specific patterns of discontinuous and continuous PCL layers, with the well-organized biopores promoting cell migration, adhesion, and proliferation.[203]

4.1.6. Respiratory system

Tissue engineering for the heart has focused on myocardial tissue and heart valves, and to a lesser extent on coronary arteries.[204] The myocardial layer of the heart is a complex 3D laminar myofibrillar tissue containing multiple cardiomyocytes and collagen fibers that gradually shift in the direction of their transmural depth, contributing to the unique cardiac biomechanical behavior. Ischemic damage to the myocardium leads to cardiomyocyte death, with the limited regenerative capacity of cardiomyocytes resulting in scar tissue formation. Cardiac scar tissue, once formed,

persists for a lifetime, reducing the pumping ability of the heart and increasing stress on the remaining myocardium. 3D printing with MA-based compounds aims to create a cardiac patch or mesh tissue with specific mechanical strength, electrical conductivity, and the ability to support cardiomyocytes, human cardiac progenitor cells, and human-induced multifunctional stem cells.[205,206] Currently, two main methods for increasing and maintaining cell viability exist; one is the simultaneous use of biocompatible substances, such as ECM[205] and methacryloyl-substituted recombinant human parasomatic elastin (MeTro),[207] and methacryloyl anhydride-based compounds in one bioink.

Moreover, the oxygen concentration of hydrogels can be enhanced through low-intensity pulsed ultrasound (LIPUS) irradiation, effectively increasing hydrogel permeability and facilitating substance exchange in a non-invasive manner. Ultrasound-controlled release of oxygen, achieved through LIPUS, reportedly improved the viability of transplanted cells and expedited the repair of infarcted tissues.[207,208] In 3D structures created from microsphere tissues using calcium peroxide and IL-10-containing GelMA, microspheres could sustain oxygen availability to support cell viability in hypoxic environments for at least five days, concurrently modulating the macrophage M2 phenotype to exert an anti-inflammatory effect (Figure 7).[209] Functional tissue-engineered heart valves have

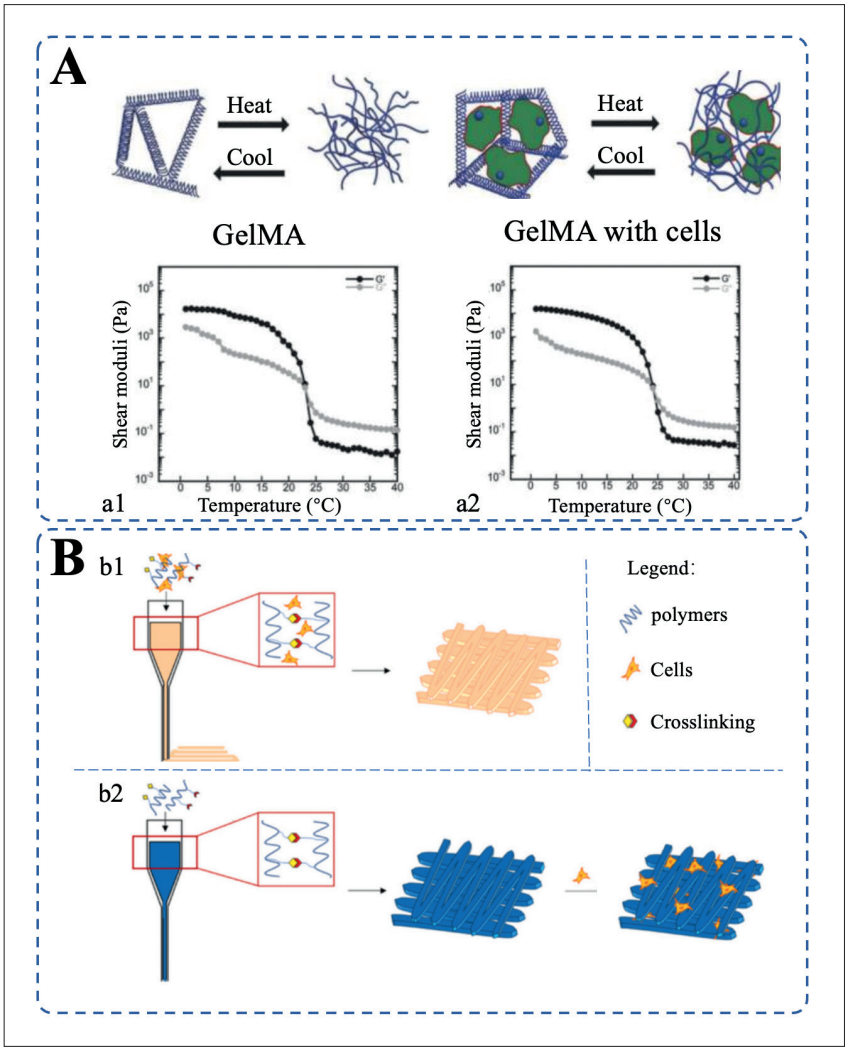

Figure 7. XXX. (A) A 3D-bioprinted scaffold printed from a silk-based bioink comprising non-mulberry silk fibroin (nSF), polyethylene glycol dimethacrylate (PEGDMA), gelatin methacrylate (GelMA), and carbon nanotubes (CNTs). (B) DNA content quantification and live dead assay of human umbilical vein endothelial cell (HUVECs) survival. (C) Beating signal of neonatal rat cardiomyocytes on the 3D-bioprinted scaffold. (D) *In vivo* immune-compatibility assessment of conductive 3D-printed constructs indicates the presence of macrophages and the formation of new blood vessels in the implants. Adapted with permission from Mehrotra et al.[209] Abbreviations: CPO, calcium peroxide; HRP, horseradish; HT, host tissue; IC, implanted construct.

been an elusive goal for approximately 30 years. Among the ongoing challenges is the requirement that engineered valve leaflets have nonlinear elastic tissue biomechanical properties, support a quiescent fibroblast phenotype, and resist calcification.[210] Scaffolds constructed using PCL-MAA with GelMA and polyethylene glycol diacrylate not only withstood the flow and pressure conditions of the aortic valve but also maintained and promoted cell viability in the spongiosum/ventricular layer and increased type I collagen production.[211] These results are summarized in Table 3. Notably, cells cultured on TEMPO-modified nanocrystalline cellulose (mNCC)-GelMA scaffolds demonstrated resistance to calcification.[210]

4.1.7. Pancreas

3D liver bioprinting is a promising technique for creating 3D liver models that can be used for *in vitro* drug testing, hepatotoxicity studies, and transplantation. Several 3D-printed MA-based bioinks, such as incorporating hepatocytes, primary human hepatocytes, and hepatic stellate cells utilizing ColMA\thioHA, have been utilized in liver tissue engineering; these bioinks maintain cell viability for more than 2 weeks and can respond to appropriate drug (acetaminophen) treatment.[212] Moreover, bioinks utilizing GelMA and antioxidant mixtures of vitamin C and vitamin E demonstrated improved cell–cell interactions and liver-specific functions, such as albumin and urea secretion, which were increased by 5- and 2.5-folds, respectively.[213] By utilizing GelMA with liver decellularized ECM (dECM) via DLP, a novel liver microtissue with an endodentate structure was constructed to achieve a larger body surface area for improved recovery of liver functions.[214] In 3D structures printed with bioinks constructed using Alg (1%), cellulose nanocrystals (CNC) (3%), and GelMA (5%), a clear cell migration was observed: fibroblasts colonized the hard 135ACG matrix and aligned themselves at the 135ACG/GelMA border due to chemotaxis, whereas HepG2 only formed spheres in the soft GelMA matrix.[215]

4.2. Bioactive factor loading

By loading hydrogels with various bioactive factors, not only the functionality of the scaffold can be increased, but also the acting time of these substances can be prolonged. These bioactive factors are summarized in Table 4.

4.2.1. Growth factors

Cytokines are a class of small or low-molecular-weight proteins that transmit information between cells and exert immunoregulatory and effector functions. Their levels in the body are low; as they are stimulants (immunogens, mitogens, or other), they can induce cells to produce low-molecular-weight soluble proteins (polypeptides), which can regulate intrinsic and adaptive immunity, promote the generation and growth of blood cells, and repair damaged tissues among other functions. Cytokines can be divided into IL, interferons, tumor necrosis factor, colony-stimulating factor, growth factors, and chemotactic cytokines.

Adding growth factors to 3D-printed hydrogel scaffolds, either by mixing them in bioink or adhering them to the surface of the final scaffolds, can promote cell growth and migration. For instance, GelMA combined with VEGF reportedly promoted wound healing, collagen deposition, and angiogenesis.[216] The addition of epidermal growth factor (EGF) to GelMA-SilMA promoted wound healing in the epidermis and dermis and enhanced the proliferation of keratinocytes and fibroblasts.[273] The addition of insulin-like growth factor-I (IGF-1) to GelMA promoted myoblast alignment and differentiation into myotubes, with the synthesized microfluidic-assisted polymer particles exhibiting successful adsorption and sustained release of IGF-1 at physiological pH for at least 21 days.[274] Regarding TGFs, the sustained release of TGF-β1[219] and TGF-β3[175] from the scaffold successfully directed the migration and differentiation of endogenous stem/progenitor cells. Short peptide cell regulatory protein-10, a TGF-β1 analog, along with KGN, promotes endogenous stem/progenitor cell migration and differentiation by upregulating the expression of RUNX1 and SOX9 at both the mRNA and protein levels.[275] IL-4[276] and IL-10[209] exert their functions in 3D-printed scaffolds primarily by modulating inflammatory responses, while also mediating the conversion of macrophages from a proinflammatory M1 phenotype to an anti-inflammatory M2 phenotype for immunomodulation.

4.2.2. Drug delivery

The physical properties of hydrogels are favorable for drug delivery, as they enable the sustained release of encapsulated drugs. Hydrogels are capable of maintaining high localized drug concentrations over long periods of time through appropriate release mechanisms, which can be based on diffusion, swelling, chemical, or other environmental stimuli. The macrostructure, microstructure (e.g., porosity), and degree of polymer crosslinking of a hydrogel affect its lattice pore size, while the hydrodynamic diameter and number of lattices in a hydrogel affect the degree of drug movement. The mechanism of drug release from hydrogels is ultimately regulated by the grid size. A drug with a smaller relative grid size can diffuse rapidly through the hydrogel, resulting in a shorter drug release time. When the size of the drug is close to the grid size, the drug release slows down significantly; when it is larger than the grid size, the drug is physically encapsulated in the grid. Constructing hydrogel scaffolds through 3D printing not only enables the precise control of scaffold dimensions and

Table 3. Application of 3D-printed methacrylic anhydride (MA) hydrogel in tissue engineering

Tissue type	MA-based biomaterials	Biological factor	3D printing method	Light curing parameters	Animal models	Effects	Ref.
Skin	GelMA	HdFs	Extrusion 3D printing	405 nm UV light for 3 min	-	Promotes the activity of healthy fibroblasts; inhibits myofibroblast activation to accelerate healing and reduce scar regeneration	[157]
	GelMA, HAMA, adECM	ADSCs	Extrusion 3D printing	405 nm UV light for 3–5 s	Mouse total skin excision model	Promotes faster neoangiogenesis, collagen production, and remodeling to accelerate wound healing	[173]
	GelMA	Epi-SCs	Extrusion, robot-assisted *in situ* printing	405 nm UV light for 10–30 s	Mouse total skin excision model	Supports SKP proliferation and maintains their properties; promotes wound healing and functional tissue skin regeneration	[158]
	GelMA, ADM	Fibroblasts, HUVECs	Extrusion 3D printing	Blue light for 30 s	Mouse total skin excision model	Promotes cell viability and proliferation and supports *in vitro* epidermal reconstruction	[159]
	GelMA	VEGF	Extrusion 3D printing	365 nm UV light for 5 min	Porcine skin wound model	Promotes wound healing, collagen deposition, and angiogenesis	[216]
Cartilage	GelMA	PRP	DLP	405 nm visible light at 30 mW/cm^2 for 30 s	Rabbit cartilage defect model	Promotes migration, osteogenic, and chondrogenic differentiation of bone marrow MSCs	[184]
	GelMA	ECM, MSCs, exosomes	DLP	405 nm visible light at 11 mW/cm^2 for 30 s	Rabbit cartilage defect model	Repairs chondrocyte mitochondrial dysfunction; enhances chondrocyte migration	[183]
	GelMA, ACMMA	dECM, auricular chondrocytes	Extrusion 3D printing	405 nm UV light at 20 mW/cm^2 for 10 s	Subcutaneous transplantation in nude mice	Microporous lugs with precise shapes and satisfactory mechanical strength	[51]
	GelMA, HAMA	Meniscus ECMMA MECM, PDGF-BB, KGN	Extrusion 3D printing	405 nm blue light at 90 mW/cm^2 for 30 s	Medial meniscus defect model in rabbit knee joint	Promotes chondrocyte migration and differentiation	[175]
	GelMA, HAMA	Chondrocytes	DLP	385–405 nm blue light for 30 s	-	Promotes chondrocyte differentiation	[217]
	GelMA, alginate	Chondrocytes	Extrusion 3D printing	-	Subcutaneous transplantation in nude mice	Promotes sustained release of nutrients and medications	[218]
	GelMA-PLA SFs, OMA	BMSCs	Extrusion 3D printing	365 nm UV light at 10 mW/cm^2 for 1 min	-	Printed structures have high mechanical strength and good biocompatibility	[195]
	GelMA, alginate	TGF-β1, chondrocytes	Extrusion 3D printing	365 nm UV light at 7 mW/cm^2 for 15 s	Subcutaneous transplantation in nude mice	Promotes chondrocyte differentiation into cartilage	[218]

(Continue...)

Table 3. Continue...

Tissue type	MA-based biomaterials	Biological factor	3D printing method	Light curing parameters	Animal models	Effects	Ref.
Cartilage	GelMA, CAM	Microtia chondrocytes	DLP	365 nm UV light at 14 mW/cm^2 for 35 s	Subcutaneous transplantation in nude mice	Auricular structures with high elasticity, high printing precision, and low swelling rate	[176]
	PACG, GelMA	Mn^{2+}, BG	Inkjet printing	-	Rat cartilage defect model	Promotes cell attachment and spreading; enhances gene expression for chondrocyte- and osteogenic-related differentiation of human bone marrow stem cells	[181]
	GelMA, HAMA, ChSMA	TGF-β1, synovial-derived MSCs	Extrusion 3D printing	405 nm blue light for 60 s	Rat model of patellar notch osteochondral defects	With good shape fidelity, it improves the biological properties and cartilage formation of synovial-derived MSCs	[219]
	GelMA	BNC	Extrusion 3D printing	405 nm UV source at 30 mW/cm^2 for 10 s	Subcutaneous transplantation in nude mice	Facilitates the secretion of GAG from regenerated cartilage; improves biomechanical properties.	[219]
	GelMA	PRP, adipose tissue-derived MSCs	Extrusion 3D printing	300–500 nm UV light at 200 mW/cm^2	-	Increases glycosaminoglycan and calcium content, mineralization, and ECM production; promotes *in vitro* osteochondral tissue formation	[185]
	GelMA	Chondrocytes	Extrusion 3D printing	405 nm UV light for 90 s	-	Promotes human chondrocyte proliferation and expression of markers related to chondrogenesis	[220]
	GelMA, PEGMA	BMSCs	Extrusion 3D printing	-	-	Supports the development of more fibrocartilage-like tissue	[221]
	GelMA, PEGDA, ChSMA	BMSCs	Extrusion 3D printing	405 nm blue light at 30 mW/cm^2 for 30 s	-	Promotes differentiation, proliferation, and extracellular mesenchymal production of bone marrow MSCs	[193]
	GelMA, PCL	Chondrocytes	Extrusion 3D printing	UV light for 20 s	-	Construction of new cartilage with mechanical properties similar to nasal cartilage	[76]
	GelMA, PEGDA, RNTK	ADSCs	DLP	355 nm UV light	-	Promotes cell growth, differentiation, and proliferation; promotes collagen II, glycosaminoglycan, and total collagen synthesis	[192]
	GelMA	ADSCs, aptamer HM69 and TGF-β3	Extrusion 3D printing	-	Rabbit femoral synovial osteochondral defect model	Recruited MSCs promote cell adhesion and proliferation, and cartilage formation	[222]

(Continue...)

Table 3. Continue...

Tissue type	MA-based biomaterials	Biological factor	3D printing method	Light curing parameters	Animal models	Effects	Ref.
Cartilage	GelMA, HAMA	Chondrocytes	Extrusion 3D printing	405 nm UV light at 30 mW /cm^2 for 4 s	Subcutaneous transplantation in nude mice	Lyophilization further improved the mechanical strength of the 3D-printed hydrogel and reduced its degradation rate	[194]
	GelMA	Human BMSCs	Extrusion 3D printing	365 nm UV light at 200 mW/cm^2 for 60 s	-	Microspheres are capable of randomly assembling into large tissues, which form dense large tissues after 72 h of incubation	[223]
	GelMA, HAMA	Human chondrocytes	Extrusion 3D printing	405 nm UV light at 300 mW/cm^2	-	Addition of HAMA to GelMA improves cartilage formation over GelMA alone (15%)	[223]
	GelMA	MSCs, TGF-β1 binding peptide, Hap	Extrusion 3D printing	-	Osteochondral defect model of rat femoral talus	Promotes chondrogenesis; induces cartilage (repair and formation) better without triggering significant inflammatory responses	[187]
	GelMA, alginate	Chondrocytes,	DLP	365 nm UV light for 120 s	-	Improves the scaffolds' mechanical properties	[186]
	Functionalized alginate, GelMA	BMSCs	Extrusion 3D printing	365 nm UV light at 5 mW/cm^2 for 15 min	-	Promoted robust cartilage formation; increases stiffness while maintaining elasticity and toughness	[224]
	GelMA-PEGDA	MSCs	DLP	-	-	Promotes the differentiation of embedded MSCs to chondrocytes	[178]
	GelMA	-	Extrusion 3D printing	UV light at 0.09 mW/cm^2 for 1 min	Chinchilla ear tympanic membrane defect model	Promotes cell invasion and proliferation	[225]
	GelMA	$CaCO_3$ granules, TGFβ1, human meniscal chondrocytes	DLP	UV light at 50 mW/cm^2 for 8 s	Longitudinal tears in human meniscus slices	Produces an organized cellular arrangement that promotes meniscus-like tissue formation	[179]
	GelMA, SFMA	PTH, Acs articular chondrocytes, BMSCs	Extrusion 3D printing	405 nm blue light for 10 s	Rabbit osteoarticular defect model	Inhibition of chondrocyte hypertrophy favors hyaline chondrocyte ECMMA production	[182]
	SilMA	Human chondrocytes	DLP	365 nm UV light for 5 s	Subcutaneous transplantation in nude mice	Ensures cell viability; promotes proliferation and differentiation	[226]

(Continue...)

Table 3. Continue...

Tissue type	MA-based biomaterials	Biological factor	3D printing method	Light curing parameters	Animal models	Effects	Ref.
Cartilage	SilMA, PEGDA	Porcine chondrocytes	Extrusion 3D printing	405 nm blue light at 1000 mW for 20 s	-	Expression of collagen II and aggregated proteoglycans is consistent with the formation of cartilage tissue	[227]
	HAMA, PCL	BMSCs	Extrusion 3D printing	-	Medial meniscectomy-induced osteoarthritis animal model	BMSCs in scaffolds survive and proliferate; BMSC-loaded brace significantly improved the joint function of the injured lower leg	[189]
	ECMMA	Rabbit ear chondrocyte	Extrusion 3D printing	UV light at 200 mW/cm^2 for 2 min	-	Promotes cell proliferation and generation of cartilage tissue	[228]
	AlgMA, PCL	BMSCs	Extrusion 3D printing	405 nm blue light for 30 s	-	Good cell survival, proliferation, morphology, type II collagen deposition, and differentiation into cartilage	[229]
	ChsMA	Chondrocytes	Extrusion 3D printing	UV light at 103 mW/cm^2 for 3 s	-	Promotes cell proliferation	[230]
	HAMA	-	Robot-assisted in-situ printing	-	Rabbit talipes cartilage defect model	Bioink can properly fill the defective area and repair cartilage damage after 12 weeks	[231]
	HAMA, ChsMA	Bovine chondrocytes	Extrusion 3D printing	365 nm UV light at 6.09 mW/cm^2 for 10 s	-	Promotes cell proliferation	[232]
Bone	PLA, HAp, GelMA	MnCO, deferoxamine NPs	FDM	365 nm UV light for 5.5 h	Rat femoral defect model	Scaffold with strong immunomodulation and angiogenesis, weak osteoclastogenesis, and superior osteogenic capacity	[233]
	GelMA, HA	Rat BMSCs, β-TCP, Sr^{2+}, MXene	Extrusion 3D printing	405 nm UV light	Chronic osteomyelitis model of rat jawbone	Promotes infection healing and bone regeneration	[166]
	GelMA, HAMA	BMMs, BMSCs	Extrusion 3D printing	405 nm blue light at 0.5 W/cm^2	Rat cranial defect model	Promotes M2-type polarization of macrophages in the microenvironment of early bone defects and further promotes bone repair	[174]
	GelMA, PEGDA, Fullon f 127 bis-acrylate F127DA	Mouse embryonic osteoblast precursor cells, rabbit BMSCs	DLP	405 nm blue light at 20 mW/cm^2 for 4 s	Rabbit femoral condylar defect model	Effective promotion of osteogenic differentiation of BMSCs	[234]
	GelMA	Rabbit BMSCs	Extrusion 3D printing	UV light at 365 nm	/	Promotes cell growth to support and effectively maintain the osteogenic process	[235]

(Continue...)

doi: 10.36922/ijb.4650

Table 3. Continue...

Tissue type	MA-based biomaterials	Biological factor	3D printing method	Light curing parameters	Animal models	Effects	Ref.
Bone	GelMA	DFO	Extrusion 3D printing	405 nm blue light for 120 s	Rat cranial defect model	Significantly promotes endothelial cell migration and tube formation, mineralized matrix deposition, and ALP expression in osteoblasts	[236]
	GelMA/PCL	BMSC ST2	FDM	405 nm blue light for 5 s	Rat cranial defect model	Promotes cell proliferation, osteogenic differentiation, and mineralization of ST2 in *in vitro* scaffold, enhancing angiogenesis and osteogenesis	[237]
	Ti-6Al-4V alloy, GelMA	BMSCs	SLS	UV light at 7.1 mW/cm^2 for 80 s	Rabbit radial bone defect model	Promotes osteogenesis and angiogenesis	[163]
	Graphene, GelMA	BMSCs	Extrusion 3D printing	405 nm blue light for 60 s	Subcutaneous transplantation in nude mice	Promotes synergistic regeneration of nerves and bone	[238]
	GelMA, PEGDA, poly aluminum silicate	HUVECs	Extrusion 3D printing	-	Rat cranial defect model	Promotes angiogenesis and osteogenesis	[239]
	GelMA	Graphene oxide, MSCs	Extrusion 3D printing	UV light for 30 s	-	Enhances cell proliferation and adhesion, and osteogenic differentiation properties	[240]
	PLA, GelMA	MSCs	FDM	-	-	Promotes osteoblast differentiation	[241]
	nHAp, GelMA	BMSCs	Extrusion 3D printing	405 nm	Subcutaneous grafting in nude mice/rabbit cranial defect model	Initiates early osteogenesis and angiogenesis by recruiting endogenous stem cells *in situ*	[242]
	Alginate, C3S, GelMA	MSCs	Extrusion 3D printing	365 nm irradiation for 4 min	-	Promotes cell adhesion, spreading, proliferation, and osteogenic differentiation while possessing good mechanical qualities	[162]
	GelMA	MC3T3-E1, glutathione	Extrusion 3D printing	UV light at 405 nm for 30 s	Rat cranial defect model	Clears ROS; promotes osteoblast proliferation and differentiation for bone repair in diabetes	[167]
	GelMA, HAp	BMSCs	Extrusion 3D printing	410 nm blue light for 1 min	Rabbit cranial defect	Promotes BMSC migration, proliferation, and osteogenic differentiation *in vitro*; promotes targeted migration of endogenous stem cells, early osteogenesis, and angiogenesis	[243]

(Continue...)

doi: 10.36922/ijb.4650

Table 3. Continue...

Tissue type	MA-based biomaterials	Biological factor	3D printing method	Light curing parameters	Animal models	Effects	Ref.
Bone	PL/GelMA/BCP	HUVECs	DLP	UV light at 405 nm for 30 s	Subcutaneous implantation on the back of rats	Regulates cell behavior and promotes the formation of vascular-like structures	[169]
	GelMA-HM5, GelMA-HZ5 (Mg/Zn-modified HAp)	-	Extrusion 3D printing	UV light at 360 nm for 5 min	-	Supports the bone	[244]
	GelMA, SilMA, GelDA, graphene oxide	BMSCs	Extrusion 3D printing	UV light at 405 nm for 2 min.	Rat cranial defect model	Effectively promotes osteogenesis *in vitro* and *in vivo*	[245]
	GelMA, Laponite	BMSCs	Extrusion 3D printing	UV light at 100 mW/cm^2 for 5 min.	-	Promotes cell proliferation and osteogenic differentiation	[246]
	GelMA, dECM	DFCs	Extrusion 3D printing	405 nm UV light for 30 s	Rat subcutaneous graft, Beagle mutt alveolar fossa bone defect model	Promotes regeneration of periodontal tissues, especially anchoring structures at the bone–ligament interface	[247]
	GelMA, BP	BP cells	Extrusion 3D printing	405 nm UV light for 1 min	-	Ensures cell migration and colonization	[248]
	Mg-PCL-GelMA	MSCs	FDM	405 nm UV light at 30 mW/cm^2 for 3 min.	-	Enhances osteogenic differentiation of encapsulated MSCs; supports bone ECM deposition; promotes mineralized nodule formation, OCN, and Col I expression	[249]
	Polyphenol CQDs, GelMA	MG-63 cells	Extrusion 3D printing	365 nm	Rat cranial defect model	Promotes angiogenesis, bone regeneration, and anti-tumor	[250]
	Sr-MBGNs, GelMA	BMSCs	Extrusion 3D printing	-	Rat cranial defect model	Releases Sr, Ca, and Si ions to enhance osteogenesis, angiogenesis, and immunomodulatory properties; promotes cell adhesion and regulates osteoblast differentiation	[170]
	MSNcapDex, GelMA	Human BMSCs	Extrusion 3D printing	UV light at 0.86 mW/cm^2 for 5 min	-	Cells survived and exhibited osteogenic differentiation biomarkers	[251]
	Nifedipine-containing alcohol plasmas and tumblestone, sodium alginate, GelMA	BMSCs	Extrusion 3D printing	405 nm	Rat cranial defect model	Promoted osteogenic differentiation and migration of bone marrow MSCs; inhibits osteoclastogenesis *in vitro*	[172]

(Continue...)

doi: 10.36922/ijb.4650

Table 3. Continue...

Tissue type	MA-based biomaterials	Biological factor	3D printing method	Light curing parameters	Animal models	Effects	Ref.
Bone	Gelatin, GelMA, alginate, nHAp	HUVECs and osteoblasts (MC3T3)	Extrusion 3D printing	360–480 nm UV light at 6.9 mW/cm^2 for 40 s	-	Promotes cell growth, angiogenesis, and gene expression	[252]
	GelMA, HAMA	hMSCs, MXene	Extrusion 3D printing	-	-	Promotes spontaneous differentiation of human BMSCs into osteoblasts	[253]
	GelMA, PEGDA	PDLSCs	Extrusion 3D printing	UV light at 2.9 mW/cm^2 for 30 s	Rat alveolar bone defect model	Promotes new bone formation	[254]
	GelMA, sodium alginate, BGM	mBMSCs, BMP2, PDGF	Extrusion 3D printing	365 nm UV light for 30 s	Rat subcutaneous graft, Beagle mutt alveolar fossa bone defect model	Promotes osteogenic differentiation and soft tissue repair.	[255]
	GelMA, nHAP	MC3T3-E1	Extrusion 3D printing	450 nm UV light for 3 min	Mouse cranial defect model	Effective repair of cranial defects and promotion of MC3T3-E1 osteogenic differentiation in mice	[256]
	GelMA, nHAP	MG63 cells, human BMSCs	DLP	440 nm blue light at 8 mW/cm^2 for 1 min	-	Promotes expression of cellular osteogenic genes	[257]
	GelMA, alginate	HUVECS, hBMSCs	Extrusion 3D printing	30 s of UV exposure	-	Induction of osteoblast differentiation and enhancement of mechanical properties	[164]
	LDH-GelMA	Osteoblasts	Extrusion 3D printing	360–480 nm UV light at 6.9 W/cm^2 for 40 s	-	Supports the survival, spreading, and proliferation of encapsulated osteoblasts in the absence of osteoinductive factors utilizing LDH	[165]
	SilMA	MRC5 cells	DLP, pneumatic extrusion	370 nm UV light at 45 W/m^2 for 60 s	-	Supports cell metabolism, adhesion, proliferation, and osteogenic differentiation	[258]
	MeGC	MG-63 cells	Extrusion 3D printing	430–485 nm UV light	-	Promotes cell proliferation and differentiation	[259]
	meHA-HAp-PEEK scaffolds	Human MSCs	FDM	UV light for 5–10 min	-	Promotes MSC adhesion and proliferation; contributes to osteogenic differentiation and extracellular mesenchymal mineralization	[260]
BLI	ColMA, BG	MSCs	Extrusion 3D printing	UV light for 1 min	Rabbit anterior cruciate ligament stripping model	Promotes specific cell differentiation, regeneration of the bone–ligament interface, and functional grafting to osseointegration	[261]

(Continue...)

Table 3. Continue...

Tissue type	MA-based biomaterials	Biological factor	3D printing method	Light curing parameters	Animal models	Effects	Ref.
Medulla spinalis	Ac-β-CD, GelMA	Neural stem cells, OSMI-4	Extrusion 3D printing	405 nm UV light at 0.6 mW/cm^2 for 14 s	Rat whole-sectional SCI model	Enhances intrinsic neuronal differentiation of neural stem cells; promotes neuronal regeneration and axonal growth in spinal cord injury model rats, leading to significant motor recovery	[202]
Medulla spinalis	GelMA	Human amniotic AEC neural-like cells	DLP	-	Rat whole-sectional SCI model	Promotes the recovery of nervous system function and motor function in rats	[262]
	PCL, GelMA, alginate	RA	Extrusion 3D printing	UV light for 1 min	-	Supports neural differentiation and patterning of EBs in response to co-printing with 1 μM RA	[203]
Coronary artery	Carbon nanotubes, ColMA	HCAECs	Extrusion 3D printing	365 nm UV light at 6.1 mW/cm^2	-	Significantly improves viscoelastic behavior and conductivity	[204]
Heart valve	PCL-MAA holder, GelMA/PEGDA	MSCs	FDM	-	-	Maintains and promotes cell viability; increases the production of type I collagen	[211]
	mNCC-GelMA	Human ADMSCs	Extrusion 3D printing	365 nm UV light for 4 min	/	Cells cultured in mNCC-GelMA demonstrate resistance to calcification	[210]
Myocardium	nSF, PEGDMA, GelMA	Cardiomyocyte, IL-10	Extrusion 3D printing	UV light for 60 s	Subcutaneous transplantation in nude mice	Upregulation of mature cardiac biomarkers, sarcomere formation, and heartbeat; regulates macrophage anti-inflammatory M2 phenotype	[209]
	GelMA-PEDOT:PSS	Cardiomyocyte	Extrusion 3D printing	450–550 nm UV light for 80 s	Subcutaneous transplantation in nude mice	Maintains high cytocompatibility and cell-spreading ability	[209]
	GeMA	Human cardiomyocytes, human cardiac fibroblasts	Extrusion 3D printing	UV light for 3–5 min	Rat AMI model	Improves long-term survival, angiogenesis, and stability of AMI rat grafts; reduces fibrosis, increases left ventricular thickness, and enhances cardiac function	[263]
	GelMA, MeTro	Cardiomyocytes	Extrusion 3D printing	405 nm blue light for 3 min	Rat subcutaneous transplantation	Displays endothelial barrier function and spontaneous beating of cardiomyocytes; reduces inflammatory response	[207]
	GelMA	Cardiomyocytes (H9C2s)	Extrusion 3D printing	365 nm UV light	-	Optimizes culture of cardiomyocytes through ERK1/2 and PI3K-Akt signaling pathways in 3D bioprinted cell-loaded GelMA scaffolds	[264]

(Continue...)

Table 3. Continue...

Tissue type	MA-based biomaterials	Biological factor	3D printing method	Light curing parameters	Animal models	Effects	Ref.
Myocardium	GelMA, collagen, fibronectin	Human iPSC-CM	Extrusion 3D printing	-	-	Creation of a pre-vascular pathway with the shape of an anterior interventricular artery within the myocardial structure that maintains cell viability	[265]
	GelMA	ND-Hb	Extrusion 3D printing	405 nm blue light	Rat myocardial infarction model	Improvement of cell viability in ND-Hb patches	[208]
	cECM, GelMA	hCPCs	Extrusion 3D printing	White light for 5 min	Rat AMI model	Promotes cell survival and vascularization	[205]
	PCL-GelMA	Human iPSCs	FDM	-	-	Supports iPSC-CM function in a 14-day culture	[206]
Biliary system	PCL, GelMA	USPIO NPs	FDM	405 nm, 3 W light source for 50 s	-	Protecting and supporting the stent improves the biocompatibility of the printed bile ducts; USPIO NPs dispersed in GelMA were used as a contrast agent for real-time monitoring of lesion repair and bile duct degradation by MRI	[266]
	GelMA	Hepatocytes, fibroblasts	DLP	25 mW/cm^2	-	Maintains >90% cell viability; enhances albumin secretion	[267]
	Alginate, CNC, GelMA	HepG2, NIH/3T3	Extrusion 3D printing	365 nm blue light for 2 min	-	Improves hepatocyte function; increases albumin production	[215]
	GelMA, liver dECM	Hepatocytes (hiHep cells)	DLP	365 nm UV light at 2.25 mW/cm^2	-	Enhances hepatocyte-specific functions and liver function recovery	[214]
	GelMA	Antioxidant mixture of vitamin C and vitamin E, HepG2 cell	Extrusion 3D printing	365 nm UV light for 3–5 min	Rabbit subcutaneous graft	Improves cell–cell interactions and liver-specific functions	[213]
	GelMA	Primary human HCC	Extrusion 3D printing	405 nm UV light at 7 mW/cm^2 for 1 min	Mouse subcutaneous transplantation	Survival for at least 28 days, albumin secretion, and debromoisoquin metabolism	[268]
	ColMA, thio hyaluronic acid	Primary human hepatocytes, hepatic stellate cells	Extrusion 3D printing	-	-	Cells remained active and responded to appropriate medication (acetaminophen) therapy for more than 2 weeks	[212]
Muscle tissue	GelMA, fibrinogen	C2C12 myoblasts	Extrusion 3D printing	365 nm UV light for 15 s	Rat subcutaneous implantation, rat bulk muscle loss model	Promotes cell growth, differentiation, and *in situ* regeneration of functional skeletal muscle	[269]
	GelMA	C2C12 myoblasts	Extrusion 3D printing	821 mJ/cm^2 light for 30 s	Tibialis anterior muscle injury mouse model	Demonstrates significant functional recovery and muscle volume restoration	[270]

(Continue...)

doi: 10.36922/ijb.4650

Table 3. Continue...

Tissue type	MA-based biomaterials	Biological factor	3D printing method	Light curing parameters	Animal models	Effects	Ref.
Muscle tissue	GelMA, collagen, decellularized ECMMA	C2C12, human ASCs	Extrusion 3D printing	20 mW/cm^2 light for 6 s	Mouse tibialis anterior muscle defect injury model	Constructs carrying ASCs significantly induced greater muscle regeneration than cellular constructs without topographical cues	[198]
	GelMA,	Mouse myoblasts (C2C12), MPT of skeletal muscles	Extrusion 3D printing	405 nm UV light	-	Maintains cell survival; cells exhibited a higher degree of cellular alignment	[271]
	SilMA	Mouse myoblasts (C2C12)	DLP	365 nm UV light	-	Promotes the differentiation of mouse adult myoblasts in hydrogels; increases the diameter and length of myotubes	[197]
	GelMA, CMCMA, AlgMA-PEGDA	Mouse myoblasts (C2C12)	Extrusion 3D printing	365 nm UV light at 3 W/cm^2	-	Provides structure and supports the formation and alignment of myotubes	[196]
	GelMA	Mouse myoblasts (C2C12), PEDOT NPs	Extrusion 3D printing	UV light for 2 min	-	Promotes proliferation, migration, and differentiation of C2C12 cells and myofiber formation	[272]
	GelMA	Mouse myoblasts (C2C12), AuNPs/ MXene nanosheets	Extrusion 3D printing	UV light for 4 min	-	Improved electrical and rheological properties led to enhanced differentiation of encapsulated myoblasts and allowed printing of highly viable (97%) stable constructs	[199]

Abbreviations: adECM, adipose derived extracellular matrix; ADSCs, adipose-derived stem cell; ADM, acellular dermal matrix; AlgMA, methacrylated sodium Alg; ALP, alkaline phosphatase; AMI, acute myocardial infarction; BCP, bidirectional calcium phosphate; BG, bioactive glass; BGM, bioactive glass microspheres; BLI, bone–ligament interface; BMMs, bone marrow-derived macrophages; BMSCs, bone marrow mesenchymal stem cells; BNC, bacterial nanocellulose; BP, bone particles; C3S, calcium trisilicate; CAM, cartilage acellular matrix; cECM, chondrocyte extracellular matrix; ChSMA, methacryloylated Chondroitin sulfate; CNC, cellulose nanocrystals; Col I, Collagen I; ColMA, methacrylated collagen; CQD, carbon quantum dot; dECM, decellularized extracellular matrix; DFCs, dental follicle cells; DLP, digital light processing; ECM, extracellular matrix; ECMMA, methacryloylated extracellular matrix; Epi-SCs, epidermal stem cells; FDM, fused deposition modeling; GAG, glycosaminoglycan; GelDA, gelatin-dopamine; GelMA, methacrylated gelatin; HA, hyaluronic acid; HAMA, hyaluronic acrylate methacrylate; Hap, hydroxyapatite; HCAECs, human coronary artery endothelial cells; HCC, hepatocellular carcinoma; hCPCs, human cardiac progenitor cells; HdFs, human skin fibroblasts; HUVECs, human umbilical cord vascular endothelial cells; iPSCs, induced pluripotent stem cells; iPSC-CM, induced pluripotent stem cell-derived cardiomyocytes; KGN, Kartogenin; LDH, layered double hydroxides; MAA, methacrylic acid; MBGN, mesoporous bioactive glass nanoparticle; mBMSCs, mouse bone marrow-derived stromal cells; MeGC, methacrylic acid glycol chitosan; MECM, mesenchymal stem cell-derived extracellular matrix; meHA, hyaluronic acid methacrylate; MeTro, methacryloyl-substituted recombinant human para-somatic elastin; mNCC, TEMPO-modified nanocrystalline cellulose; mNG, mNCC-GelMA; MPT, minimal processing tissue; MRI, magnetic resonance imaging; MSCs, mesenchymal stem cells; MSNCaPDex, mesoporous silica nanoparticles functionalized with calcium, phosphate, and dexamethasone; ND-Hb, hemoglobin wrapped into nanodroplets; nHAP, nanohydroxyapatite; NPs, nanoparticles; nSF, non-mulberry silk fibroin; OCN, osteocalcin; OMA, oxidized methacrylate; PACG, N-acryloyl-2-glycine; PCL, polycaprolactone; PDGF-BB, platelet-derived growth factor-BB; PDLSCs, periodontal membrane stem cells; PEDOT, poly(3,4-ethylenedioxythiophene); PSS, polystyrene sulfonate; PEEK, polyetheretherketone; PEGDA, polyethylene glycol diacrylate; PEGDMA, polyethylene glycol dimethacrylate; PEGMA, poly(ethylene glycol) methacrylate; PL, platelet lysate; PLA, polylactic acid; PRP, platelet-rich plasma; PTH, parathyroid hormone; RA, retinoic acid; RNTK, rosette nanotubes; ROS, reactive oxygen species; SCI, spinal cord injury; SF, silk fibroin; SilMA, methacryloylated SF; SKPs, skin-derived precursors; SLS, selective laser sintering; USPIO, ultrasmall superparamagnetic iron oxide; UV, ultraviolet; VEGF, vascular endothelial growth factor.

doi: 10.36922/ijb.4650

pore sizes to match drug sizes, but also facilitates a targeted drug delivery system for precision therapy.

Hydrogel scaffolds for controlling the release of Mn^{2+}, Sr^{2+}, Si^{4+}, and B^{3+} were constructed using GelMA. A burst release was observed during the first 3 days due to the rapid leakage of ions near the surface. These ions gradually diffused out of the printed porous hydrogel scaffolds over approximately 25 days.[181] Zhang et al.[233] used 3D printing to construct 3D GelMA scaffolds loaded with MnCO, which could trigger a sustained release of CO and Mn^{2+} through a Fenton-like reaction with endogenous hydrogen peroxide produced at the implanted tissue site, thereby significantly reducing the inflammatory response by upregulating the M2 macrophage phenotype. MXenes have a favorable photothermal effect. Under near-infrared light irradiation, they kill both Gram-positive and Gram-negative bacteria and can be used to treat infected bone defects by constructing 3D scaffolds for delivery to infected bones.[166,253] The addition of antitumor cells to these scaffolds can kill tumor cells through targeted transport. Dutta et al. constructed 3D scaffolds that could release antitumor drugs (≈49%) to kill osteosarcoma cells.[168] Vitamins are a class of essential organic compounds that play a critical role in the metabolism of substances. Retinoic acid (RA) promoted the neural differentiation of EBs incorporated in PCL-GelMA-Alg.[203] Additionally, RA exhibited the ability to scavenge intracellular ROS generated during photocrosslinking, a property further enhanced by incorporating an antioxidant mixture of vitamin C and vitamin E into GelMA.[213]

4.2.3. Exosomes

Exosomes are membranous vesicles released into the ECM by intracellular multivesicular bodies fused to the cell membrane. Almost all types of cells can produce and release exosomes. They possess a nanosized lipid inclusion structure with a diameter of 30–100 nm and contain proteins, mRNAs, and microRNAs. Exosomes have been recognized as biomarkers of diagnostic/drug responses or as intercellular communication vectors for transferring biologically active noncoding RNA or proteins between cells. Compared with the use of cells combined with hydrogels, this cell-free treatment avoids immune rejection and loss of cell viability for achieving therapeutic effects.

Several studies have combined exosomes with hydrogels for the treatment of various conditions, such as diabetes, chronic wound healing,[277] regeneration of cartilage defects,[278] and spinal cord repair.[279] However, *in situ* crosslinking is utilized for the generation of most hydrogel constructs, resulting in hydrogels with low porosity. The preparation of scaffolds using physical freeze-drying and crosslinking methods allows for the generation of hydrogel scaffolds with higher porosity, yielding promising results in terms of cellular encapsulation. Emerging technologies, such as 3D printing, enable the synthesis of radically oriented channels that guide cell migration for therapeutic purposes.[280] Two key issues are associated with the 3D printing of scaffolds delivering exosomes using methacryloyl compounds: survival of exosomes (toxicity of photoinitiators and physical extrusion of the printing process can affect exosome survival) and the rate of exosome release (exosomes are characterized by rapid clearance from the bloodstream, limiting the duration of their therapeutic effect). In a study by Born et al., a deliverable MSC-derived GelMA hydrogel scaffold demonstrating anti-inflammatory and pro-angiogenic effects was constructed using an extrusion printer. This study also demonstrated that the initial release rate of exosomes can be controlled by different photoinitiator concentrations and that the bioactivity of MSC extracellular vesicles (EV) in endothelial gap closure assays was retained after bioprinting.[281] In a study by Chen et al., GelMA hydrogel scaffolds loaded with exosomes from ADSCs were constructed using SLA printing and demonstrated effectiveness in repairing mitochondrial dysfunction in chondrocytes, enhancing chondrocyte migration, and polarizing synovial macrophages toward the M2 phenotype, thereby promoting cartilage regeneration.[183] Hu et al. utilized DLP printing to construct a GelMA hydrogel scaffold loaded with exosomes derived from epidermal stem cells of human umbilical cord mesenchymal stem cells (hUC-MSCs-sEVs) and demonstrated that hUC-MSCs-sEVs, by delivering miR-23a-3p, activated the PTEN/AKT signaling pathway, subsequently promoting calcium deposition, endothelial network formation, and osteogenic differentiation.[282]

4.2.4. Bioactive substances

Introducing bioactive tissues into hydrogel scaffolds not only increases the biocompatibility of hydrogels but also increases the bioactive factors and primitive cell colonization in hydrogels. Many bioactive substances can work well combined with cell-active substrates in bioinks. PRP contains a large number of growth factors, such as PDGF, TGF-β, and IGF-1, which play a significant role in maintaining cell activity and inducing differentiation and colonization.[184,283] If bone particles (BPs) are included in GelMA for co-printing, the cells initially contained in BPs can migrate and colonize the bioprinted scaffolds while maintaining their ability to express early osteogenic markers for bone regeneration purposes. Similarly, Tavares-Negrete et al. developed GelMA hydrogels supplemented with minimal processing tissue (MPT) constructs to create dense skeletal muscle-like tissue.[271] Constructs supplemented with MPT also maintained

their 3D integrity for 28 days. In contrast, similar original GelMA constructs only maintained their structure for 14 days or less. C2C12 cells embedded in MPT-supplemented constructs exhibited a higher degree of cellular alignment and achieved significantly higher densities than cells loaded in the original GelMA constructs. Their findings suggested that the addition of MPT contains abundant biochemical and topological cues such as growth factors, glycosaminoglycans, and structurally conserved proteins (e.g., collagen).[271]

4.2.5. Other functional substances

The recruitment of the above functional substances to enable the therapeutic effect can be achieved by loading some other recruiting substances. For example, Yang et al. constructed a 3D-bioprinted bifunctional scaffold made of GelMA and PCL based on the MSC-specific recruitment mediated by the aptamer HM69 and the cellular cartilage formation enhanced by growth factors; this aptamer specifically recognizes and recruits MSCs.[222] Ding et al. revealed that a hydrogel scaffold carrying a bioactive peptide linkage that selectively adsorbs TGF-β1 not only provides cell growth space but also induces endogenous TGF-β1 recruitment to promote cartilage formation.[187]

4.3. Organoids/organ-on-chip

An organ-on-chip is a microfluidic cell culture device created using microchip fabrication methods (Figure 8A). This device incorporates continuous perfusion chambers with multicell layer structures, tissue interfaces, physicochemical microenvironments, and a simulated human vascular circulation. Organ-on-chip have diverse applications, including high-throughput drug screening, drug uptake and metabolism studies, drug development, modeling the human circulatory system, drug toxicology assessments, artificial biomimetic microenvironments, studying intercellular interactions, ECM interactions, and serving as a novel *in vitro* culture platform.

Notably, organ-on-chip addresses the limitations of animal models by offering controlled experimental conditions. Organoids, with their unique advantages in drug absorption, metabolism, and toxicity studies, enable the determination of key pharmacokinetic parameters, such as drug absorption, distribution, metabolism, elimination, and toxicity. This approach allows for rapid screening of various drugs for antitumor effects and assessments of liver and kidney toxicity. Moreover, organ-on-chip offers low sample usage, high throughput, safety, and minimal environmental impact.

In addition, an organoid is a 3D *in vitro* cell culture system that is highly similar to the source tissue or organ *in vivo*. These culture systems can replicate the complex spatial morphology of differentiated tissues and exhibit cell-to-cell and cell-to-surrounding matrix interactions and spatial location patterns. In turn, they are capable of achieving similar physiological responses to differentiated tissues and organs *in vivo*, with a high degree of similarity to the source tissue. Compared with the traditional 2D cell culture model, the 3D cultured organoid contains multiple cell types, breaking through the pure physical contact between cells, forming closer cell-to-cell and cell-to-matrix interactions. These results in the formation of functional "micro-organs" that better simulate organogenesis and physiology, making them valuable in basic research. Moreover, it can be used to better simulate the process of organogenesis and the physiological and pathological state of organs and tissues and thus has a broad application prospect in basic research and clinical diagnosis and treatment.

Furthermore, 3D bioprinting technology can be employed to precisely control cell distribution and differentiation through layered printing, enabling the construction of human organ-like structures with high fidelity. This can expand our knowledge of human development and tissue and organ regeneration mechanisms and promote the application of organ-like and organ chips in tissue biology, disease model construction, toxicology, pharmacology, and personalized medicine.[286] Currently, the use of MA-based compounds has been realized in the liver,[287,288] pancreas,[283] blood vessels,[289] myocardium,[290] atrioventricular nodes,[291] malignant tumors,[292,293] skeletal muscle,[291] bones and joints,[294] and periodontal ligament-alveolar bone (Table 5).[295]

MA-based hydrogels are gradually being used in the 3D printing of biological scaffolds due to their robust biological properties and flexible, tunable properties, with strong potential in organoid construction. Reportedly, structures obtained by 3D printing can provide topographical cues for cell migration, differentiation, and proliferation. Further, dECM and GelMA structures with topographical cues displayed increased gene expression levels by 1.5–1.8 fold,[296] providing cues for gene expression and proliferation.

Van der Valk et al. employed GelMA/HAMA and extrusion 3D printing to construct biomodels that enhance microcalcification by mimicking the mechanical environment of the natural Aortic valve (AV) node.[291] The median Young's modulus of the atrioventricular node midlayer was 37.1, 15.4, and 26.9 kPa for fiber, sponge, and ventricle, respectively. By adjusting the ratio of the bioinks, they observed that the modulus of the fibers and sponges matched that of the 3D 5% GelMA/1% HAMA UV-crosslinked hydrogel. Their study revealed the effective use

Table 4. Application of 3D-printed methacrylic anhydride (MA) hydrogel in active biological factor loading

Active biological factor	MA biomaterials	3D printing	Light curing parameters	Effect	Ref.
Cytokine					
VEGF	GelMA	Extrusion 3D printing	365 nm UV light for 5 min	Promotes wound healing, collagen deposition, and angiogenesis	[216]
EGF	GelMA, SilMA	DLP	365 nm UV light for 4 s at 6.09 mW/cm^2	Enhanced wound healing in the epidermis and dermis with proliferation of keratinocytes and fibroblasts	[273]
IGF-1	GelMA	Extrusion 3D printing	365 nm UV light for 25 s at 180 mW/cm^2	Promotes alignment of myoblasts and differentiation into myotubes	[274]
PDGF-BB, chondro-inducible KGN	GelMA, HAMA	-	-	Promotion of cell migration and synergistic promotion of MSC chondrogenic differentiation	[175]
TGF-β1	GelMA, HAMA, ChsMA	Extrusion 3D printing	405 nm blue light for 60 s	Enhanced the aggregation, proliferation, and differentiation of SMSCs	[219]
TGF-β1 binding peptide	GelMA	Extrusion 3D printing		Promotes the recruitment of TGF-β1, with favorable therapeutic effects	[187]
TGF-β3	GelMA, HAMA	Extrusion 3D printing	405 nm blue light for 60 s	Sustained release of TGF-β3 from scaffolds successfully directs migration and differentiation of endogenous stem/progenitor cells	[219]
IL-4	GelMA, dextrose (PGelDex)	Extrusion 3D printing, handheld, DLP	360–480 nm UV light for 30 s at 10 mW/cm^2	Mediates the conversion of macrophages from a pro-inflammatory M1 phenotype to an anti-inflammatory M2 phenotype for immunomodulation	[276]
IL-10	GelMA, SilMA	Extrusion 3D printing	405 nm UV light for 20 s at 1000 mW	Mediates the conversion of macrophages from pro-inflammatory M1 phenotype to anti-inflammatory M2 phenotype for immunomodulation; cell viability maintained in anoxic environment for at least 5 days	[209]
Therapeutic drugs					
Mn^{2+}, Sr^{2+}, Si^{4+}, B^{3+}	GelMA, PACG	Inkjet	-	Promotes bone regeneration	[181]
MXene	GelMA	Extrusion 3D printing	405 nm UV light for 15 s	MXene has a good photothermal effect and kills both Gram-positive and Gram-negative bacteria under near-infrared light	[166]
DOXH	GelMA	Extrusion 3D printing	400 nm UV light for 2 min	DOXH facilitates diabetic wound regeneration by regulating ROS scavenging and macrophage polarization to the M2 phenotype	[284]
DC	HAMA	Extrusion 3D printing	-	Anti-cancer properties	[189]
Anti-tumor drugs	GelMA	Extrusion 3D printing	365 nm UV light for 60 s	Release of anti-tumor drugs (≈49%), which kill osteosarcoma cells	[168]
RA	GelMA, PCL	Extrusion 3D printing	UV light for 60 s	Induction of neural differentiation in EBs	[203]

(Continue...)

Table 4. Continue...

Active biological factor	MA biomaterials	3D printing	Light curing parameters	Effect	Ref.
Antioxidant mixture of vitamin C and E	GelMA	Extrusion 3D printing	365 nm UV light for 3–5 min	Enhances scavenging of intracellular ROS formed during photocrosslinking	[213]
Exosomes					
HADSC exosomes	GelMA	SLA	405 nm UV light for 30 s at 11 mW/cm^2	Effective repair of chondrocyte mitochondrial dysfunction, enhancement of chondrocyte migration, and polarization of synovial macrophages toward the M2 phenotype	[281]
MSCs exosomes	GelMA	Extrusion 3D printing	UV light at 850 mW/cm^2	Anti-inflammatory and pro-angiogenic	[183]
hUC-MSCs-sEVs	GelMA, nanoclay hydrogel	DLP	365 nm UV light for 2 min	Activates the PTEN/AKT signaling via miR-23a-3p; promotes calcium deposition and endothelial network formation; induces osteogenic differentiation and angiogenesis	[282]
Human MSC exosomes	HAMA	Extrusion 3D printing	-	Improves proliferation, migration, and angiogenic capacity of human fibroblasts and human endothelial cells; enhances expression of markers associated with wound healing	[285]
Nucleic acid					
Fitness HM69	GelMA	Extrusion 3D printing	-	This aptamer specifically recognizes and recruits MSCs, provides a favorable microenvironment for cell adhesion and proliferation, and promotes cartilage formation, improving the repair of total cartilage defects in rabbits	[222]
Bioactive substance					
BP	GelMA	Extrusion 3D printing	-	Cells migrate and colonize the bioprinted scaffold while maintaining their ability to express early osteogenic markers	[248]
MPT of skeletal muscles	GelMA	Extrusion 3D printing	405 nm UV light	MPT contains abundant biochemical and topological clues such as growth factors, GAGs, and structurally conserved proteins (e.g., collagen)	[271]
Cytoplasm					
MSCs	GelMA-dextrose (PGelDex)	Extrusion, DLP, handheld printing	360–480 nm UV light for 30 s at 10 mW/cm^2	Inhibits the activation and proliferation of immune cells (e.g., monocytes and macrophages) through the paracrine release of bioactive molecules, particularly interleukins	[276]

Abbreviations: BP, bone pellets; ChsMA, methacryloylated Chondroitin sulfate; DC, diclofenac sodium; DLP, digital light processing; DOXH, doxycycline hyclate; EBs, embryoid bodies; EGF, endothelial growth factor; GAG, glycosaminoglycans; GelMA, methacrylated gelatin; HADSC, human adipose-derived stem cell; HAMA, hyaluronic acrylate methacrylate; hUC-MSCs-sEVs, human umbilical cord mesenchymal stem cell-derived small extracellular vesicle; IGF-1, insulin-like growth factor-I; KGN, Kartogenin; MSC, mesenchymal stem cell; MPT, minimal processing tissue; PACG, poly(*N*-acryloyl 2-glycine); PDGF-BB, platelet-derived growth factor-BB; RA, retinoic acid; ROS, reactive oxygen species; SilMA, methacryloylated SF; SLA, stereolithography; SMSCs, synovial mesenchymal stem cells; UV, ultraviolet; VEGF, vascular endothelial growth factor.

doi: 10.36922/ijb.4650

of heart valve mechanobiology for high-throughput drug screening in calcific aortic valve disease (Figure 8B).[291]

For the vascular system, Zhang et al. utilized sacrificial 3D bioprinting to fabricate hollow microchannel-like vascular chips containing a fused endothelial layer. The microchannels were embedded in GelMA hydrogel with human endothelial cells attached to the surface. Human whole blood was injected into the microchannel to form a thrombus, and tissue plasminogen activator (tPA) was continuously infused as a thrombolytic agent, demonstrating potential lysis of nonfibrotic thrombi. They further observed that in hydrogels containing fibroblasts and damaged endothelium, fibroblast migration into the clot and type I collagen deposition had occurred, confirming the mimicry of the model in generalizing the fibrotic process *in vivo*.[289]

For malignant tumors, Sanchez-Salazar et al. utilized GelMA and reported >75% survival of microtumors cultured with Caco2 cells during a 10-day incubation period.[292] Microtumors treated with 5-fluorouracil displayed <20% cell survival and lower VEGF-A and E-cadherin expression than untreated controls. The tumor microarray device was demonstrated to be suitable for studying cancer biology and performing drug response assays.[292] Furthermore, Chen et al. utilized MDA-MB-231 and MCF7 human breast cancer cell lines, HT-29 human colon cancer cell lines, and NCI-H23 human lung cancer cell lines co-printed with GelMA; they demonstrated that GelMA exhibits similar properties to matrix gel in tumorsphere cultures and 3D tumor invasiveness studies.[293] This established the effectiveness of the 3D GelMA culture in multiple tumors and its potential for replacing stromal gel in tumor invasiveness assessments.[293]

Based on the mechanical strength of 5% (wt/vol) GelMA similar to that of healthy liver tissue, Ma et al. utilized photopolymerization of the hydrogel matrix to encapsulate hiPSC-derived hepatocytes along with endothelial and mesenchymal supporting cells.[297] This complementary pattern mimicked the hepatic lobular structure, resulting in a patient-specific liver model that closely resembled the natural tissue structure and cellular composition. Furthermore, 2% (wt/vol) glyceryl methacrylate-hyaluronate mixed with 5% (wt/vol) GelMA in a 1:1 ratio for encapsulating supporting endothelial and mesenchymal cells was found to promote endothelial cell proliferation and support blood vessel formation.[297] In a study by Gu et al., acoustic differential bioassembly was utilized to differentially assemble hiPSC-derived hepatospheres and endothelial cells and porous GelMA-encapsulated HUVECs in a microgel into a hexagonal cellular structure that mimicked the umbilical and sinusoidal structures in the liver lobule. This hepatic lobule model reconstructed hepatic metabolic and synthetic functions, such as albumin secretion and urea production.[298]

4.4. Adhesive tissue engineering scaffolds

Adhesive tissue engineering scaffolds (ATES) have emerged as an innovative alternative to sutures and bio-adhesives for ensuring implantation into target tissues. Relying on their inherent tissue adhesion properties, ATES systems enable minimally invasive delivery of various scaffolds. Here, we present the development of first-in-class 3D-bioprinted ATES constructs using functionalized hydrogel bioinks (Table 6). Two ATES delivery strategies—*in situ* printing and post-printing transfer—were tested using two bioprinting methods: embedded- versus air-printing. Dopamine-modified HA methacrylate and GelMA were used as the main bioink components, allowing for the fabrication of scaffolds with enhanced adhesion and crosslinking properties. Dopamine modification improved the adhesive properties of the HAMA-dopa/GelMA constructs under different loading conditions while maintaining their structural fidelity, stability, mechanical properties, and biocompatibility. While direct printing onto the adhesive yielded superior bond strength, embedded printing followed by transfer to the target tissue displayed greater potential for translational applications. In summary, these results demonstrated the potential of bioprinted ATES as off-the-shelf medical devices for different biomedical applications.[300]

The robust adhesive properties of an adhesive bioink consisting of gelatin methacryloyl, gelatin, HA methacrylate, and skin secretions of Chinese giant salamander enabled good extrusion bioprinting under humid conditions. This bioink also demonstrated strong adhesion to various surfaces with different chemistries, likely due to the different bonds presented in the bioink formulation. Thus, this bioink is capable of fabricating complex planar and volumetric structures using extrusion bioprinting.[301]

4.5. Biosensor

A biosensor is an analytical device consisting of a biosensitive element (sensing element) and a signal converter (transducer) (Table 6). The role of the biosensitive element is to recognize the target material, mainly antibodies, enzymes, nucleic acids, cells, and other biological substances, as well as similar molecules, such as aptamer, peptide, and molecularly imprinted polymers. Signal conversion devices serve to convert the interaction between a biosensitive element and a target molecule into a different signal. For example, an enzyme catalyzes a chemical reaction with a specific substance, which is then

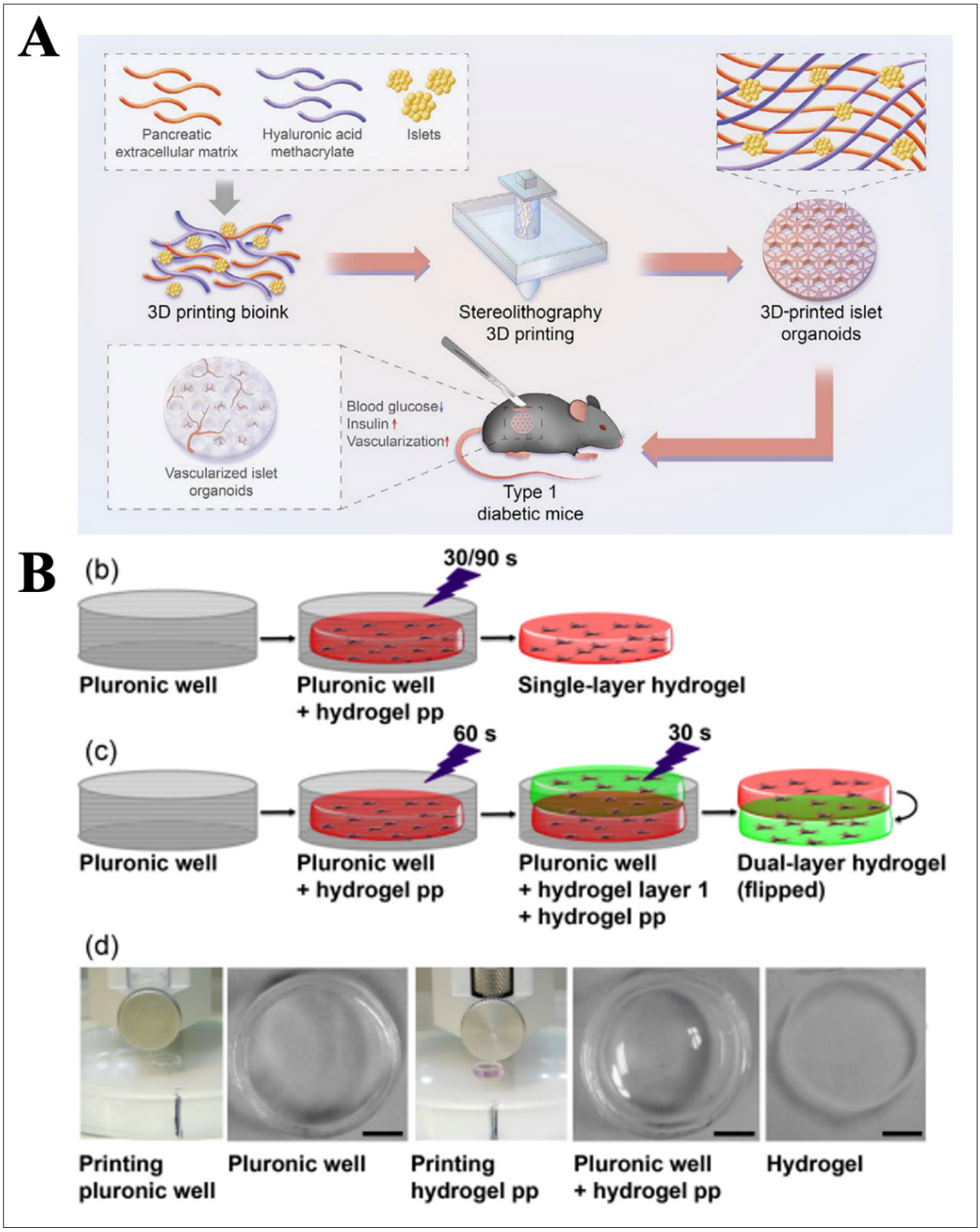

Figure 8. Organoids and organ chips. (A) 3D-printed HAMA/pECM pancreatic islet organoids. Adapted with permission from Wang et al.[299] (B) A 3D-printed model of calcific aortic valve disease (CAVD) prepared by encapsulating human aortic valvular interstitial cells (VICs) with GelMA and HAMA. Adapted with permission from van der Valk et al.[291] Abbreviations: GelMA, methacrylated gelatin; HAMA, hyaluronic acrylate methacrylate; pECM, pancreatic extracellular matrix.

converted into an electrical signal; a biological antibody captures a specific antigen, which is then converted into a light signal through labeled fluorescence.

Electrochemical biosensors based on 3D printing technology can prevent artificial errors and provide high-throughput detection. Wei et al. utilized a carbon nanofiber (CN)/GelMA conductive composite hydrogel printed on eight-channel screen-printed carbon electrodes to form tight intercellular contacts that maintain cell viability.[302] To improve the conductivity of the biosensors, they chose a 3D honeycomb-printed filler pattern. The electrochemical impedance spectroscopy technique was used to evaluate the toxicity of fungal toxins. The electrochemical method is simple, effective, and functions in real-time, which provides a new direction for cytotoxicity evaluation tools that can be used for producing toxins in bulk. Differences in the print fill pattern and number of graphically printed layers during extrusion-based 3D bioprinting can lead to the formation of different morphological structures of composite hydrogels on screen-printed electrodes, which can affect the electrochemical signals of the constructed sensors. Therefore, they explored the effects of five common print fill patterns and different graphic print layers on the electrical signals.[302] In addition, it was observed that different concentrations of GelMA hydrogels would exhibit different processing performance and biocompatibility characteristics. The electrical conductivity of different concentrations of GelMA hydrogels and their effects on cell viability were evaluated, revealing a survival rate of cells in 5–7.5% concentrations of GelMA hydrogels greater than 93%. Finally, the combined toxicity of deoxynivalenol (DON), 3-acetyldeoxynivalenol (3-ADON), and 15-acetyldeoxynivalenol (15-ADON) was analyzed by employing the combined index method, and the type of toxic combined effect was determined. Accordingly, a new method for evaluating the combined toxicity of mycotoxins was proposed, which has potential applications in food safety and evaluation.[302]

Wan et al. designed a green, rapid, and efficient method for constructing fluorescent nanosystems based on polyethyleneimine (PEI) and functionalized HAp using simple physical adsorption.[303] First, HAp nanorods were

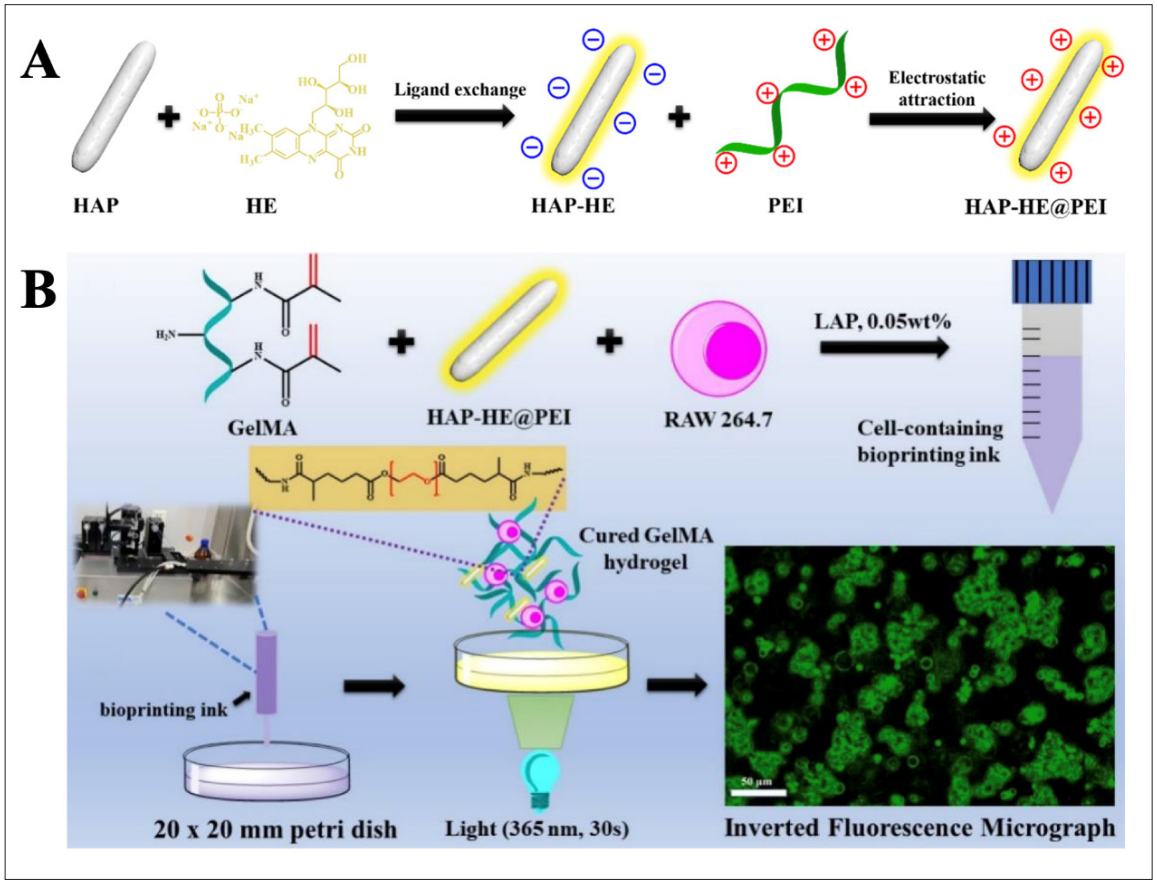

Figure 9. A fluorescent nanosystem based on PEI and functionalized HAP. (A) Preparation of HAP-HE@PEI with a positively charged surface. (B) Bioink preparation and printing for 3D cell imaging. Adapted with permission from Wan et al.[303] Abbreviations: GelMA, methacrylated gelatin; HAP, hydroxyapatite; HE, riboflavin sodium phosphate; LAP, lithium phenyl-2,4,6-trimethylbenzoylphosphinate; PEI, polyethyleneimine.

Table 5. Application of 3D-printed methacrylic anhydride (MA) hydrogel in organoid/organ chip

Organoid/ organ-on-chip	MA biomaterials	Bioactive substances	3D printing	Light curing parameters	Effects	Ref.
Aortic valve organoid	GelMA, HAMA	VIC	Extrusion 3D printing	365 nm UV light for 60 s at 2.5 mW/cm^2	Potentiates microcalcification by mimicking the native AV mechanical environment; reveals valvular mechanobiology and facilitates high-throughput drug screening in CAVD	[291]
Heart-on-a-chip	GelMA, PCL	Cardiac myocytes	Extrusion 3D printing; electrospinning	UV light for 30 s at 12 mW/cm^2	Established a 3D anisotropic HoC platform for evaluating DIC and cardioprotective efficacy; the 3D-printed micrometer-scale scaffold frames mimic the interwoven myocardium anatomical structure and the branched-aligned nanofibers network to guide cellular arrangements	[304]
	GelMA, PCL	Neonatal mouse cardiomyocytes	DLP	365 nm UV light for 18 s at 6 mW/cm^2	The constructed 3D cardiac microtissue *in vitro* modeling system has great potential for cardiac disease modeling and drug screening	[305]
Thrombosis-on-a-chip	GelMA	Endothelial cell	Extrusion 3D printing	UV light at 850 mW/cm^2	Injection of human whole blood into microchannels to form thrombi and continuous infusion of tPA as a thrombolytic agent demonstrated the potential lysis of nonfibrotic thrombi	[289]
Liver organoid	GelMA	Huh7, HepaRG stem cells	Extrusion 3D printing	365 nm UV light for 60 s at 2.5 mW/cm^2	Promotes fibrillar collagen deposition for liver fibrosis studies	[287]
Liver-on-a-chip	GelMA	HepG2/C3A cells	Extrusion 3D printing	UV light for 15 s at 850 mW	Treatment with 15 mM acetaminophen induces a toxic response in liver constructs, suggesting this liver microarray platform for toxicity assessment	[288]
Islet organoid	GelMA	Pancreatic ECM, PRP, mouse islet β cells (MIN6)	Extrusion 3D printing	405 nm UV light for 30 s	Specific bioinks with coordinated immunomodulatory responses, indicated by abundant M2-polarized macrophages, were prepared and characterized to attenuate inflammation; maintains cellular activity, enhances glucose sensitivity, and promotes angiogenesis.	[283]
	HAMA	Pancreatic dECM	SLA	405 nm UV light for 10 s	Maintenance of islet cell adhesion and morphology through the Rac1/ROCK/MLCK signaling pathway improved islet function and activity; favors the formation of a new vascular network	[299]
Bone organoid	GelMA, AlgMA, HAP	BMSCs	DLP	-	Guides osteogenesis, mineralization, cell layer formation, modeling, and remodeling, ultimately promoting bone organoid development	[306]

(Continue...)

Table 5. Continue...

Organoid/ organ-on-chip	MA biomaterials	Bioactive substances	3D printing	Light curing parameters	Effects	Ref.
Skeletal muscle organoid	GelMA, dECM-MA	Myoblasts (C2C12)	Extrusion 3D printing	UV light at 300 mW/cm^2	3D-printed dECM-based structures with topographical cues have the potential to bioengineer functional skeletal muscle tissuev	[296]
Knee joint-on-a-chip	GelMA	Cartilage, synovium, and adipose tissue	Extrusion 3D printing	395 nm UV light for 60 s	Drugs can be tested by systemic administration in all mid-streams or intra-articular administration by adding the drug to a shared synovial analog stream; perfusion of a shared stream through cartilage, synovium, and adipose tissue enables tissue crosstalk	[294]
Knee joint adipose tissue-on-a-chip	GelMA	ASCs	-	-	Adipose tissue-like organ could be constructed to study the role of the infrapatellar fat pad in the pathobiology of knee OA	[307]
PDL-AB-on-a-chip	GelMA, HAp magnetic iron oxide nanoparticles	Human PDL fibroblasts, human osteoblasts	Extrusion 3D printing	365 nm UV light for 120 s	Preliminary tetracycline interaction studies suggest that 3D microtissue cells within the model can uptake the drug	[307]
Tumor-on-a-chip	GelMA/alginate hydrogel microspheres	Caco2 cells	Extrusion 3D printing, DLP	365 nm UV light for 30 s	An organ chip suitable was constructed for studying cancer biology and performing drug response assays	[307]
	GelMA-hydrolyzed collagen	Lung cancer cell	Extrusion 3D printing	-	The efficacy of this hydrogel in 3D tumor cultures is demonstrated, as well as its potential to replace stromal gels in the assessment of tumor aggressiveness	[293]
	GelMA	Adipocyte- and iPSC-derived MSCs\endothelial cells, patient-derived neuroblastoma spheroids	Extrusion 3D printing	365 nm UV light for 125 s	Created a novel medium-throughput bio-fabrication platform suitable for studying tumor angiogenesis and metastasis in future precision medicine; demonstrated that micro-vessels are attracted to and grow into tumors by tumor spheres and that neuroblastoma cells invade the tumor environment once the spheres are destroyed	[308]

Abbreviations: AlgMA, methacrylated sodium Alg; ASCs, adipose tissue-derived mesenchymal stem cells; AV, aortic valve; BMSCs, bone marrow mesenchymal stem cells; CAVD, calcific aortic valve disease; dECM, decellularized extracellular matrix; DIC, disseminated intravascular coagulation; DLP, digital light processing; ECM, extracellular matrix; GelMA, methacrylated gelatin; HAMA, hyaluronic acrylate methacrylate; HAP, hydroxyapatite; Hoc, Heart-on-a-chip; iPSC, induced pluripotent stem cells; PCL, polycaprolactone; PDL, periodontal ligament; AB, alveolar bone; PRP, platelet-rich plasma; SLA, stereolithography; UV, ultraviolet; VIC, valvular interstitial cell.

doi: 10.36922/ijb.4650

Table 6. Application of 3D-printed methacrylic anhydride (MA) hydrogel in adhesive tissue engineering scaffolds (ATESs) and biosensors

Component	MA biomaterials	Bioactive substances	3D printing	Light curing parameters	Effects	Ref.
ATESs	Dopa-HAMA, GelMA	-	Extrusion 3D printing	365 nm UV light	Dopamine modification improved adhesive properties while maintaining structural fidelity, stability, mechanical properties, and biocompatibility	[289]
	GelMA, HAMA	Skin secretion of *Andrias davidianus*	Extrusion 3D printing	360–480 nm UV light for 30 s at 10 mW/cm^2	Promotes adhesion of the scaffold in wet conditions; maintains high cell viability	[301]
Biosensors	GelMA, CN	Human lung cancer cell A549	Extruded	405 nm UV light for 10–20 s	A new method for evaluating the combined toxicity of mycotoxins	[302]
	GelMa, HAP-HE@PEI	Macrophages RAW 264.7 cells	Inkjet	UV light for 30 s	A promising candidate for bioimaging, drug delivery, and bioprinting; can be rapidly taken up by NIH-3T3 fibroblasts and successfully applied to cellular imaging	[303]

Abbreviations: CN, carbon nanofiber; Dopa, dopamine; GelMA, methacrylated gelatin; HAMA, hyaluronic acrylate methacrylate; HAP, hydroxyapatite; HE, riboflavin sodium phosphate; PEI, polyethyleneimine; UV, ultraviolet.

functionalized with riboflavin sodium phosphate (HE) to impart fluorescent properties based on the ligand exchange process. Next, PEI was attached to the surface of HE-functionalized HAP (HAP-HE@PEI) using electrostatic attraction. The fluorescent HAP-HE@PEI nanosystems were rapidly absorbed by NIH-3T3 fibroblasts and successfully applied to cellular imaging. Additionally, they prepared doxorubicin hydrochloride (DOX) with a high loading of HAp-HE@PEI; the *in vitro* release results revealed that the maximum release of DOX at pH 5.4 was significantly higher (31.83%) than that at pH 7.2 (9.90%). Consequently, DOX can be employed as a drug delivery vehicle for cancer therapy. Finally, a 3D cell culture of RAW 264.7 macrophages using GelMA hydrogel-printed HAP-HE@PEI as 3D inkjet printing ink displayed good biocompatibility. In conclusion, due to the enhanced affinity of HAP-HE@PEI for cell membranes, this method has potential in bioimaging, drug delivery, and bioprinting (Figure 9).[303]

5. Conclusion

Among the currently used MA-based bioinks, GelMA remains the mainstream choice with established and reproducible printing parameters. While the preparation and 3D printing processes of GelMA hydrogels are well-established, a systematic research framework for other MA-based bioinks, encompassing nomenclature, preparation, light-curing processes, and applications, is lacking. In this review, although many MA hydrogels have demonstrated significant therapeutic and clinical potential, further research on their application is warranted. In addition, the biological potential of the precursor compounds remains underexplored, presenting opportunities for future investigation and advancement.

In this review, we introduced various 3D printing technologies for use in bioclinical applications. The current conventional method is extrusion printing combined with light curing, followed by DLP and SLA. We discussed the advantages and disadvantages of various printing modalities, among which extrusion printing stood out due to the lightweight and low cost of the device; however, it exhibits a low printing speed and poor cell activity of printed cells. To promote the development of translational medicine, future research should utilize other bioprinting modalities and explore methods that are more economical and compatible with clinical applications. Moreover, results on 3D-printed scaffolds are limited to *in vitro* or animal experiments; 3D printing should be tested in clinical settings. Some emergent studies proposed *in situ* printing, handheld 3D pens, and other emerging 3D printing technologies.[309] This enables the combination of computer-aided technology with 3D printing to obtain personalized 3D-printed stents.

In summation, the fusion of MA-based compounds with 3D biotechnology yields bioscaffolds with high biocompatibility and customizable mechanical properties. These versatile scaffolds can be utilized in tissue engineering, drug delivery, organoids, organ chips, biosensing, and more applications. Future advancements in this technology can be achieved by employing multifaceted and multiparameter methods to better support both research and clinical treatment.

Acknowledgments

None

Funding

This work was supported by the Hunan Provincial Health Commission Scientific Research Project, China (C202304106744).

Conflict of interest

The authors declared no potential conflicts of interest with respect to the research, authorship, and publication of this article.

Author contributions

Conceptualization: Naisi Shen, Bairong Fang, Liangle Liu
Investigation: Naisi Shen, Zhen Li, Pu Yang, Xiangjun Liu, Yikun Ju, Yue Hu
Writing – original draft: Naisi Shen
Writing – review & editing: All authors

Ethics approval and consent to participate

Not applicable.

Consent for publication

Not applicable.

Availability of data

Not applicable.

References

1. Ravi M, Paramesh V, Kaviya SR, Anuradha E, Solomon FD. 3D cell culture systems: advantages and applications. *J Cell Physiol*. 2015;230:16-26. doi: 10.1002/jcp.24683
2. Shankar V, van Blitterswijk C, Vrij E, Giselbrecht S. Automated, high-throughput phenotypic screening and analysis platform to study pre- and post-implantation morphogenesis in stem cell-derived embryo-like structures. *Adv Sci (Weinh)*. 2023;11(4):2304987. doi: 10.1002/advs.202304987
3. Jensen C, Teng Y. Is it time to start transitioning from 2D to 3D cell culture?, *Front Mol Biosci*. 2020;7:33. doi: 10.3389/fmolb.2020.00033
4. Groll J, Burdick JA, Cho DW, et al. A definition of bioinks and their distinction from biomaterial inks. *Biofabrication*. 2018;11:013001. doi: 10.1088/1758-5090/aaec52
5. Raja IS, Kang MS, Hong SW, et al. State-of-the-art techniques for promoting tissue regeneration: combination of three-dimensional bioprinting and carbon nanomaterials. *Int J Bioprint*. 2023;9:635. doi: 10.18063/ijb.v9i1.635
6. Mandrycky C, Wang Z, Kim K, Kim DH. 3D bioprinting for engineering complex tissues. *Biotechnol Adv*. 2016;34:422-434. doi: 10.1016/j.biotechadv.2015.12.011
7. Peng X, Wu S, Sun X, et al. 4D printing of freestanding liquid crystal elastomers via hybrid additive manufacturing. *Adv Mater*. 2022;34:e2204890. doi: 10.1002/adma.202204890
8. Mainik P, Spiegel CA, Blasco E. Recent advances in multi-photon 3D laser printing: active materials and applications. *Adv Mater.* 2024;36(11):e2310100. doi: 10.1002/adma.202310100
9. Tuan RS, Boland G, Tuli R. Adult mesenchymal stem cells and cell-based tissue engineering. *Arthritis Res Ther*. 2003;5:32-45. doi: 10.1186/ar614
10. Klebe RJ. Cytoscribing: a method for micropositioning cells and the construction of two- and three-dimensional synthetic tissues. *Exp Cell Res*. 1988;179:362-373. doi: 10.1016/0014-4827(88)90275-3
11. Li X, Liu B, Pei B, et al. Inkjet bioprinting of biomaterials. *Chem Rev*. 2020;120:10793-10833. doi: 10.1021/acs.chemrev.0c00008
12. Miri AK, Mirzaee I, Hassan S, et al. Effective bioprinting resolution in tissue model fabrication. *Lab Chip*. 2019;19: 2019-2037. doi: 10.1039/c8lc01037d
13. Cui X, Boland T, D'Lima DD, Lotz MK. Thermal inkjet printing in tissue engineering and regenerative medicine. *Recent Pat Drug Deliv Formul*. 2012;6:149-155. doi: 10.2174/187221112800672949
14. Guillemot F, Souquet A, Catros S, et al. High-throughput laser printing of cells and biomaterials for tissue engineering. *Acta Biomater*. 2010;6:2494-2500. doi: 10.1016/j.actbio.2009.09.029
15. Pepper ME, Seshadri V, Burg TC, Burg KJ, Groff RE. Characterizing the effects of cell settling on bioprinter output. *Biofabrication*. 2012;4:011001. doi: 10.1088/1758-5082/4/1/011001
16. Courson R, Bratash O, Maziz A, et al. Rapid prototyping of a polymer MEMS droplet dispenser by laser-assisted 3D printing. *Microsyst Nanoeng*. 2023;9:85. doi: 10.1038/s41378-023-00559-3
17. Gruene M, Deiwick A, Koch L, et al. Laser printing of stem cells for biofabrication of scaffold-free autologous grafts. *Tissue Eng Part C Methods*. 2011;17:79-87.

doi: 10.1089/ten.TEC.2010.0359

18. Daly AC, Prendergast ME, Hughes AJ, Burdick JA. Bioprinting for the biologist. *Cell*. 2021;184:18-32. doi: 10.1016/j.cell.2020.12.002

19. Askari M, Afzali Naniz M, Kouhi M, Saberi A, Zolfagharian A, Bodaghi M. Recent progress in extrusion 3D bioprinting of hydrogel biomaterials for tissue regeneration: a comprehensive review with focus on advanced fabrication techniques. *Biomater Sci*. 2021;9:535-573. doi: 10.1039/d0bm00973c

20. Rocca M, Fragasso A, Liu W, Heinrich MA, Zhang YS. Embedded multimaterial extrusion bioprinting. *SLAS Technol*. 2018;23:154-163. doi: 10.1177/2472630317742071

21. Xu L, Varkey M, Jorgensen A, et al. Bioprinting small diameter blood vessel constructs with an endothelial and smooth muscle cell bilayer in a single step. *Biofabrication*. 2020;12:045012. doi: 10.1088/1758-5090/aba2b6

22. Lian L, Zhou C, Tang G, et al. Uniaxial and coaxial vertical embedded extrusion bioprinting. *Adv Healthc Mater*. 2022;11(9):e2102411. doi: 10.1002/adhm.202102411

23. Malekpour A, Chen X. Printability and cell viability in extrusion-based bioprinting from experimental, computational, and machine learning views. *J Funct Biomater*. 2022;13(2):40. doi: 10.3390/jfb13020040

24. Lan X, Adesida A, Boluk Y. Rheological and viscoelastic properties of collagens and their role in bioprinting by micro-extrusion. *Biomed Mater*. 2022;17(6). doi: 10.1088/1748-605X/ac9b06

25. Tappa K, Jammalamadaka U. Novel biomaterials used in medical 3D printing techniques. *J Funct Biomater*. 2018;9(1):17. doi: 10.3390/jfb9010017

26. Ismail KI, Yap TC, Ahmed R. 3D-printed fiber-reinforced polymer composites by fused deposition modelling (FDM): fiber length and fiber implementation techniques. *Polymers (Basel)*. 2022;14(21):4659. doi: 10.3390/polym14214659

27. Krueger L, Miles JA, Popat A. 3D printing hybrid materials using fused deposition modelling for solid oral dosage forms. *J Control Release*. 2022;351:444-455. doi: 10.1016/j.jconrel.2022.09.032

28. Kumar H, Kim K. Stereolithography 3D bioprinting. *Methods Mol Biol*. 2020;2140:93-108. doi: 10.1007/978-1-0716-0520-2_6

29. Morano C, Pagnotta L. Additive manufactured parts produced using selective laser sintering technology: comparison between porosity of pure and blended polymers. *Polymers (Basel)*. 2023;15(22):4446. doi: 10.3390/polym15224446

30. Mazzoli A. Selective laser sintering in biomedical engineering. *Med Biol Eng Comput*. 2013;51(3):245-256. doi: 10.1007/s11517-012-1001-x

31. Shirazi SF, Gharehkhani S, Mehrali M, et al. A review on powder-based additive manufacturing for tissue engineering: selective laser sintering and inkjet 3D printing. *Sci Technol Adv Mater*. 2015;16:033502. doi: 10.1088/1468-6996/16/3/033502

32. Su X, Wang T, Guo S. Applications of 3D printed bone tissue engineering scaffolds in the stem cell field. *Regen Ther*. 2021;16:63-72. doi: 10.1016/j.reth.2021.01.007

33. Kafle A, Luis E, Silwal R, Pan HM, Shrestha PL, Bastola AK. 3D/4D printing of polymers: fused deposition modelling (FDM), selective laser sintering (SLS), and stereolithography (SLA). *Polymers (Basel)*. 2021;13(18):3101. doi: 10.3390/polym13183101

34. Li YC, Zhang YS, Akpek A, Shin SR, Khademhosseini A. 4D bioprinting: the next-generation technology for biofabrication enabled by stimuli-responsive materials. *Biofabrication*. 2016;9:012001. doi: 10.1088/1758-5090/9/1/012001

35. Ong CS, Nam L, Ong K, et al. 3D and 4D bioprinting of the myocardium: current approaches, challenges, and future prospects. *Biomed Res Int*. 2018;2018: 6497242. doi: 10.1155/2018/6497242

36. Miao S, Cui H, Nowicki M, et al. Stereolithographic 4D bioprinting of multiresponsive architectures for neural engineering. *Adv Biosyst*. 2018;2(9):1800101. doi: 10.1002/adbi.201800101

37. Hua M, Wu D, Wu S, Ma Y, Alsaid Y, He X. 4D printable tough and thermoresponsive hydrogels. *ACS Appl Mater Interfaces*. 2021;13:12689-12697. doi: 10.1021/acsami.0c17532

38. Guo Y, Belgodere JA, Ma Y, Jung JP, Bharti B. Directed printing and reconfiguration of thermoresponsive Silica-pNIPAM nanocomposites. *Macromol Rapid Commun*. 2019;40(13):e1900191. doi: 10.1002/marc.201900191

39. Pan HM, Goto A. Topology-dependent pH-responsive actuation and shape memory programming for biomimetic 4D printing. *Macromol Rapid Commun*. 2023;44:e2300074. doi: 10.1002/marc.202300074

40. Tahouni Y, Cheng T, Lajewski S, et al. Codesign of biobased cellulose-filled filaments and mesostructures for 4D printing humidity responsive smart structures. *3D Print Addit Manuf*. 2023;10(1):1-14. doi: 10.1089/3dp.2022.0061

41. Wychowaniec JK, Brougham DF. Emerging magnetic fabrication technologies provide controllable hierarchically-structured biomaterials and stimulus response for biomedical applications. *Adv Sci (Weinh)*. 2022;9:e2202278.

doi: 10.1002/advs.202202278.

42. Capakova Z, Radaszkiewicz KA, Acharya TH, et al. The biocompatibility of polyaniline and polypyrrole 2: doping with organic phosphonates. *Mater Sci Eng C Mater Biol Appl*. 2020;113:110986. doi: 10.1016/j.msec.2020.110986.

43. Noroozi R, Bodaghi M, Jafari H, Zolfagharian A, Fotouhi M. Shape-adaptive metastructures with variable Bandgap regions by 4D printing. *Polymers (Basel)*. 2020;12(3):519. doi: 10.3390/polym12030519

44. Ashammakhi N, Ahadian S, Zengjie F, et al. Advances and future perspectives in 4D bioprinting. *Biotechnol J*. 2018;13:e1800148. doi: 10.1002/biot.201800148

45. Kuribayashi-Shigetomi K, Onoe H, Takeuchi S. Cell origami: self-folding of three-dimensional cell-laden microstructures driven by cell traction force. *PLoS One*. 2012;7:e51085. doi: 10.1371/journal.pone.0051085

46. Devillard R, Pages E, Correa MM, et al. Cell patterning by laser-assisted bioprinting. *Methods Cell Biol*. 2014;119:159-174. doi: 10.1016/B978-0-12-416742-1.00009-3

47. Placone JK, Engler AJ. Recent advances in extrusion-based 3D printing for biomedical applications. *Adv Healthc Mater*. 2018;7:e1701161. doi: 10.1002/adhm.201701161.

48. Hwang HH, Zhu W, Victorine G, Lawrence N, Chen S. 3D-printing of functional biomedical microdevices via light- and extrusion-based approaches. *Small Methods*. 2018;2(2):1700277. doi: 10.1002/smtd.201700277

49. Murphy SV, Atala A. 3D bioprinting of tissues and organs. *Nat Biotechnol*. 2014;32:773-785. doi: 10.1038/nbt.2958

50. Cadamuro F, Nicotra F, Russo L. 3D printed tissue models: from hydrogels to biomedical applications. *J Control Release*. 2023;354:726-745. doi: 10.1016/j.jconrel.2023.01.048

51. Jia L, Hua Y, Zeng J, et al. Bioprinting and regeneration of auricular cartilage using a bioactive bioink based on microporous photocrosslinkable acellular cartilage matrix. *Bioact Mater*. 2022;16:66-81. doi: 10.1016/j.bioactmat.2022.02.032

52. Ojansivu M, Rashad A, Ahlinder A, et al. Wood-based nanocellulose and bioactive glass modified gelatin-alginate bioinks for 3D bioprinting of bone cells. *Biofabrication*. 2019;11:035010. doi: 10.1088/1758-5090/ab0692

53. Moncal KK, Ozbolat V, Datta P, Heo DN, Ozbolat IT. Thermally-controlled extrusion-based bioprinting of collagen. *J Mater Sci Mater Med*. 2019;30:55. doi: 10.1007/s10856-019-6258-2

54. Benson K, Galla HJ, Kehr NS. Cell adhesion behavior in 3D hydrogel scaffolds functionalized with D- or L-aminoacids. *Macromol Biosci*. 2014;14:793-798. doi: 10.1002/mabi.201300485

55. Sigaux N, Pourchet L, Breton P, Brosset S, Louvrier A, Marquette CA. 3D bioprinting:principles, fantasies and prospects. *J Stomatol Oral Maxillofac Surg*. 2019;120:128-132. doi: 10.1016/j.jormas.2018.12.014

56. Yao B, Hu T, Cui X, Song W, Fu X, Huang S. Enzymatically degradable alginate/gelatin bioink promotes cellular behavior and degradation in vitro and in vivo. *Biofabrication*. 2019;11:045020. doi: 10.1088/1758-5090/ab38ef

57. Duan B, Hockaday LA, Kang KH, Butcher JT. 3D bioprinting of heterogeneous aortic valve conduits with alginate/gelatin hydrogels. *J Biomed Mater Res A*. 2013;101:1255-1264. doi: 10.1002/jbm.a.34420

58. Michael S, Sorg H, Peck CT, et al. Tissue engineered skin substitutes created by laser-assisted bioprinting form skin-like structures in the dorsal skin fold chamber in mice. *PLoS One*. 2013;8:e57741. doi: 10.1371/journal.pone.0057741

59. Visser J, Peters B, Burger TJ, et al. Biofabrication of multi-material anatomically shaped tissue constructs. *Biofabrication*. 2013;5:035007. doi: 10.1088/1758-5082/5/3/035007

60. Owens CM, Marga F, Forgacs G, Heesch CM. Biofabrication and testing of a fully cellular nerve graft. *Biofabrication*. 2013;5:045007. doi: 10.1088/1758-5082/5/4/045007

61. Xiao S, Zhao T, Wang J, et al. Gelatin methacrylate (GelMA)-based hydrogels for cell transplantation: an effective strategy for tissue engineering. *Stem Cell Rev Rep*. 2019;15:664-679. doi: 10.1007/s12015-019-09893-4

62. Ozbolat IT, Yu Y. Bioprinting toward organ fabrication: challenges and future trends. *IEEE Trans Biomed Eng*. 2013;60:691-699. doi: 10.1109/TBME.2013.2243912

63. Kolesky DB, Truby RL, Gladman AS, Busbee TA, Homan KA, Lewis JA. 3D bioprinting of vascularized, heterogeneous cell-laden tissue constructs. *Adv Mater*. 2014;26:3124-3130. doi: 10.1002/adma.201305506

64. Abdollahi Baghban S, Ebrahimi M, Bagheri-Khoulenjani S, Khorasani M. A highly efficient microwave-assisted synthesis of an LED-curable methacrylated gelatin for bio applications. *RSC Adv*. 2021;11:14996-15009. doi: 10.1039/d1ra01269j

65. Purcell BP, Elser JA, Mu A, Margulies KB, Burdick JA. Synergistic effects of SDF-1alpha chemokine and hyaluronic acid release from degradable hydrogels on directing bone marrow derived cell homing to the myocardium. *Biomaterials*. 2012;33:7849-7857.

doi: 10.1016/j.biomaterials.2012.07.005

66. Burkhart A, Ritter H. Influence of cyclodextrin on the UCST- and LCST-behavior of poly(2-methacrylamido-caprolactam)-co-(N,N-dimethylacrylamide). *Beilstein J Org Chem*. 2014;10:1951-1958.
doi: 10.3762/bjoc.10.203

67. Yue K, Trujillo-de Santiago G, Alvarez MM, Tamayol A, Annabi N, Khademhosseini A. Synthesis, properties, and biomedical applications of gelatin methacryloyl (GelMA) hydrogels. *Biomaterials*. 2015;73:254-271.
doi: 10.1016/j.biomaterials.2015.08.045

68. Schuurmans CCL, Mihajlovic M, Hiemstra C, Ito K, Hennink WE, Vermonden T. Hyaluronic acid and chondroitin sulfate (meth)acrylate-based hydrogels for tissue engineering: synthesis, characteristics and pre-clinical evaluation. *Biomaterials*. 2021;268:120602.
doi: 10.1016/j.biomaterials.2020.120602

69. Nichol JW, Koshy ST, Bae H, Hwang CM, Yamanlar S, Khademhosseini A. Cell-laden microengineered gelatin methacrylate hydrogels. *Biomaterials*. 2010;31:5536-5544.
doi: 10.1016/j.biomaterials.2010.03.064

70. Sun M, Sun X, Wang Z, Guo S, Yu G, Yang H. Synthesis and properties of gelatin methacryloyl (GelMA) hydrogels and their recent applications in load-bearing tissue. *Polymers (Basel)*. 2018;10(11):1290.
doi: 10.3390/polym10111290

71. Zhu M, Wang Y, Ferracci G, Zheng J, Cho NJ, Lee BH. Gelatin methacryloyl and its hydrogels with an exceptional degree of controllability and batch-to-batch consistency. *Sci Rep*. 2019;9:6863.
doi: 10.1038/s41598-019-42186-x

72. Janmaleki M, Liu J, Kamkar M, Azarmanesh M, Sundararaj U, Nezhad AS. Role of temperature on bio-printability of gelatin methacryloyl bioink in two-step cross-linking strategy for tissue engineering applications. *Biomed Mater*. 2020;16:015021.
doi: 10.1088/1748-605X/abbcc9

73. He Q, Cheng Y, Deng Y, Wen F, Lai Y, Li H. Conductive hydrogel for flexible bioelectronic device: current progress and future perspective. *Adv Funct Mater*. 2024;34(1):2308974.
doi: 10.1002/adfm.202308974

74. Goodarzi Hosseinabadi H, Dogan E, Miri AK, Ionov L. Digital light processing bioprinting advances for microtissue models. *ACS Biomater Sci Eng*. 2022;8:1381-1395.
doi: 10.1021/acsbiomaterials.1c01509

75. Li L, Scheiger JM, Levkin PA. Design and applications of photoresponsive hydrogels. *Adv. Mater*. 2019;31:e1807333.
doi: 10.1002/adma.201807333

76. Ruiz-Cantu L, Gleadall A, Faris C, Segal J, Shakesheff K, Yang J. Multi-material 3D bioprinting of porous constructs for cartilage regeneration. *Mater Sci Eng C Mater Biol Appl*. 2020;109:110578.
doi: 10.1016/j.msec.2019.110578

77. Raees S, Ullah F, Javed F, et al. Classification, processing, and applications of bioink and 3D bioprinting: a detailed review. *Int J Biol Macromol*.2023;232:123476.
doi: 10.1016/j.ijbiomac.2023.123476.

78. Lu D, Zeng Z, Geng Z, et al. Macroporous methacrylated hyaluronic acid hydrogel with different pore sizes for in vitro and in vivo evaluation of vascularization. *Biomed Mater*. 2022;17.
doi: 10.1088/1748-605X/ac494b

79. Chimene D, Kaunas R, Gaharwar AK. Hydrogel bioink reinforcement for additive manufacturing: a focused review of emerging strategies. *Adv Mater*. 2020;32:e1902026.
doi: 10.1002/adma.201902026

80. Klotz BJ, Gawlitta D, Rosenberg A, Malda J, Melchels FPW. Gelatin-methacryloyl hydrogels: towards biofabrication-based tissue repair. *Trends Biotechnol*. 2016;34:394-407.
doi: 10.1016/j.tibtech.2016.01.002

81. Kurian AG, Singh RK, Patel KD, Lee JH, Kim HW. Multifunctional GelMA platforms with nanomaterials for advanced tissue therapeutics. *Bioact Mater*. 2022;8:267-295.
doi: 10.1016/j.bioactmat.2021.06.027

82. Dong Z, Yuan Q, Huang K, Xu W, Liu G, Gu Z. Gelatin methacryloyl (GelMA)-based biomaterials for bone regeneration. *RSC Adv*. 2019;9:17737-17744.
doi: 10.1039/c9ra02695a.

83. Schuurman W, Levett PA, Pot MW, et al. Gelatin-methacrylamide hydrogels as potential biomaterials for fabrication of tissue-engineered cartilage constructs. *Macromol Biosci*. 2013;13:551-561.
doi: 10.1002/mabi.201200471

84. Zheng H, Zuo B. Functional silk fibroin hydrogels: preparation, properties and applications. *J Mater Chem B*. 2021;9:1238-1258.
doi: 10.1039/d0tb02099k

85. Liu H, Sun Z, Guo C. Chemical modification of silk proteins: current status and future prospects. *Adv Fiber Mater*. 2022;4:705-719.
doi: 10.1007/s42765-022-00144-9.

86. Sun W, Gregory DA, Tomeh MA, Zhao X. Silk fibroin as a functional biomaterial for tissue engineering. *Int J Mol Sci*. 2021;22(3):1499.
doi: 10.3390/ijms22031499

87. Kim SH, Hong H, Ajiteru O, et al. 3D bioprinted silk fibroin hydrogels for tissue engineering. *Nat Protoc*. 2021;16:5484-5532.
doi: 10.1038/s41596-021-00622-1

88. Kim SH, Seo YB, Yeon YK, et al. 4D-bioprinted silk hydrogels for tissue engineering. *Biomaterials*. 2020;260:120281.

doi: 10.1016/j.biomaterials.2020.120281.

89. Kim SH, Yeon YK, Lee JM, et al. Precisely printable and biocompatible silk fibroin bioink for digital light processing 3D printing. *Nat Commun*. 2018;9:1620. doi: 10.1038/s41467-018-03759-y

90. Liu J, Shi L, Deng Y, et al. Silk sericin-based materials for biomedical applications. *Biomaterials*. 2022;287: 121638. doi: 10.1016/j.biomaterials.2022.121638

91. Qi C, Liu J, Jin Y, et al. Photo-crosslinkable, injectable sericin hydrogel as 3D biomimetic extracellular matrix for minimally invasive repairing cartilage. *Biomaterials*. 2018;163:89-104. doi: 10.1016/j.biomaterials.2018.02.016

92. Spada A, Emami J, Tuszynski JA, Lavasanifar A. The uniqueness of albumin as a Carrier in Nanodrug Delivery. *Mol Pharm*. 2021;18:1862-1894. doi: 10.1021/acs.molpharmaceut.1c00046

93. Khanna S, Singh AK, Behera SP, Gupta S. Thermoresponsive BSA hydrogels with phase tunability. *Mater Sci Eng C Mater Biol Appl*. 2021;119:111590. doi: 10.1016/j.msec.2020.111590.

94. Chen Y, Zhai MJ, Mehwish N, et al. Comparison of globular albumin methacryloyl and random-coil gelatin methacryloyl: preparation, hydrogel properties, cell behaviors, and mineralization. *Int J Biol Macromol*. 2022;204:692-708. doi: 10.1016/j.ijbiomac.2022.02.028

95. Patrawalla NY, Kajave NS, Albanna MZ, Kishore V. Collagen and beyond: a comprehensive comparison of human ECM properties derived from various tissue sources for regenerative medicine applications. *J Funct Biomater*. 2023;14(7):363. doi: 10.3390/jfb14070363

96. Marques CF, Diogo GS, Pina S, Oliveira JM, Silva TH, Reis RL. Collagen-based bioinks for hard tissue engineering applications: a comprehensive review. *J Mater Sci Mater Med*. 2019;30:32. doi: 10.1007/s10856-019-6234-x

97. Wang Z, Yang Y, Gao Y, Xu Z, Yang S, Jin M. Establishing a novel 3D printing bioinks system with recombinant human collagen. *Int J Biol Macromol*. 2022;211:400-409. doi: 10.1016/j.ijbiomac.2022.05.088

98. Mostert D, Jorba I, Groenen BGW, et al. Methacrylated human recombinant collagen peptide as a hydrogel for manipulating and monitoring stiffness-related cardiac cell behavior. *iScience*. 2023;26:106423. doi: 10.1016/j.isci.2023.106423

99. Zhou J, Wen B, Xie H, et al. Advances in the preparation and assessment of the biological activities of chitosan oligosaccharides with different structural characteristics. *Food Funct*. 2021;12:926-951. doi: 10.1039/d0fo02768e

100. Yang M, Wang H, Li K, Chen Z, Seamirumi DT. A new soft tissue constructed with chitosan for wound dressings-incorporating nanoparticles for medical and nursing therapeutic efficacy. *Regen Ther*. 2023;24:103-111. doi: 10.1016/j.reth.2023.06.005

101. Ailincai D, Cibotaru S, Anisiei A, et al. Marin, mesoporous chitosan nanofibers loaded with norfloxacin and coated with phenylboronic acid perform as bioabsorbable active dressings to accelerate the healing of burn wounds. *Carbohydr Polym*. 2023;318:121135. doi: 10.1016/j.carbpol.2023.121135.

102. Yang Y, Ma Y, Wang J, et al. Chitosan-based mussel-inspired hydrogel for rapid self-healing and high adhesion of tissue adhesion and wound dressings. *Carbohydr Polym*. 2023;316:121083. doi: 10.1016/j.carbpol.2023.121083

103. Wang W, Xue C, Mao X. Chitosan: structural modification, biological activity and application. *Int J Biol Macromol*. 2020;164:4532-4546. doi: 10.1016/j.ijbiomac.2020.09.042

104. Shen Y, Tang H, Huang X, et al. DLP printing photocurable chitosan to build bio-constructs for tissue engineering. *Carbohydr Polym*. 2020;235:115970. doi: 10.1016/j.carbpol.2020.115970

105. Aguirre G, Billon L. Water-borne synthesis of multi-responsive and biodegradable chitosan-crosslinked microgels: towards self-assembled films with adaptable properties. *Carbohydr Polym*. 2023;318:121099. doi: 10.1016/j.carbpol.2023.121099

106. Song F, Kong Y, Shao C, et al. Chitosan-based multifunctional flexible hemostatic bio-hydrogel. *Acta Biomater*. 2021;136:170-183. doi: 10.1016/j.actbio.2021.09.056

107. He X, Liu X, Yang J, et al. Tannic acid-reinforced methacrylated chitosan/methacrylated silk fibroin hydrogels with multifunctionality for accelerating wound healing. Carbohydr Polym. 2020;247:116689. doi: 10.1016/j.carbpol.2020.116689

108. Wei H, Yu S, Zhang Y, et al. Injectable chitosan/xyloglucan composite hydrogel with mechanical adaptivity and endogenous bioactivity for skin repair. *Carbohydr Polym*. 2023;313:120904. doi: 10.1016/j.carbpol.2023.120904

109. Yoon SJ, Kim SH, Choi JW, Chun HJ, Yang DH. Guided cortical and cancellous bone formation using a minimally invasive technique of BMSC- and BMP-2-laden visible light-cured carboxymethyl chitosan hydrogels. *Int J Biol Macromol*. 2023;227:641-653. doi: 10.1016/j.ijbiomac.2022.12.137

110. Chen Y, Sheng W, Lin J, et al. Magnesium oxide nanoparticle coordinated phosphate-functionalized chitosan injectable hydrogel for osteogenesis and angiogenesis in bone regeneration. *ACS Appl Mater Interfaces*. 2022;14:7592-7608.

doi: 10.1021/acsami.1c21260

111. Carvalho CR, Wrobel S, Meyer C, et al. Gellan Gum-based luminal fillers for peripheral nerve regeneration: an in vivo study in the rat sciatic nerve repair model. *Biomater Sci*. 2018;6:1059-1075. doi: 10.1039/c7bm01101f

112. Chen F, Huang G, Huang H. Preparation and application of dextran and its derivatives as carriers. *Int J Biol Macromol*. 2020;145:827-834. doi: 10.1016/j.ijbiomac.2019.11.151

113. Sun G, Mao JJ. Engineering dextran-based scaffolds for drug delivery and tissue repair. *Nanomedicine (Lond)*. 2012;7:1771-1784. doi: 10.2217/nnm.12.149

114. Yang R, Xue W, Liao H, et al. Injectable polylysine and dextran hydrogels with robust antibacterial and ROS-scavenging activity for wound healing. *Int J Biol Macromol*. 2022;223:950-960. doi: 10.1016/j.ijbiomac.2022.11.065

115. Zhao B, Zhang Y, Li D, Mo X, Pan J. Hofmeister effect-enhanced gelatin/oxidized dextran hydrogels with improved mechanical properties and biocompatibility for wound healing. *Acta Biomater*. 2022;151:235-253. doi: 10.1016/j.actbio.2022.08.009

116. Kolahdoozan M, Rahimi T, Taghizadeh A, Aghaei H. Preparation of new hydrogels by visible light cross-linking of dextran methacrylate and poly(ethylene glycol)-maleic acid copolymer. *Int J Biol Macromol*. 2023;227:1221-1233. doi: 10.1016/j.ijbiomac.2022.11.309

117. Huang S, Liu H, Huang S, Fu T, Xue W, Guo R. Dextran methacrylate hydrogel microneedles loaded with doxorubicin and trametinib for continuous transdermal administration of melanoma. *Carbohydr Polym*. 2020;246:116650. doi: 10.1016/j.carbpol.2020.116650

118. Wang H, Zhou L, Liao J, et al. Cell-laden photocrosslinked GelMA-DexMA copolymer hydrogels with tunable mechanical properties for tissue engineering. *J Mater Sci Mater Med*. 2014;25:2173-2183. doi: 10.1007/s10856-014-5261-x

119. Sun G, Zhang X, Shen YI, et al. Dextran hydrogel scaffolds enhance angiogenic responses and promote complete skin regeneration during burn wound healing. *Proc Natl Acad Sci U S A*. 2011;108: 20976-20981. doi: 10.1073/pnas.1115973108

120. Dhamecha D, Movsas R, Sano U, Menon JU. Applications of alginate microspheres in therapeutics delivery and cell culture: past, present and future. *Int J Pharm*. 2019;569:118627. doi: 10.1016/j.ijpharm.2019.118627

121. Rastogi P, Kandasubramanian B. Review of alginate-based hydrogel bioprinting for application in tissue engineering. *Biofabrication*. 2019;11:042001. doi: 10.1088/1758-5090/ab331e

122. Charron PN, Fenn SL, Poniz A, Oldinski RA. Mechanical properties and failure analysis of visible light crosslinked alginate-based tissue sealants. *J Mech Behav Biomed Mater*. 2016;59:314-321. doi: 10.1016/j.jmbbm.2016.02.003

123. Samorezov JE, Morlock CM, Alsberg E. Dual ionic and photo-crosslinked alginate hydrogels for micropatterned spatial control of material properties and cell behavior. *Bioconjug Chem*. 2015;26:1339-1347. doi: 10.1021/acs.bioconjchem.5b00117

124. Gao Y, Jin X. Dual crosslinked methacrylated alginate hydrogel micron fibers and tissue constructs for cell biology. Mar Drugs. 2019;17:557. doi: 10.3390/md17100557

125. Garcia-Lizarribar A, Villasante A, Lopez-Martin JA, et al. 3D bioprinted functional skeletal muscle models have potential applications for studies of muscle wasting in cancer cachexia. *Biomater Adv*. 2023;150:213426. doi: 10.1016/j.bioadv.2023.213426

126. Fenn SL, Miao T, Scherrer RM, Floreani RA. Dual-cross-linked methacrylated alginate sub-microspheres for intracellular chemotherapeutic delivery. *ACS Appl Mater Interfaces*. 2016;8:17775-17783. doi: 10.1021/acsami.6b03245

127. Wang Y, Li S, Xu X, Tan Y, Liu XW, Fang J. Chemoenzymatic synthesis of homogeneous chondroitin polymers and its derivatives. *Carbohydr Polym*. 2020;232:115822. doi: 10.1016/j.carbpol.2019.115822

128. Bishnoi M, Jain A, Hurkat P, Jain SK. Chondroitin sulphate: a focus on osteoarthritis. *Glycoconj J*. 2016;33:693-705. doi: 10.1007/s10719-016-9665-3

129. Mencio CP, Hussein RK, Yu P, Geller HM. The role of chondroitin sulfate proteoglycans in nervous system development. *J Histochem Cytochem*. 2021;69:61-80. doi: 10.1369/0022155420959147

130. Ida-Yonemochi H, Takeuchi K, Ohshima H. Role of chondroitin sulfate in the developmental and healing process of the dental pulp in mice. *Cell Tissue Res*. 2022;388:133-148. doi: 10.1007/s00441-022-03575-3

131. Lin JZ, Duan MR, Lin N, Zhao WJ. The emerging role of the chondroitin sulfate proteoglycan family in neurodegenerative diseases. *Rev Neurosci*. 2021;32:737-750. doi: 10.1515/revneuro-2020-0146

132. Yang S, Gigout S, Molinaro A, et al. Chondroitin 6-sulphate is required for neuroplasticity and memory in ageing. *Mol Psychiatry*. 2021;26:5658-5668. doi: 10.1038/s41380-021-01208-9

133. Morla S. Glycosaminoglycans and glycosaminoglycan mimetics in cancer and inflammation. *Int J Mol Sci*. 2019;20(8):1963. doi: 10.3390/ijms20081963

134. Grzanna MW, Au RY, Au AY, Rashmir AM, Frondoza CG. Avocado/soybean unsaponifiables, glucosamine and chondroitin sulfate combination inhibits proinflammatory cox-2 expression and prostaglandin e2 production in tendon-derived cells. *J Med Food*. 2020;23:139-146. doi: 10.1089/jmf.2019.0022

135. Pudelko A, Wisowski G, Olczyk K, Kozma EM. The dual role of the glycosaminoglycan chondroitin-6-sulfate in the development, progression and metastasis of cancer. *FEBS J*. 2019;286:1815-1837. doi: 10.1111/febs.14748

136. Ornell KJ, Lozada D, Phan NV, Coburn JM. Controlling methacryloyl substitution of chondroitin sulfate: injectable hydrogels with tunable long-term drug release profiles. *J Mater Chem B*. 2019;7:2151-2161. doi: 10.1039/c8tb03020k

137. He Y, Sun M, Wang J, et al. Chondroitin sulfate microspheres anchored with drug-loaded liposomes play a dual antioxidant role in the treatment of osteoarthritis. *Acta Biomater*. 2022;151:512-527. doi: 10.1016/j.actbio.2022.07.052

138. Liu C, Fan L, Xing J, et al. Inhibition of astrocytic differentiation of transplanted neural stem cells by chondroitin sulfate methacrylate hydrogels for the repair of injured spinal cord. *Biomater Sci*. 2019;7:1995-2008. doi: 10.1039/c8bm01363b

139. Silva ED, Babo PS, Costa-Almeida R, et al. Multifunctional magnetic-responsive hydrogels to engineer tendon-to-bone interface. *Nanomedicine*. 2018;14:2375-2385. doi: 10.1016/j.nano.2017.06.002

140. Le HV, Le Cerf D. Colloidal polyelectrolyte complexes from hyaluronic acid: preparation and biomedical applications. *Small*. 2022;18:e2204283. doi: 10.1002/smll.202204283.

141. Xia C, Chen P, Mei S, et al. Photo-crosslinked HAMA hydrogel with cordycepin encapsulated chitosan microspheres for osteoarthritis treatment. *Oncotarget*. 2017;8: 2835-2849. doi: 10.18632/oncotarget.13748

142. Mouser VH, Abbadessa A, Levato R, et al. Development of a thermosensitive HAMA-containing bio-ink for the fabrication of composite cartilage repair constructs. *Biofabrication*. 2017;9:015026. doi: 10.1088/1758-5090/aa6265

143. Wei S, Wang Z, Liang X, et al. A composite hydrogel with antibacterial and promoted cell proliferation dual properties for healing of infected wounds. *Am J Transl Res*. 2023;15:4467-4486.

144. Xu Z, Liu G, Liu P, et al. Hyaluronic acid-based glucose-responsive antioxidant hydrogel platform for enhanced diabetic wound repair. *Acta Biomater*. 2022;147:147-157. doi: 10.1016/j.actbio.2022.05.047

145. Shen J, Chen A, Cai Z, et al. Exhausted local lactate accumulation via injectable nanozyme-functionalized hydrogel microsphere for inflammation relief and tissue regeneration. *Bioact Mater*. 2022;12:153-168. doi: 10.1016/j.bioactmat.2021.10.013

146. Shen X, Li S, Zhao X, et al. Dual-crosslinked regenerative hydrogel for sutureless long-term repair of corneal defect. *Bioact Mater*. 2023;20:434-448. doi: 10.1016/j.bioactmat.2022.06.006

147. Jung M, Han Y, Woo C, Ki CS. Pulmonary tissue-mimetic hydrogel niches for small cell lung cancer cell culture. *J Mater Chem B*. 2021;9:1858-1866. doi: 10.1039/d0tb02609c

148. Schuurmans CCL, Abbadessa A, Bengtson MA, et al. Complex coacervation-based loading and tunable release of a cationic protein from monodisperse glycosaminoglycan microgels. *Soft Matter*. 2018;14:6327-6341. doi: 10.1039/c8sm00686e

149. Wang L, Cao H, Jiang H, Fang Y, Jiang D. A novel 3D bio-printing "liver lobule" microtissue biosensor for the detection of AFB(1). *Food Res Int*. 2023;168:112778. doi: 10.1016/j.foodres.2023.112778

150. Huang YC, Liu ZH, Kuo CY, Chen JP. Photo-crosslinked hyaluronic acid/carboxymethyl cellulose composite hydrogel as a dural substitute to prevent post-surgical adhesion. *Int J Mol Sci*. 2022;23:6177. doi: 10.3390/ijms23116177

151. Yu Y, Xiao H, Tang G, et al. Biomimetic hydrogel derived from decellularized dermal matrix facilitates skin wounds healing. *Mater Today Bio*. 2023;21:100725. doi: 10.1016/j.mtbio.2023.100725

152. Liu F, Wang X, Li Y, et al. Dendrimer-modified gelatin methacrylate hydrogels carrying adipose-derived stromal/stem cells promote cartilage regeneration. *Stem Cell Res Ther*. 2022;13:26. doi: 10.1186/s13287-022-02705-6

153. Lim KS, Levato R, Costa PF, et al. Bio-resin for high resolution lithography-based biofabrication of complex cell-laden constructs. *Biofabrication*. 2018;10:034101. doi: 10.1088/1758-5090/aac00c

154. Simaan-Yameen H, Bar-Am O, Saar G, Seliktar D. Methacrylated fibrinogen hydrogels for 3D cell culture and delivery. *Acta Biomater*. 2023;164:94-110. doi: 10.1016/j.actbio.2023.03.046

155. Powers JG, Higham C, Broussard K, Phillips TJ. Wound healing and treating wounds: chronic wound care and management. *J Am Acad Dermatol*. 2016;74:607-625; quiz625-606. doi: 10.1016/j.jaad.2015.08.070

156. Wilkinson HN, Hardman MJ. Wound healing: cellular mechanisms and pathological outcomes. *Open Biol*. 2020;10:200223.

doi: 10.1098/rsob.200223

157. R Ibañez RI, do Amaral R, Reis RL, Marques AP, Murphy CM, O'Brien FJ. 3D-printed gelatin methacrylate scaffolds with controlled architecture and stiffness modulate the fibroblast phenotype towards dermal regeneration. *Polymers (Basel)*. 2021;13(15):2510. doi: 10.3390/polym13152510

158. Chen H, Ma X, Gao T, Zhao W, Xu T, Liu Z. Robot-assisted in situ bioprinting of gelatin methacrylate hydrogels with stem cells induces hair follicle-inclusive skin regeneration. *Biomed Pharmacother*. 2023;158:114140. doi: 10.1016/j.biopha.2022.114140

159. Jin R, Cui Y, Chen H, et al. Three-dimensional bioprinting of a full-thickness functional skin model using acellular dermal matrix and gelatin methacrylamide bioink. *Acta Biomater*. 2021;131:248-261. doi: 10.1016/j.actbio.2021.07.012

160. Zhang L, Yang G, Johnson BN, Jia X. Three-dimensional (3D) printed scaffold and material selection for bone repair. *Acta Biomater*. 2019;84:16-33. doi: 10.1016/j.actbio.2018.11.039

161. Ji C, Qiu M, Ruan H, et al. Transcriptome analysis revealed the symbiosis niche of 3d scaffolds to accelerate bone defect healing. *Adv Sci (Weinh)*. 2022;9:e2105194. doi: 10.1002/advs.202105194

162. Beheshtizadeh N, Farzin A, Rezvantalab S, et al. 3D printing of complicated GelMA-coated Alginate/Tri-calcium silicate scaffold for accelerated bone regeneration. *Int J Biol Macromol*. 2023;229:636-653. doi: 10.1016/j.ijbiomac.2022.12.267

163. Ma L, Wang X, Zhou Y, et al. Biomimetic Ti-6Al-4V alloy/gelatin methacrylate hybrid scaffold with enhanced osteogenic and angiogenic capabilities for large bone defect restoration. *Bioact Mater*. 2021;6:3437-3448. doi: 10.1016/j.bioactmat.2021.03.010

164. Ghahri T, Salehi Z, Aghajanpour S, et al. Development of osteon-like scaffold-cell construct by quadruple coaxial extrusion-based 3D bioprinting of nanocomposite hydrogel. *Biomater Adv*. 2023;145:213254. doi: 10.1016/j.bioadv.2022.213254

165. Alarcin E, Izbudak B, Yuce E, et al. Optimization of methacrylated gelatin /layered double hydroxides nanocomposite cell-laden hydrogel bioinks with high printability for 3D extrusion bioprinting. *J Biomed Mater Res A*. 2023;111:209-223. doi: 10.1002/jbm.a.37450

166. Nie R, Sun Y, Lv H, et al. 3D printing of MXene composite hydrogel scaffolds for photothermal antibacterial activity and bone regeneration in infected bone defect models. *Nanoscale*. 2022;14:8112-8129. doi: 10.1039/d2nr02176e

167. Wang L, Shen M, Hou Q, Wu Z, Xu J, Wang L. 3D printing of reduced glutathione grafted gelatine methacrylate hydrogel scaffold promotes diabetic bone regeneration by activating PI3K/Akt signaling pathway. *Int J Biol Macromol*. 2022;222:1175-1191. doi: 10.1016/j.ijbiomac.2022.09.236

168. Dutta SD, Ganguly K, Hexiu J, Randhawa A, Moniruzzaman M, Lim KT. A 3D bioprinted nanoengineered hydrogel with photoactivated drug delivery for tumor apoptosis and simultaneous bone regeneration via macrophage immunomodulation. *Macromol Biosci*. 2023;23(9):e2300096. doi: 10.1002/mabi.202300096

169. Liu G, Zhang B, Wan T, et al. A 3D-printed biphasic calcium phosphate scaffold loaded with platelet lysate/gelatin methacrylate to promote vascularization. *J Mater Chem B*. 2022;10:3138-3151. doi: 10.1039/d2tb00006g

170. Xu Z, Qi X, Bao M, et al. Biomineralization inspired 3D printed bioactive glass nanocomposite scaffolds orchestrate diabetic bone regeneration by remodeling micromilieu. *Bioact Mater*. 2023;25:239-255. doi: 10.1016/j.bioactmat.2023.01.024

171. Yang J, Fatima K, Zhou X, He C. Meticulously engineered three-dimensional-printed scaffold with microarchitecture and controlled peptide release for enhanced bone regeneration. *Biomater Transl*. 2024;5:69-83. doi: 10.12336/biomatertransl.2024.01.007

172. Li S, Li Z, Yang J, Ha Y, Zhou X, He C. Inhibition of sympathetic activation by delivering calcium channel blockers from a 3D printed scaffold to promote bone defect repair. *Adv Healthc Mater*. 2022;11:e2200785. doi: 10.1002/adhm.202200785

173. Zhang D, Fu Q, Fu H, Zeng J, Jia L, Chen M. 3D-bioprinted human lipoaspirate-derived cell-laden skin constructs for healing of full-thickness skin defects. *Int J Bioprint*. 2023;9:718. doi: 10.18063/ijb.718

174. Yu K, Huangfu H, Qin Q, et al. Application of bone marrow-derived macrophages combined with bone mesenchymal stem cells in dual-channel three-dimensional bioprinting scaffolds for early immune regulation and osteogenic induction in rat calvarial defects. *ACS Appl Mater Interfaces*. 2022;14:47052-47065. doi: 10.1021/acsami.2c13557

175. Yang Z, Cao F, Li H, et al. Microenvironmentally optimized 3D-printed TGFbeta-functionalized scaffolds facilitate endogenous cartilage regeneration in sheep. *Acta Biomater*. 2022;150:181-198. doi: 10.1016/j.actbio.2022.07.029

176. Xie X, Wu S, Mou S, Guo N, Wang Z, Sun J. Microtissue-based bioink as a chondrocyte microshelter for DLP bioprinting. *Adv Healthc Mater*. 2022;11:e2201877.

doi: 10.1002/adhm.202201877

177. Galliger Z, Vogt CD, Helms HR, Panoskaltsis-Mortari A. Extracellular matrix microparticles improve GelMA bioink resolution for 3D bioprinting at ambient temperature. *Macromol Mater Eng*. 2022;307(10):2200196. doi: 10.1002/mame.202200196

178. Zhu W, Cui H, Boualam B, et al. 3D bioprinting mesenchymal stem cell-laden construct with core-shell nanospheres for cartilage tissue engineering. *Nanotechnology*. 2018;29:185101. doi: 10.1088/1361-6528/aaafa1

179. Grogan SP, Chung PH, Soman P, et al. Digital micromirror device projection printing system for meniscus tissue engineering. *Acta Biomater*. 2013;9:7218-7226. doi: 10.1016/j.actbio.2013.03.020

180. Gong L, Li J, Zhang J, et al. An interleukin-4-loaded bi-layer 3D printed scaffold promotes osteochondral regeneration. *Acta Biomater*. 2020;117:246-260. doi: 10.1016/j.actbio.2020.09.039

181. Gao F, Xu Z, Liang Q, et al. Osteochondral regeneration with 3d-printed biodegradable high-strength supramolecular polymer reinforced-gelatin hydrogel scaffolds. *Adv Sci (Weinh)*. 2019;6:1900867. doi: 10.1002/advs.201900867

182. Deng C, Yang J, He H, et al. 3D bio-printed biphasic scaffolds with dual modification of silk fibroin for the integrated repair of osteochondral defects. *Biomater Sci*. 2021;9:4891-4903. doi: 10.1039/d1bm00535a

183. Chen P, Zheng L, Wang Y, et al. Desktop-stereolithography 3D printing of a radially oriented extracellular matrix/mesenchymal stem cell exosome bioink for osteochondral defect regeneration. *Theranostics*. 2019;9:2439-2459. doi: 10.7150/thno.31017

184. Jiang G, Li S, Yu K, et al. A 3D-printed PRP-GelMA hydrogel promotes osteochondral regeneration through M2 macrophage polarization in a rabbit model. *Acta Biomater*. 2021;128:150-162. doi: 10.1016/j.actbio.2021.04.010

185. Irmak G, Gumusderelioglu M. Patients- and tissue-specific bio-inks with photoactivated PRP and methacrylated gelatin for the fabrication of osteochondral constructs, *Mater Sci Eng C Mater Biol Appl*. 2021;125:112092. doi: 10.1016/j.msec.2021.112092

186. Zhang X, Yan Z, Guan G, et al. Polyethylene glycol diacrylate scaffold filled with cell-laden methacrylamide gelatin/alginate hydrogels used for cartilage repair. *J Biomater Appl*. 2022;36:1019-1032. doi: 10.1177/08853282211044853

187. Ding X, Gao J, Yu X, et al. 3D-printed porous scaffolds of hydrogels modified with TGF-beta1 binding peptides to promote in vivo cartilage regeneration and animal gait restoration. *ACS Appl Mater Interfaces*. 2022;14:15982-15995. doi: 10.1021/acsami.2c00761

188. Gao J, Ding X, Yu X, et al. Cell-free bilayered porous scaffolds for osteochondral regeneration fabricated by continuous 3D-printing using nascent physical hydrogel as ink. *Adv Healthc Mater*. 2021;10:e2001404. doi: 10.1002/adhm.202001404

189. Liu Y, Peng L, Li L, et al. 3D-bioprinted BMSC-laden biomimetic multiphasic scaffolds for efficient repair of osteochondral defects in an osteoarthritic rat model. *Biomaterials*. 2021;279:121216. doi: 10.1016/j.biomaterials.2021.121216

190. Martyniak K, Lokshina A, Cruz MA, Karimzadeh M, Kemp R, Kean TJ. Biomaterial composition and stiffness as decisive properties of 3D bioprinted constructs for type II collagen stimulation. *Acta Biomater*. 2022;152:221-234. doi: 10.1016/j.actbio.2022.08.058

191. Ege D, Hasirci V. Is 3D printing promising for osteochondral tissue regeneration? *ACS Appl Bio Mater*. 2023;6:1431-1444. doi: 10.1021/acsabm.3c00093

192. Zhou X, Tenaglio S, Esworthy T, et al. Three-dimensional printing biologically inspired DNA-based gradient scaffolds for cartilage tissue regeneration. *ACS Appl Mater Interfaces*. 2020;12:33219-33228. doi: 10.1021/acsami.0c07918

193. Guan J, Yuan FZ, Mao ZM, et al. Fabrication of 3D-printed interpenetrating hydrogel scaffolds for promoting chondrogenic differentiation. *Polymers (Basel)*. 2021;13(13):2146. doi: 10.3390/polym13132146

194. Xia H, Zhao D, Zhu H, et al. Lyophilized scaffolds fabricated from 3d-printed photocurable natural hydrogel for cartilage regeneration. *ACS Appl Mater Interfaces*. 2018;10:31704-31715. doi: 10.1021/acsami.8b10926

195. Wang M, Zhao J, Luo Y, et al. 3D contour printing of anatomically mimetic cartilage grafts with microfiber-reinforced double-network bioink. *Macromol Biosci*. 2022;22:e2200179. doi: 10.1002/mabi.202200179

196. Garcia-Lizarribar A, Fernandez-Garibay X, Velasco-Mallorqui F, Castano AG, Samitier J, Ramon-Azcon J. Composite biomaterials as long-lasting scaffolds for 3D bioprinting of highly aligned muscle tissue. *Macromol Biosci*. 2018;18:e1800167. doi: 10.1002/mabi.201800167.

197. Ajiteru O, Choi KY, Lim TH, et al. A digital light processing 3D printed magnetic bioreactor system using silk magnetic bioink. *Biofabrication*. 2021;13(3). doi: 10.1088/1758-5090/abfaee

198. Lee J, Lee H, Jin EJ, Ryu D, Kim GH. 3D bioprinting using a new photo-crosslinking method for muscle tissue restoration. *NPJ Regen Med*. 2023;8:18. doi: 10.1038/s41536-023-00292-5

199. Boularaoui S, Shanti A, Lanotte M, et al. Nanocomposite conductive bioinks based on low-concentration gelma and mxene nanosheets/gold nanoparticles providing enhanced printability of functional skeletal muscle tissues. *ACS Biomater Sci Eng*. 2021;7:5810-5822.
doi: 10.1021/acsbiomaterials.1c01193

200. Koffler J, Zhu W, Qu X, et al. Biomimetic 3D-printed scaffolds for spinal cord injury repair. *Nat Med*. 2019;25:263-269.
doi: 10.1038/s41591-018-0296-z

201. Poongodi R, Chen YL, Yang TH, et al. Bio-scaffolds as cell or exosome carriers for nerve injury repair. *Int J Mol Sci*. 2021;22(24):13347.
doi: 10.3390/ijms222413347

202. Liu X, Song S, Chen Z, et al. Release of O-GlcNAc transferase inhibitor promotes neuronal differentiation of neural stem cells in 3D bioprinted supramolecular hydrogel scaffold for spinal cord injury repair, *Acta Biomater*. 2022;151:148-162.
doi: 10.1016/j.actbio.2022.08.031

203. Hamid OA, Eltaher HM, Sottile V, Yang J. 3D bioprinting of a stem cell-laden, multi-material tubular composite: an approach for spinal cord repair. *Mater Sci Eng C Mater Biol Appl*. 2021;120:111707.
doi: 10.1016/j.msec.2020.111707

204. Izadifar M, Chapman D, Babyn P, Chen X, Kelly ME. UV-assisted 3D bioprinting of nanoreinforced hybrid cardiac patch for myocardial tissue engineering. *Tissue Eng Part C Methods*. 2018;24:74-88.
doi: 10.1089/ten.TEC.2017.0346

205. Bejleri D, Streeter BW, Nachlas ALY, et al. A bioprinted cardiac patch composed of cardiac-specific extracellular matrix and progenitor cells for heart repair. *Adv Healthc Mater*. 2018;7:e1800672.
doi: 10.1002/adhm.201800672

206. Brazhkina O, Park JH, Park HJ, et al. Designing a 3D printing based auxetic cardiac patch with hiPSC-CMs for heart repair. *J Cardiovasc Dev Dis*. 2021;8(12):172.
doi: 10.3390/jcdd8120172

207. Lee S, Sani ES, Spencer AR, et al. Human-recombinant-elastin-based bioinks for 3D bioprinting of vascularized soft tissues. *Adv Mater*. 2020;32:e2003915.
doi: 10.1002/adma.202003915

208. Wang H, Guo Y, Hu Y, et al. Ultrasound-controlled nano oxygen carriers enhancing cell viability in 3D GelMA hydrogel for the treatment of myocardial infarction. *Int J Biol Macromol*. 2023;244:125139.
doi: 10.1016/j.ijbiomac.2023.125139

209. Mehrotra S, Singh RD, Bandyopadhyay A, Janani G, Dey S, Mandal BB. Engineering microsphere-loaded non-mulberry silk-based 3D bioprinted vascularized cardiac patches with oxygen-releasing and immunomodulatory potential. *ACS Appl Mater Interfaces*. 2021;13:50744-50759.
doi: 10.1021/acsami.1c14118

210. Ma N, Cheung DY, Butcher JT. Incorporating nanocrystalline cellulose into a multifunctional hydrogel for heart valve tissue engineering applications. *J Biomed Mater Res A*. 2022; 110:76-91.
doi: 10.1002/jbm.a.37267

211. Nachlas ALY, Li S, Streeter BW, et al. A multilayered valve leaflet promotes cell-laden collagen type I production and aortic valve hemodynamics. *Biomaterials*. 2020;240:119838.
doi: 10.1016/j.biomaterials.2020.119838

212. Mazzocchi A, Devarasetty M, Huntwork R, Soker S, Skardal A. Optimization of collagen type I-hyaluronan hybrid bioink for 3D bioprinted liver microenvironments. *Biofabrication*. 2018;11:015003.
doi: 10.1088/1758-5090/aae543

213. S. J, S. Velayudhan, A.K. Pr, Biocompatibility evaluation of antioxidant cocktail loaded gelatin methacrylamide as bioink for extrusion-based 3D bioprinting, *Biomed Mater*. 2023;18(4).
doi: 10.1088/1748-605X/acd82f

214. Mao Q, Wang Y, Li Y, et al. Fabrication of liver microtissue with liver decellularized extracellular matrix (dECM) bioink by digital light processing (DLP) bioprinting. *Mater Sci Eng C Mater Biol Appl*. 2020;109:110625.
doi: 10.1016/j.msec.2020.110625

215. Wu Y, Wenger A, Golzar H, Tang XS. 3D bioprinting of bicellular liver lobule-mimetic structures via microextrusion of cellulose nanocrystal-incorporated shear-thinning bioink. Sci Rep. 2020;10:20648.
doi: 10.1038/s41598-020-77146-3

216. Jang MJ, Bae SK, Jung YS, et al. Enhanced wound healing using a 3D printed VEGF-mimicking peptide incorporated hydrogel patch in a pig model. *Biomed Mater*. 2021;16(4).
doi: 10.1088/1748-605X/abf1a8

217. Lam T, Dehne T, Kruger JP, et al. Photopolymerizable gelatin and hyaluronic acid for stereolithographic 3D bioprinting of tissue-engineered cartilage. *J Biomed Mater Res B Appl Biomater*. 2019:107:2649-2657.
doi: 10.1002/jbm.b.34354

218. Yin P, Su W, Li T, et al. A modular hydrogel bioink containing microsphere-embedded chondrocytes for 3D-printed multiscale composite scaffolds for cartilage repair. iScience 2023;26:107349.
doi: 10.1016/j.isci.2023.107349

219. Sang S, Mao X, Cao Y, et al. 3D Bioprinting Using Synovium-Derived MSC-Laden Photo-Cross-Linked ECM Bioink for Cartilage Regeneration. *ACS Appl Mater Interfaces*. 2023.
doi: 10.1021/acsami.2c19058

220. Chen YW, Lin YH, Lin TL, et al. 3D-biofabricated chondrocyte-laden decellularized extracellular matrix-contained gelatin methacrylate auxetic scaffolds under cyclic tensile stimulation for cartilage regeneration, *Biofabrication*. 2023;15(4).
doi: 10.1088/1758-5090/ace5e1

221. Daly AC, Critchley SE, Rencsok EM, Kelly DJ. A comparison of different bioinks for 3D bioprinting of fibrocartilage and hyaline cartilage. *Biofabrication*. 2016;8:045002. doi: 10.1088/1758-5090/8/4/045002

222. Yang Z, Zhao T, Gao C, et al. 3D-bioprinted difunctional scaffold for in situ cartilage regeneration based on aptamer-directed cell recruitment and growth factor-enhanced cell chondrogenesis. *ACS Appl Mater Interfaces*. 2021;13:23369-23383. doi: 10.1021/acsami.1c01844

223. De Moor L, Fernandez S, Vercruysse C, et al. Hybrid bioprinting of chondrogenically induced human mesenchymal stem cell spheroids. *Front Bioeng Biotechnol*. 2020;8:484. doi: 10.3389/fbioe.2020.00484

224. Wang B, Diaz-Payno PJ, Browe DC, et al. Affinity-bound growth factor within sulfated interpenetrating network bioinks for bioprinting cartilaginous tissues. *Acta Biomater*. 2021;128:130-142. doi: 10.1016/j.actbio.2021.04.016

225. Kuo CY, Wilson E, Fuson A, et al. Repair of tympanic membrane perforations with customized bioprinted ear grafts using Chinchilla models. *Tissue Eng Part A*. 2018;24:527-535. doi: 10.1089/ten.TEA.2017.0246

226. Hong H, Seo YB, Kim DY, et al. Digital light processing 3D printed silk fibroin hydrogel for cartilage tissue engineering. *Biomaterials*. 2020;232:119679. doi: 10.1016/j.biomaterials.2019.119679

227. Bandyopadhyay A, Mandal BB, Bhardwaj N. 3D bioprinting of photo-crosslinkable silk methacrylate (SilMA)-polyethylene glycol diacrylate (PEGDA) bioink for cartilage tissue engineering. *J Biomed Mater Res A*. 2022;110:884-898. doi: 10.1002/jbm.a.37336

228. Visscher DO, Lee H, van Zuijlen PPM, et al. A photo-crosslinkable cartilage-derived extracellular matrix bioink for auricular cartilage tissue engineering. *Acta Biomater*. 2021;121:193-203. doi: 10.1016/j.actbio.2020.11.029

229. Cao Y, Cheng P, Sang S, et al. Mesenchymal stem cells loaded on 3D-printed gradient poly(epsilon-caprolactone)/methacrylated alginate composite scaffolds for cartilage tissue engineering. *Regen Biomater*. 2021;8:rbab019. doi: 10.1093/rb/rbab019

230. Abbadessa A, Blokzijl MM, Mouser VH, et al. A thermo-responsive and photo-polymerizable chondroitin sulfate-based hydrogel for 3D printing applications. *Carbohydr Polym*. 2016;149:163-174. doi: 10.1016/j.carbpol.2016.04.080

231. Ma K, Zhao T, Yang L, et al. Application of robotic-assisted in situ 3D printing in cartilage regeneration with HAMA hydrogel: an in vivo study. *J Adv Res*. 2020;23:123-132. doi: 10.1016/j.jare.2020.01.010

232. Kesti M, Muller M, Becher J, et al. A versatile bioink for three-dimensional printing of cellular scaffolds based on thermally and photo-triggered tandem gelation. *Acta Biomater*. 2015;11:162-172. doi: 10.1016/j.actbio.2014.09.033

233. Zhang J, Tong D, Song H, et al. Osteoimmunity-regulating biomimetically hierarchical scaffold for augmented bone regeneration. *Adv Mater*. 2022;34:e2202044. doi: 10.1002/adma.202202044

234. Gao J, Li M, Cheng J, et al. 3D-printed GelMA/PEGDA/F127DA scaffolds for bone regeneration. *J Funct Biomater*. 2023;14:96. doi: 10.3390/jfb14020096

235. Leu Alexa R, Cucuruz A, Ghitulica CD, et al. 3D printable composite biomaterials based on GelMA and hydroxyapatite powders doped with cerium ions for bone tissue regeneration. *Int J Mol Sci*. 2022;23:1841. doi: 10.3390/ijms23031841

236. Li Z, Li S, Yang J, et al. 3D bioprinted gelatin/gellan gum-based scaffold with double-crosslinking network for vascularized bone regeneration. *Carbohydr Polym*. 2020;290:119469. doi: 10.1016/j.carbpol.2022.119469

237. Liu G, Chen J, Wang X, Liu Y, Ma Y, Tu X. Functionalized 3D-printed ST2/gelatin methacryloyl/polcaprolactone scaffolds for enhancing bone regeneration with vascularization. Int J Mol Sci. 2022;23(15):8347. doi: 10.3390/ijms23158347

238. Zhang X, Zhang H, Zhang Y, et al. 3D printed reduced graphene oxide-GelMA hybrid hydrogel scaffolds for potential neuralized bone regeneration. *J Mater Chem B*. 2023;11:1288-1301. doi: 10.1039/d2tb01979e

239. Xu C, Chang Y, Xu Y, et al. Silicon-phosphorus-nanosheets-integrated 3D-printable hydrogel as a bioactive and biodegradable scaffold for vascularized bone regeneration. *Adv Healthc Mater*. 2022;11:e2101911. doi: 10.1002/adhm.202101911

240. Jiang Y, Zhou D, Yang B. 3D bioprinted GelMA/GO composite induces osteoblastic differentiation. *J Biomater Appl*. 2022;37:527-537. doi: 10.1177/08853282221098235

241. Ashwin B, Abinaya B, Prasith TP, et al. 3D-poly (lactic acid) scaffolds coated with gelatin and mucic acid for bone tissue engineering. *Int J Biol Macromol.* 2020;162:523-532. doi: 10.1016/j.ijbiomac.2020.06.157

242. Tong L, Pu X, Liu Q, et al. Nanostructured 3D-printed hybrid scaffold accelerates bone regeneration by photointegrating nanohydroxyapatite. *Adv Sci (Weinh)*. 2023;10:e2300038. doi: 10.1002/advs.202300038

243. Pu X, Tong L, Wang X, et al. Bioinspired hydrogel anchoring 3DP GelMA/HAp scaffolds accelerates bone reconstruction. *ACS Appl Mater Interfaces*. 2022;14:20591-20602.

doi: 10.1021/acsami.1c25015

244. Leu Alexa R, Cucuruz A, Ghitulica CD, et al. 3D printed composite scaffolds of GelMA and hydroxyapatite nanopowders doped with Mg/Zn ions to evaluate the expression of genes and proteins of osteogenic markers. *Nanomaterials (Basel)*. 2022;12(19):3420. doi: 10.3390/nano12193420

245. Sun X, Yang J, Ma J, et al. Three-dimensional bioprinted BMSCs-laden highly adhesive artificial periosteum containing gelatin-dopamine and graphene oxide nanosheets promoting bone defect repair. *Biofabrication*. 2023;15(2). doi: 10.1088/1758-5090/acb73e

246. Dong L, Bu Z, Xiong Y, et al. Facile extrusion 3D printing of gelatine methacrylate/Laponite nanocomposite hydrogel with high concentration nanoclay for bone tissue regeneration. *Int J Biol Macromol*. 2021;188:72-81. doi: 10.1016/j.ijbiomac.2021.07.199

247. Yang X, Ma Y, Wang X, et al. A 3D-bioprinted functional module based on decellularized extracellular matrix bioink for periodontal regeneration. *Adv Sci (Weinh)*. 2023;10:e2205041. doi: 10.1002/advs.202205041

248. Ratheesh G, Vaquette C, Xiao Y. Patient-specific bone particles bioprinting for bone tissue engineering. *Adv Healthc Mater*. 2020;9(23):e2001323. doi: 10.1002/adhm.202001323

249. Alcala-Orozco CR, Mutreja I, Cui X, Hooper GJ, Lim KS, Woodfield TBF. Hybrid biofabrication of 3D osteoconductive constructs comprising Mg-based nanocomposites and cell-laden bioinks for bone repair. *Bone*. 2022;154:116198. doi: 10.1016/j.bone.2021.116198

250. Dutta SD, Ganguly K, Hexiu J, Randhawa A, Moniruzzaman M, Lim KT. A 3D bioprinted nanoengineered hydrogel with photoactivated drug delivery for tumor apoptosis and simultaneous bone regeneration via macrophage immunomodulation. *Macromol Biosci*. 2023;23:e2300096. doi: 10.1002/mabi.202300096

251. Tavares MT, Gaspar VM, Monteiro MV, S Farinha JP, Baleizão C, Mano JF. GelMA/bioactive silica nanocomposite bioinks for stem cell osteogenic differentiation. *Biofabrication*. 2021;13(3). doi: 10.1088/1758-5090/abdc86

252. Shahabipour F, Tavafoghi M, Aninwene GE, et al. Coaxial 3D bioprinting of tri-polymer scaffolds to improve the osteogenic and vasculogenic potential of cells in co-culture models. *J Biomed Mater Res A*. 2022;110:1077-1089. doi: 10.1002/jbm.a.37354

253. Lee SH, Kang MS, Jeon S, et al. 3D bioprinting of human mesenchymal stem cells-laden hydrogels incorporating MXene for spontaneous osteodifferentiation. *Heliyon*. 2023;9:e14490. doi: 10.1016/j.heliyon.2023.e14490

254. Ma Y, Ji Y, Zhong T, et al. Bioprinting-based PDLSC-ECM screening for in vivo repair of alveolar bone defect using cell-laden, injectable and photocrosslinkable hydrogels. *ACS Biomater Sci Eng*. 2017;3:3534-3545. doi: 10.1021/acsbiomaterials.7b00601

255. Miao G, Liang L, Li W, et al. 3D bioprinting of a bioactive composite scaffold for cell delivery in periodontal tissue regeneration. *Biomolecules*. 2023;13(7):1062. doi: 10.3390/biom13071062

256. Guo L, Chen H, Li Y, Zhou J, Chen J. Biocompatible scaffolds constructed by chondroitin sulfate microspheres conjugated 3D-printed frameworks for bone repair. *Carbohydr Polym*. 2023;299:120188. doi: 10.1016/j.carbpol.2022.120188

257. Su JJ, Lin CH, Chen H, Lee SY, Lin YM. Biofabrication of cell-laden gelatin methacryloyl hydrogels with incorporation of silanized hydroxyapatite by visible light projection. *Polymers (Basel)*. 2021;13(14):2354. doi: 10.3390/polym13142354

258. Bucciarelli A, Petretta M, Grigolo B, et al. Methacrylated silk fibroin additive manufacturing of shape memory constructs with possible application in bone regeneration. *Gels*. 2022;8(12):833. doi: 10.3390/gels8120833

259. Chang HK, Yang DH, Ha MY, et al. 3D printing of cell-laden visible light curable glycol chitosan bioink for bone tissue engineering. *Carbohydr Polym*. 2022;287:119328. doi: 10.1016/j.carbpol.2022.119328

260. Ferroni L, D'Amora U, Leo S, et al. PEEK and hyaluronan-based 3d printed structures: promising combination to improve bone regeneration. *Molecules*. 2022;27(24):8749. doi: 10.3390/molecules27248749

261. Kajave NS, Schmitt T, Patrawalla NY, Kishore V. Design-build-validate strategy to 3D print bioglass gradients for anterior cruciate ligament enthesis reconstruction. *Tissue Eng Part C Methods*. 2022;28:158-167. doi: 10.1089/ten.TEC.2022.0035

262. Qiu C, Sun Y, Li J, et al. Therapeutic effect of biomimetic scaffold loaded with human amniotic epithelial cell-derived neural-like cells for spinal cord injury. *Bioengineering (Basel)*. 2022;9(10):535. doi: 10.3390/bioengineering9100535

263. Kim KS, Joo HJ, Choi SC, et al. Transplantation of 3D bio-printed cardiac mesh improves cardiac function and vessel formation via ANGPT1/Tie2 pathway in rats with acute myocardial infarction. *Biofabrication*. 2021;13(4). doi: 10.1088/1758-5090/ac1e78

264. Hu Y, Jia Y, Wang H, et al. Low-intensity pulsed ultrasound promotes cell viability and inhibits apoptosis of H9C2 cardiomyocytes in 3D bioprinting scaffolds via PI3K-Akt and ERK1/2 pathways. *J Biomater Appl*. 2022; 37:402-414. doi: 10.1177/08853282221102669

265. Ainsworth MJ, Chirico N, de Ruijter M, et al. Convergence of melt electrowriting and extrusion-based bioprinting for vascular patterning of a myocardial construct. *Biofabrication*. 2023;15(3). doi: 10.1088/1758-5090/ace07f

266. Li H, Yin Y, Xiang Y, Liu H, Guo R. A novel 3D printing PCL/GelMA scaffold containing USPIO for MRI-guided bile duct repair. *Biomed Mater*. 2020;15:045004. doi: 10.1088/1748-605X/ab797a

267. Cui J, Wang H, Shi Q, Sun T, Huang Q, Fukuda T. Multicellular co-culture in three-dimensional gelatin methacryloyl hydrogels for liver tissue engineering. *Molecules*. 2019;24(9):1762. doi: 10.3390/molecules24091762

268. Cuvellier M, Rose S, Ezan F, et al. In vitrolong term differentiation and functionality of three-dimensional bioprinted primary human hepatocytes: application forin vivoengraftment. *Biofabrication*. 2022;14(3). doi: 10.1088/1758-5090/ac7825

269. Li T, Hou J, Wang L, et al. Bioprinted anisotropic scaffolds with fast stress relaxation bioink for engineering 3D skeletal muscle and repairing volumetric muscle loss. *Acta Biomater*. 2023;156:21-36. doi: 10.1016/j.actbio.2022.08.037

270. Hwangbo H, Lee H, Jin EJ, et al. Bio-printing of aligned GelMa-based cell-laden structure for muscle tissue regeneration. *Bioact Mater*. 2022;8:57-70. doi: 10.1016/j.bioactmat.2021.06.031

271. Tavares-Negrete JA, Pedroza-Gonzalez SC, Frias-Sanchez AI, et al. Supplementation of GelMA with minimally processed tissue promotes the formation of densely packed skeletal-muscle-like tissues. *ACS Biomater Sci Eng*. 2023;9:3462-3475. doi: 10.1021/acsbiomaterials.2c01521

272. Wang Y, Wang Q, Luo S, et al. 3D bioprinting of conductive hydrogel for enhanced myogenic differentiation. *Regen Biomater*. 2021;8:rbab035. doi: 10.1093/rb/rbab035

273. Choi KY, Ajiteru O, Hong H, et al. A digital light processing 3D-printed artificial skin model and full-thickness wound models using silk fibroin bioink. *Acta Biomater*. 2023;164:159-174. doi: 10.1016/j.actbio.2023.04.034

274. de Barros NR, Darabi MA, Ma X, et al. Enhanced maturation of 3D bioprinted skeletal muscle tissue constructs encapsulating soluble factor-releasing microparticles. *Macromol Biosci*. 2023;23(12):e2300276. doi: 10.1002/mabi.202300276

275. Liu G, Guo Q, Liu C, et al. Cytomodulin-10 modified GelMA hydrogel with kartogenin for in-situ osteochondral regeneration. *Acta Biomater*. 2023;169:317-333. doi: 10.1016/j.actbio.2023.08.013

276. Wang M, Li W, Luo Z, et al. A multifunctional micropore-forming bioink with enhanced anti-bacterial and anti-inflammatory properties. *Biofabrication*. 2022;14(2). doi: 10.1088/1758-5090/ac5936

277. Wang C, Wang M, Xu T, et al. Engineering bioactive self-healing antibacterial exosomes hydrogel for promoting chronic diabetic wound healing and complete skin regeneration. *Theranostics*. 2019;9:65-76. doi: 10.7150/thno.29766

278. Zhang FX, Liu P, Ding W, et al. Injectable mussel-inspired highly adhesive hydrogel with exosomes for endogenous cell recruitment and cartilage defect regeneration. *Biomaterials*. 2021;278:121169. doi: 10.1016/j.biomaterials.2021.121169

279. Fan L, Liu C, Chen X, et al. Exosomes-loaded electroconductive hydrogel synergistically promotes tissue repair after spinal cord injury via immunoregulation and enhancement of myelinated axon growth. *Adv Sci (Weinh)*. 2022;9:e2105586. doi: 10.1002/advs.202105586

280. Khayambashi P, Iyer J, Pillai S, Upadhyay A, Zhang Y, Tran SD. Hydrogel encapsulation of mesenchymal stem cells and their derived exosomes for tissue engineering. *Int J Mol Sci*. 2021;22(2):684. doi: 10.3390/ijms22020684

281. Born LJ, McLoughlin ST, Dutta D, et al. Sustained released of bioactive mesenchymal stromal cell-derived extracellular vesicles from 3D-printed gelatin methacrylate hydrogels. *J Biomed Mater Res A*. 2022;110:1190-1198. doi: 10.1002/jbm.a.37362

282. Hu H, Zhang H, Bu Z, et al. Small extracellular vesicles released from bioglass/hydrogel scaffold promote vascularized bone regeneration by transferring miR-23a-3p. *Int J Nanomedicine*. 2022;17:6201-6220. doi: 10.2147/IJN.S389471

283. Zhu B, Wang D, Pan H, et al. Three-in-one customized bioink for islet organoid: GelMA/ECM/PRP orchestrate pro-angiogenic and immunoregulatory function. *Colloids Surf B Biointerfaces*. 2023;221:113017. doi: 10.1016/j.colsurfb.2022.113017

284. Cao W, Peng S, Yao Y, et al. A nanofibrous membrane loaded with doxycycline and printed with conductive hydrogel strips promotes diabetic wound healing in vivo. *Acta Biomater*. 2022;152:60-73. doi: 10.1016/j.actbio.2022.08.048

285. Ferroni L, Gardin C, D'Amora U, et al. Exosomes of mesenchymal stem cells delivered from methacrylated hyaluronic acid patch improve the regenerative properties of endothelial and dermal cells. *Biomater Adv*. 2022;139:213000. doi: 10.1016/j.bioadv.2022.213000

286. Liu H, Wang Y, Cui K, Guo Y, Zhang X, Qin J. Advances in hydrogels in organoids and organs-on-a-chip. *Adv Mater*. 2019;31:e1902042. doi: 10.1002/adma.201902042

287. Cuvellier M, Ezan F, Oliveira H, et al. 3D culture of HepaRG cells in GelMa and its application to bioprinting of a multicellular hepatic model. *Biomaterials*. 2021;269:120611. doi: 10.1016/j.biomaterials.2020.120611

288. Bhise NS, Manoharan V, Massa S, et al. A liver-on-a-chip platform with bioprinted hepatic spheroids. *Biofabrication*. 2016;8:014101. doi: 10.1088/1758-5090/8/1/014101

289. Zhang YS, Davoudi F, Walch P, et al. Bioprinted thrombosis-on-a-chip. *Lab Chip*. 2016;16:4097-4105. doi: 10.1039/c6lc00380j

290. Liu S, Wang Z, Chen X, et al. Multiscale anisotropic scaffold integrating 3D printing and electrospinning techniques as a heart-on-a-chip platform for evaluating drug-induced cardiotoxicity. *Adv Healthc Mater*. 2023;12(24):e2300719. doi: 10.1002/adhm.202300719

291. van der Valk DC, van der Ven CFT, Blaser MC, et al. Engineering a 3D-bioprinted model of human heart valve disease using nanoindentation-based biomechanics. *Nanomaterials (Basel)*. 2018;8(5):296. doi: 10.3390/nano8050296

292. Sanchez-Salazar MG, Crespo-Lopez Oliver R, Ramos-Meizoso S, et al. 3D-printed tumor-on-chip for the culture of colorectal cancer microspheres: mass transport characterization and anti-cancer drug assays. *Bioengineering (Basel)*. 2023;10(5):554. doi: 10.3390/bioengineering10050554

293. Chen Z, Wang F, Zhang J, et al. Study on development of composite hydrogels with tunable structures and properties for tumor-on-a-chip research. *Front Bioeng Biotechnol*. 2020;8:611796. doi: 10.3389/fbioe.2020.611796

294. Makarcyzk MJ, Li ZA, Yu I, et al. Creation of a knee joint-on-a-chip for modeling joint diseases and testing drugs. *J Vis Exp*. 2023;(191):10.3791/64186. doi: 10.3791/64186

295. Vurat MT, Seker S, Lalegul-Ulker O, et al. Development of a multicellular 3D-bioprinted microtissue model of human periodontal ligament-alveolar bone biointerface: towards a pre-clinical model of periodontal diseases and personalized periodontal tissue engineering. *Genes Dis*. 2022;9:1008-1023. doi: 10.1016/j.gendis.2020.11.011

296. Kim W, Lee H, Lee J, et al. Efficient myotube formation in 3D bioprinted tissue construct by biochemical and topographical cues. *Biomaterials*. 2020;230:119632. doi: 10.1016/j.biomaterials.2019.119632

297. Ma X, Qu X, Zhu W, et al. Deterministically patterned biomimetic human iPSC-derived hepatic model via rapid 3D bioprinting. *Proc Natl Acad Sci U S A*. 2016;113:2206-2211. doi: 10.1073/pnas.1524510113

298. Gu L, Jiang S, Xu X, et al. Size- and density-dependent acoustic differential bioassembly of spatially-defined heterocellular architecture. *Biofabrication*. 2022;15(1). doi: 10.1088/1758-5090/aca79c

299. Wang D, Guo Y, Zhu J, et al. Hyaluronic acid methacrylate/pancreatic extracellular matrix as a potential 3D printing bioink for constructing islet organoids. *Acta Biomater*. 2023;165:86-101. doi: 10.1016/j.actbio.2022.06.036

300. Chen S, Tomov ML, Ning L, et al. Extrusion-based 3D bioprinting of adhesive tissue engineering scaffolds using hybrid functionalized hydrogel bioinks. *Adv Biol (Weinh)*. 2023;7:e2300124. doi: 10.1002/adbi.202300124

301. Li W, Wang M, Wang S, et al. An adhesive bioink toward biofabrication under wet conditions. *Small*. 2023;19(50):e2205078. doi: 10.1002/smll.202205078

302. Wei K, Sun J, Gao Q, et al. 3D "honeycomb" cell/carbon nanofiber/gelatin methacryloyl (GelMA) modified screen-printed electrode for electrochemical assessment of the combined toxicity of deoxynivalenol family mycotoxins. *Bioelectrochemistry*. 2021;139:107743. doi: 10.1016/j.bioelechem.2021.107743

303. Wan W, Li Z, Wang X, Tian F, Yang J. Surface-fabrication of fluorescent hydroxyapatite for cancer cell imaging and bio-printing applications. *Biosensors (Basel)*. 2022;12(6):419. doi: 10.3390/bios12060419

304. Liu S, Wang Z, Chen X, et al. Multiscale anisotropic scaffold integrating 3D printing and electrospinning techniques as a heart-on-a-chip platform for evaluating drug-induced cardiotoxicity. *Adv Healthc Mater*. 2023;12:e2300719. doi: 10.1002/adhm.202300719

305. Liu J, Miller K, Ma X, et al. Direct 3D bioprinting of cardiac micro-tissues mimicking native myocardium. *Biomaterials*. 2020;256:120204. doi: 10.1016/j.biomaterials.2020.120204

306. Wang J, Wu Y, Li G, et al. Engineering large-scale self-mineralizing bone organoids with bone matrix-inspired hydroxyapatite hybrid bioinks. *Adv Mater*. 2024;36:e2309875. doi: 10.1002/adma.202309875

307. O'Donnell BT, Al-Ghadban S, Ives CJ, et al. Adipose tissue-derived stem cells retain their adipocyte differentiation potential in three-dimensional hydrogels and bioreactors (dagger). *Biomolecules*. 2020;10:1070. doi: 10.3390/biom10071070

308. Nothdurfter D, Ploner C, Coraca-Huber DC, et al. 3D bioprinted, vascularized neuroblastoma tumor environment in fluidic chip devices for precision medicine drug testing. *Biofabrication*. 2022;14(3). doi: 10.1088/1758-5090/ac5fb7.

309. Bhattacharyya A, Ham HW, Sonh J, et al. 3D bioprinting of complex tissue scaffolds with in situ homogeneously mixed alginate-chitosan-kaolin bioink using advanced portable biopen. *Carbohydr Polym*. 2023;317:121046. doi: 10.1016/j.carbpol.2023.121046